SYNTHESIS, CHARACTERIZATION AND CATALYTIC PROPERTIES OF EU-1 ZEOLITES

A THESIS
SUBMITTED TO THE
UNIVERSITY OF POONA
FOR THE DEGREE OF
DOCTOR OF PHILOSOPHY
(IN CHEMISTRY)

BY

GADE NARSINGA RAO
M. Sc.

PHYSICAL CHEMISTRY DIVISION
NATIONAL CHEMICAL LABORATORY
PUNE - 411 008, INDIA

MAY 1990

CONTENTS

CHAPTER 1

GENERAL INTRODUCTION

CONTENTS

1.1 INTRODUCTION

Zeolites are, microporous, crystalline, hydrated aluminosilicates containing cavities and channels. Structurally, they possess a framework based on an infinitely extending three-dimensional network of SiO_4 and AlO_4 tetrahedra linked through oxygen atoms forming a rigid three dimensional structure. The negative charge on the alumina tetrahedra is compensated by cations resulting in an electrically neutral framework. The structural formula of the crystallographic unit cell of a zeolite is expressed as,

$$M_{X/n}[(AlO_2)_X\ (SiO_2)_Y].Z\ H_2O$$

where M is the cation of valence n, Z is the number of water molecules and Y/X is the structure characteristic ratio. The sum (X+Y) represents the total number of tetrahedra in the unit cell. $[(AlO_2)_X\ (SiO_2)_Y]$ indicates the framework composition.

1.2 HISTORICAL BACKGROUND

The history of zeolites began with the discovery of stilbite in 1756. Cronstedt[1] first recognized a group of minerals consisting of hydrated aluminosilicates. Because the minerals exhibited intumescence when heated in a blowpipe flame, he named them as "Zeolites", a Greek word meaning the "boiling stone". In 1840, Damour[2] noticed that zeolites could be reversibly dehydrated without alteration of the structure and morphology. In 1896, Friedel[3] observed that hydrated zeolites could occlude molecules such as alcohol and benzene. The dehydrated chabazite

adsorbed[4] vapours of ammonia, air, hydrogen and carbondisulfide. Weigel and Steinhoff[5] observed that naturally occuring chabazite adsorbed vapours of water, methanol, ethanol and formic acid readily, while acetone, benzene and ether were excluded. To account for this phenomenon of selective sorption, McBain[6] interpreted these results in terms of molecular size difference and proposed the term "Molecular Sieves".

1.3 CLASSIFICATION OF ZEOLITES

Presently, there exists about 40 species of natural zeolites and more than 150[7] synthetic zeolites. Classification of zeolites has been made on the basis of their morphological characteristics, crystal structure, chemical composition, effective pore diameter and natural occurrence. The classification of zeolites based on morphology was given by Bragg[8]. The fibrous zeolites are noted as having the linkages of their tetrahedra more numerous in one crystallograhic direction. The lamellar zeolites are noted by having their structural linkages more numerous in one plane and are characterized by a platy cleavage. The so-called framework structures have similar bonding strength of their tetrahedra in all directions. Several different structural classifications of zeolites have been proposed[9,10]. Meier[11], however, has classified them into seven groups, based on differences in their secondary building units. With the addition of new synthetic and natural zeolites, Barrer[12] extended the number of groups to 10.

Classification of zeolites according to their chemical composition has been made on the basis of their silica-to-alumina ratios[13]. From this, four distinct groups have been formed: 1) low silica zeolites, 2) intermediate silica zeolites, 3) high silica zeolites and 4) pure silica zeolites. Table 1.1 shows this type of classification.

It is also convenient to classify zeolites according to their effective pore diameter, since this indicates the largest size molecule that can be absorbed into their pore systems. Barrer[14] has made such a classification of zeolites into five groups. Sand[15] later modified this classification into three major groups, according to the largest membered ring present in the structure of each zeolites. Table 1.2 shows this type of classification. Recently, very large pore aluminophosphate molecular sieve (VPI-5)[16,17] containing 18-membered rings has been discovered.

Zeolite EU-1 is a novel high silica zeolite[18], developed by Imperial Chemical Industries. It was prepared[18] with SiO_2/Al_2O_3 ratios between 20 and 100 from mixtures containing hexamethonium cation. Casci and Lowe[19] followed the changes in pH during synthesis of EU-1 and showed that this technique can be used to give mechanistic information and to establish when the crystallization of the desired phase has been completed. Recently the synthesis of three related zeolites, EU-7, EU-12 and EU-13, have also been disclosed[20,21,22].

Table 1.1. CLASSIFICATION OF ZEOLITES ACCORDING TO CHEMICAL COMPOSITION*

LOW Si/Al ZEOLITES (1-1.5)

A, X, sodalite

INTERMEDIATE Si/Al ZEOLITES (2-5)

(a) Natural zeolites

Erionite, chabazite, clinoptilolite, mordenite

(b) Synthetic zeolites

Y, L, Large-port Mordenite, Omega

HIGH Si/Al ZEOLITES (10-SEVERAL THOUSANDS)

(a) By thermochemical modification

Highly siliceous variants of Y, mordenite, erionite

(b) By direct synthesis

ZSM-5, ZSM-11, EU-1, EU-2, Beta

SILICA MOLECULAR SIEVES (SEVERAL THOUSANDS TO ∞)

Silicalite

* Ref. 13

Table 1.2. CLASSIFICATION OF ZEOLITES ACCORDING TO EFFECTIVE POR DIAMETER*.

Small port (8-membered ring)	Intermediate port (10-membered ring)	Large port (12-membered ring
Li-A	dachiardite	cancrinite
bikitaite	epistilbite	Linde X, Y,
brewsterite	ferrierite	gmelinite
chabazite	heulandite	mazzite
TMA-E	laumontite	mordenite
edingtonite	ZSM-5	offretite
erionite	ZSM-11	ZSM-12
gismondine	EU-1 (ZSM-50)	Omega
ZK-5	Stilbite	Beta
Levynite	ZSM-23	
Linde A	Theta-1 (ZSM-22)	
merlinoite	ZSM-48 (EU-2)	
natrolite		
paulingite		
phillipsite		
Rho		
thomsonite		
yugawaralite		

* Ref. 15.

Zeolite EU-1 belongs to the family of a high silica medium pore system[13-15]. Since the present work deals with the "Synthesis, characterization and catalytic properties of EU-1 zeolite", further discussions relating to this medium-pore zeolite is presented in later sections.

1.4 ZEOLITE SYNTHESIS

1.4.1 SYNTHESIS OF ALUMINOSILICATE ZEOLITES

Zeolites are synthesized by crystallising reactive aluminosilicate gels with alkali and alkaline earth metal hydroxides, under hydrothermal conditions. The early era of the discovery of zeolites in the late 1940's and the early 1950's, led to about 20 novel synthetic zeolites[23]. The chemistry[24] involved the use of highly reactive alkaline aluminosilicate gels. The crystallization was carried out at low temperatures and autogeneous pressure. It was observed that the cation played a dominant role in directing the formation of specific structures[25,26]. The zeolites synthesised in the earlier stages used only two alkali cations, namely sodium and potassium, or their mixtures. A second important variable in the synthesis as well as in properties was the Si/Al ratio. Increase in the Si/Al in the reaction mixture resulted in synthesis of zeolites with intermediate Si/Al ratio, such as zeolite T[27] and L, still using the same two alkali cations.

The next major advance in synthesis of new zeolite materials was the introduction of alkylammonium cations during the

hydrothermal synthesis of zeolites. In the early 1960's, the tetramethylammonium cation (TMA) was introduced as the first organic cation in zeolite synthesis[28-30]. There are various examples[28] of zeolite formation in presence of TMA-hydroxide, for example, N-A[31], ZK-4[32], and α[33], all having A type structure but higher silica to alumina ratios. Subsequently, the addition of alkyl ammonium cations to sodium aluminosilicate gels led to the formation of new zeolite structure types, examplified by zeolite ZK-5[34] Omega[35,36], and zeolite N[37]. MOBIL reported[38] incorporation of alkylammonium and other nitrogeneous organic molecules[26], such as TEA, TPA, TBA and pyrrolidine, to highly siliceous gels (Si/Al=10 to 100) resulting in the formation of a series of high silica zeolite materials. These compositions represent high silica analogs of previously known structure types. Examples are ZSM-21[39], a ferrierite-type and ZSM-34[40], an erionite-offretite type, as well as new structure types such as ZSM-5[41], ZSM-11[42], ZSM-12[43], and zeolite beta[44]. Subsequently, the use of mixed alkylammonium cations other than the classical TPA cation was demonstrated by Kulkarni et al.[45] and Kotasthane et al.[46]. Recently Casci[47] and others[48,49,50,51] have reported the synthesis of a series of new high-silica zeolites such as EU-1, EU-2, EU-4, ZSM-23 and ZSM-39 by the addition of bis-quaternary ammonium compounds.

The addition of alkylammonim cations to pure silica systems ultimately resulted in silica molecular sieves; for example silicalite-1[52] and fluoride silicalite[53] with TPA;

silicalite-2, structurally related to the zeolite ZSM-11[54] with TBA[55]; and TEA-silicalite[56], an apparent structural analog of zeolite ZSM-12, with TEA.

1.4.2 ZEOLITE SYNTHESIS WITH ISOMORPHOUS SUBSTITUTION

Considerable work has been reported[57] in producing clay minerals, in which isomorphous replacements are effected by elements not usually found in naturally occurring clay minerals. Under high pressures, Group I-VIII elements can replace silicon/aluminium in zeolite frameworks under high temperature conditions[58,59]. In a series of high temperature preparations, Eitel et al.[60] introduced Y, La and Nd in place of aluminium in synthetic nepheline type phases. All these replacements refer to syntheses at high temperatures in the absence of water. Zeolite formation at low temperatures under alkaline aqueous conditions poses a very different situation.

It is of interest to examine the claims [61] that the zeolites bearing such metallic elements in their framework have been made. Zeolites having the ZSM-5 topology were synthesized, in which iron and chromium were considered to occupy some of the tetrahedral framework sites. The iron bearing ZSM-5 was prepared[12] from a reaction mixture containing silica, ferric-oxide and caustic soda, with incorporation of hexamethylene diamine as the organic base. This was crystallized in the low temperature range, 140-160^{o}C, for 2 to 4 days. The chromium bearing ZSM-5 was also prepared under similar conditions. Barrer

et al.[62] synthesised iron-bearing cancrinite from kaolinite by heating at 80°C for 5 days.

In recent years the introduction of foreign atoms into zeolite framework has created a great interest since the physical properties and consequently the catalytic properties of zeolites are changed to a large extent by such isomorphous substitution. It has been established[63] that isomorphous substitution of Si and Al, by P, Ge, B and Fe in zeolites modify the acid strength and catalytic properties of various zeolites. Based on the above information, the recent claims in the patent literature[64-66], as well as published materials[46,67] are of great importance. An important family of molecular sieve materials, aluminophosphates was synthesized by Wilson et al.[68]. These represent the first family of framework oxide molecular sieve without silica and have been designated as "ALPO". Recently, Davis[16] discovered a very large pore (18 membered rings) alumino-phosphate molecular sieve VPI-5. The substitution of silicon for aluminium and phosphorous in the alumino phosphate framework resulted in the silico-alumino phosphate (SAPO) molecular seives which were disclosed by Lok et al.[69].

Thus, it is observed from the above literature survey that, variation in two important parameters, namely the cation-base system and the silica to alumina ratio, has generally been used in the synthesis of a variety of zeolites. However, their synthesis still uses the basic reactive gel crystallization method developed by Milton[24] in the late 1940's. The use of a

variety of organic cations has made possible the extension of zeolite science into the high Si/Al region. Secondly, many other structure types have also been made with the use of organic cations (Table 1.3)[70]. Modification of zeolite framework by isomorphous substitution is also possible, particularly under low temperature and aqueous alkaline conditions.

1.5 THE FRAMEWORK TOPOLOGY OF ZEOLITE EU-1

Zeolite EU-1 is a novel, high-silica material. Briscoe et al.[71] reported the structure of EU-1. It has 10-membered ring openings (0.58 X 0.41 nm), and an unidimensional, non-intersecting channels system in the [100] direction. Figure 1.1 depicts a schematic diagram of the channel/side-pocket network of EU-1. The side pockets are 0.68 X 0.58 nm in cross-section and 0.81 nm in depth in the [001] directions. Based on the electron diffraction studies Briscoe[71] showed that the unit cell has a orthorhombic symmetry with lattice parameters a =13.7, b=22.3 and c=20.2 A^{o}. The unit cell contains a total of 112 T-atoms and its framework density is 1.81 T/1000 $A^{o\ 3}$. The composition of the unit cell in Na form for EU-1 is

$$Na_n\ [Al_n\ Si_{112-n}\ O_{224}]\ .\ H_2O$$

where n < 19 and typically nearly 3.6. The number of aluminium atoms per unit-cell is obtained from the relation

$$N_{Al} = 112/1+R$$

where $R = N_{Si}/N_{Al}$ and N_{Si}, N_{Al} are gm. atoms of silicon and aluminium respectively.

Table 1.3. ORGANIC TEMPLATE-ZEOLITE STRUCTURE RELATIONSHIPS*

Organic	Zeolite Structure
Tetraethylammonium (TEA)	Beta
	ZSM-8
	ZSM-12
	ZSM-20
	ZSM-25
	Mordenite
Methyltriethylammonium	ZSM-12
Tetrapropylammonium	ZSM-5
n-propylamine	ZSM-5
choline	ZSM-38
	ZSM43
	CZH-5
TMA+TEA	ZSM-39
Pyrrolidine	ZSM-35
	ZSM-21
1,2 Diaminoethane	ZSM-5
	ZSM-21
DDO	ZSM-10
	ZK-5
MQ	LZ-132
	NU-3
Neopentylamine	Mordenite
Dihexamethylenetriamine	ZSM-30
BP	LOSOD
Hexamethonium Bromide (HMBr)	EU-1
	EU-2
Pentaerythritol (PTE)	NU-5

*.Ref. 70.

BP = (5-azoniaspiro (4,4) nonance)$^+$ or (bispyrrolidinium)$^+$

Choline = (2-hydroxyethyl)trimethylammonium)$^+$

DDO = (1,4-dimethyl-1,4-diazoniabicyclo(2,2,2)octane)$^+$

MQ (or MEQ) = (1-methylazobicyclo(2,2,2)octane)$^+$ or

(methylquinuclidine)$^+$

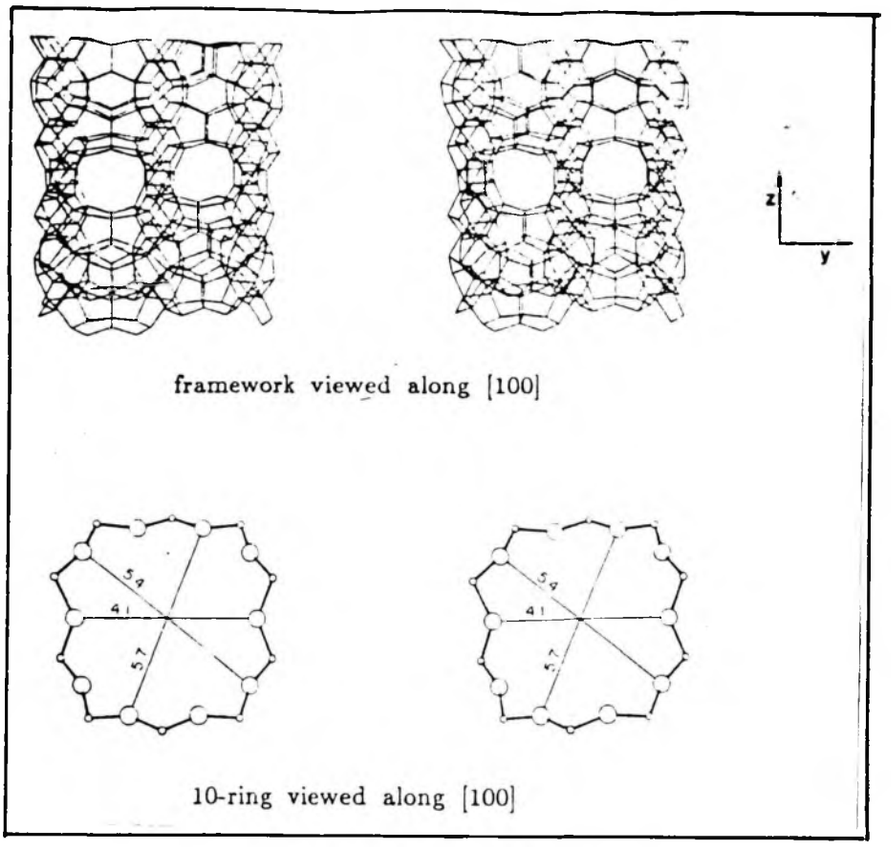

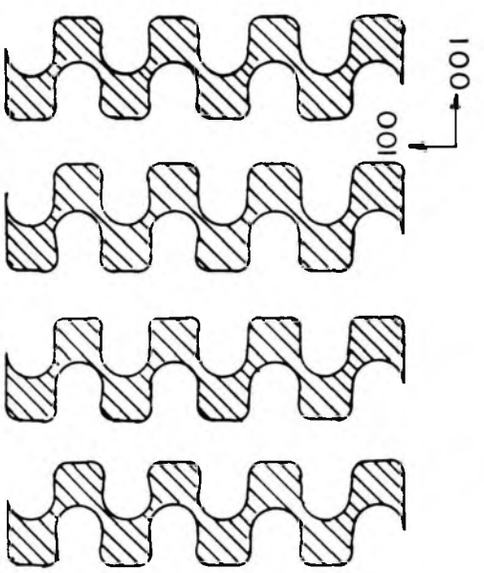

FIG. 1.1 SCHEMATIC OF THE STEREO DIAGRAMES AND CHANNEL NETWORK OF ZEOLITE EU-1. THE CHANNELS RUN IN THE (100) DIRECTION AND THE SIDE POCKETS IN (001) DIRECTIONS OFF THESE.

Based on the similarities in XRD powder patterns of EU-1, ZSM-50[72] and TPZ-3[73], it was proposed[71] that these two zeolites also possess the framework topology of EU-1, designated as EUO.

1.6 PHYSICO-CHEMICAL CHARACTERIZATION OF ZEOLITES

1.6.1 X-RAY DIFFRACTION

X-ray diffraction is one of the most important classical techniques which has been utilised not only to determine the zeolite structures but also for quantitative phase identification and to understand the kinetics and mechanism of zeolite crystallization[45,74-77]. The apparent framework symmetry change with small change in the lattice parameters has been reported[78] for ZSM-5 zeolites using X-ray diffraction technique. In addition, a reversible transformation of framework symmetry on increasing Si/Al ratio in ZSM-5 framework has been observed. Bibby et al.[79] reported the use of X-ray diffraction technique for estimating the average alumina content, from the change in unit cell volume in the ZSM-5 crystals. The use of unit cell volume studies in identifying and confirming structural incorporation of elements other than aluminum has been reported[80]. Simulated X-ray powder diffraction patterns have been compared[81,82] with experimental data to select the most likely structure for further refinement.

1.6.2 INFRARED SPECTROSCOPY

Infrared spectroscopy, is a sensitive technique for the investigation of structural details of the zeolite framework vibrations and is complementary to X-ray structure analysis. In addition, it can be used to confirm acid characteristics and isomorphous substitution. The mid-infrared spectra contains the fundamental framework vibrations of the $Si(Al)O_4$ groupings. Infrared data on the fundamental vibrations in the mid-ir (200-1300 cm^{-1}) region have been published[83-85] for many mineral and synthetic zeolites. Systematic investigations on the framework structure of zeolites A, N-A, X, Y, ZK-5, Omega, in the mid-infrared region have been reported[86]. Flanigen and Grose[87] have used the mid-infrared spectroscopy to characterise the framework of phosphate zeolites and to establish phosphorous substitution in the framework. Kutz[88] used IR spectroscopy for boron substitution into the silicate framework of the ZSM-5 type structure. Wu et al.[89] studied the decomposition of tetramethylammonium cations in Y-zeolite and observed that the absorption bands, typical of the amine near 3028, 2965, 2930 and 1480 cm^{-1} decreased and absorption bands near 3735, 3637 and 3550 cm^{-1}, typical of decationized Y, appeared on decomposition.

The bands characteristic of the hydroxyl functions in the infrared spectrum around 3000 cm^{-1} have been associated with the acidity and related to the acid activities of molecular sieves[90]. The acidic properties of OH groups in zeolites, as well as properties of Lewis and Bronsted acid centres of HZSM-5

have been extensively investigated[91-93]. The hydroxyl groups are characterized by the presence of IR absorption bands at 3600 and 3720 cm^{-1}, corresponding to strong and weak Bronsted acid sites respectively[93]. In general the framework hydroxyl vibration occur between 3660 cm^{-1} and 3600 cm^{-1}. The absorption bands in Faujasite appear at the higher wavenumbers while for ZSM-5 it appears at the lower end[94]. Structural incorporation of B, Fe or Ga in place of aluminum shifts the OH vibration to higher wavenumber, which correlates well with the resultant acidities[95].

1.6.3 NUCLEAR MAGNETIC RESONANCE SPECTROSCOPY (NMR)

The existence of discrete sites in zeolites, characterized by different environments can be detected with the help of high resolution solid state ^{27}Al and ^{29}Si n.m.r. spectroscopy. ^{29}Si n.m.r. has been used to provide information as to the number, concentration and structure of the constituent species[96-99]. Cavell et al.[100] have discussed differences in the number, nature and distribution of ^{29}Si species detectable by NMR in the solutions. A small intensity and rather broad resonance is sometimes observed at ca. 103 ppm in the high resolution solid state ^{29}Si n.m.r. spectra of ZSM-5 zeolites[101]. This resonance is due to silanol groups which are associated with the presence of defects in the zeolite lattice. The position of the ^{29}Si n.m.r. resonance was not only dependent on the number of T atoms in the first cationic coordinate sphere of Si but also on the

actual geometry of the T-O-T linkages[102]. Barrer et al.[103] studied the adsorbent-adsorbate interactions by using the ^{13}C n.m.r. technique.

Dibble et al.[104] have demonstrated the applicability of ^{27}Al n.m.r. to investigate the mechanism of zeolite precipitation. Derouane et al.[105] have studied the effect of pH and replacement of Na^+ by Cs^+, on the formation of aluminosilicate precursor species during the synthesis of ZSM-5 type zeolite. They observed that, in the absence of silicate species, TPA cations interact with aluminate anions, less so, however, in the presence of large amount of alkali cations. The application of MASNMR to characterize the zeolite structures has been published[106].

1.6.4 TEMPERATURE PROGRAMMED DESORPTION (TPD)

Temperature programmed desorption (TPD) of ammonia is commonly used to measure both acid site concentration and strength. Acidic properties of ZSM-5 type pentasil zeolites have been reported by Vadrine et al.[107,108]. Anderson et al.[109] studied TPD of ammonia on NaZSM-5, HZSM-5, and silicalite to assess the energetic distribution of sorption sites for the bases. They observed two desorption peaks for chemisorbed ammonia on HZSM-5 with maxima at about 403 and 773 K. Only 773 K peak was thought to be connected with the active sites in the methanol conversion processes. Jacobs et al.[110] studied the ammonia desorption from US-Y and ZSM-5 zeolites and observed that

both the zeolites released ammonia over a large temperature range, indicating the existence of weak, medium and strong acid sites. The amount of ammonia desorbed above 753 K clearly indicated the abundance of very strong acid sites on ZSM-5.

Topsoe et al.[93] investigated acidic properties of HZSM-5 by TPD of ammonia from fresh and partially deactivated catalysts. Three different states α, β and γ of chemi-sorbed ammonia in the range 333-373, 423-473, and 693-778 K were observed for fresh catalyst. In case of partially deactivated sample (during the reaction of methanol to hydrocarbon at 645 K) the β state was absent and α -state was strongly reduced. The activation energies for the desorption of ammonia from α, β and γ states were found to be 84.6, 96.7 and 162.3 KJ $mole^{-1}$, respectively.

1.6.5 THERMAL STABILITY OF ZEOLITES

It has been observed that the structure of zeolite either breaks down at elevated temperature resulting in the formation of amorphous phase or structural transformation occurs in some zeolites (e.g. ZSM-5) at high temperature[52,111]. The thermal stability of zeolite is an important parameter for their application as hydrocarbon/cracking reactions. The thermoanalytical data (TG, DTA) and XRD are useful in evaluating thermal stability of zeolites. The shape and temperature of DTA exotherm is ofen used in characterising the thermal stability of zeolites[112].

It is known that the thermal stability of zeolitic framework

structure increases with the silica to alumina ratio[113] and the method of thermal/acid treatment[114] or ion exchange. The structure of ZSM-5 changed from orthorhombic to monoclinic symmetry by mere calcination[111], when the SiO_2/Al_2O_3 ratio was greater than 170. The monoclinic symmetry remained unchanged by NH_4^+ ion-exchange, but the symmetry was reformed to orthorhombic in some of the specimens by protonation. The silica-alumina ratio was found to play a major role on the symmetry change of ZSM-5. Zeolite ZSM-5 possesses an exceptionally high degree of thermal and hydrothermal stability. Silicalite, the end member of ZSM-5 series is stable in air upto 1373 K and is converted slowly to amorphous silica at 1573 K[52].

1.6.6 SORPTION AND DIFFUSION STUDIES

A property that has been utilized extensively in characterizing zeolitic materials is their ability to adsorb selected molecules. Zeolites are highly porous, crystalline adsorbents with pore opening of fixed and uniform dimensions. The channels and cavities which uniformly occupy the entire volume of the adsorbent provide the essential internal surface for adsorption. The unique molecular sieving properties of the zeolites are determined by their pore dimensions. The synthetic zeolites have been characterized by their sorption capacities for various organic compounds. The molecular exclusion properties of these zeolites have been used to estimate their pore opening and shape selective properties.

Sorption of various gases and vapours on natural as well as synthetic zeolites bave been extensively studied by Barrer and coworkers[115-117]. They estimated[118,119] various thermodynamic parameters such as entropy, heat and free energy of sorption. Sorption of various hydrocarbons on ZSM-5 pentasil zeolites have also been reported[120,121]. From the knowledge of the critical dimensions of adsorbed molecules, the channel length occupied per unit cell by adsorbates has been evaluated[120]. A theoretical channel length has been calculated for ZSM-5 zeolites, amounting to a total value of 0.88 nm for both types of channels and 0.55 nm for elliptical channels alone[120]. Anderson et al.[109] compared the sorption behaviour of some hydrocarbons with more than six carbon atoms on HZSM-5, NaZSM-5, and silicalite at 298 K and P/P_O=0.5. The lower accessibility to the inner pore structure of NaZSM-5 was attributed to the blocking of channels by the Na^+ ions. They concluded that the openings of HZSM-5 and silicalite should fall in between 0.58 nm and 0.61 nm and for NaZSM-5 between 0.43 nm and 0.56 nm. The sorption property of silicalite has also been reported by Flanigen et al.[52].

It is well-known in heterogeneous catalysis that diffusion and adsorption processes affect the overall rate of the chemical transformation at the catalytic site. Two types of diffusions have been treated extensively in describing molecular transport. These two types are Knudsen diffusion and bulk diffusion. Kundsen flow occurs when the mean free path of molecule is

comparable to the pore diameter. Such conditions are usual in gas reactions on catalysts with the pore diameters in the range of 30-1000 ^{o}A. When the mean free path is much smaller than the pore diameter, molecular collisions are more frequent than collisions with the wall. The rate of diffusion under such conditions is independent of the pore radius and is known as bulk diffusion.

Diffusion in crystalline zeolites is characterized by pore diameters which are of the same order of magnitude as the diffusing molecule. The movement of molecules in zeolite pores has aspects of both adsorption and diffusion. Meisel et al.[122], investigated the relative intracrystalline mobility of hydrocarbons in the ZSM-5 channel systems and found that n-paraffins and monomethyl paraffins diffuse more rapidly than dimethyl substituted paraffins. Activation energies for diffusion for some alkyl benzenes in sodium-ZSM-5 at 523 K and 623 K have been reported by Weisz[123]. Olson et al.[124] reported some composition-dependent properties of ZSM-5. It has been observed that the ion-exchange capacity, the catalytic activity and hydrophobicity are linearly dependent on the aluminum content in the framework.

1.7 CATALYTIC REACTIONS OVER ZEOLITES

Crystalline zeolites are outstanding heterogeneous catalysts. The use of zeolites as catalysts is based on their characteristic properties such as crystallographically well-

defined structure, high thermal and hydrothermal stability and molecular sieve action. The structural features are of special interest in the various hydrocarbon conversion reactions. Weisz and coworkers[125] showed that the locus of the catalytic activity lies within the intracrystalline pores. Recently, several reviews discussing shape selectivity in catalysis have been published[123,126-128].

Active sites in zeolite catalysts are usually acidic sites. Acid sites are introduced into Na, K-zeolites by acid treatment or ammonium exchange and deammoniation or ion exchange with multivalent cations such as alkaline or rare earth ions.

In 1960, Weisz[129], Frilette and coworkers[130] first reported molecular shape selective cracking and compared the performance of sodium and calcium X zeolites in cracking of paraffins, olefins and alkylaromatics. Since then, a large number of processes have been developed. Recently, the synthesis of shape selective zeolites of ZSM-5 type has caused a breakthrough in the field of catalysis. In a relatively short time, a large number of novel commercial processes have been developed which use ZSM-5 zeolite catalysts. Prominent among the reactions catalysed by ZSM-5 zeolites are the conversion of methanol and other oxygenated compounds to gasoline[131-133], isomerization of xylenes[134], alkylation of benzene and toluene with ethylene and methanol respectively, to produce ethyl benzene and p-xylene selectively[135,136]. Synthesis gas has been converted to aromatic hydrocarbons in the presence of

polyfunctional catalyst systems containing ZSM-5 zeolites[137,138]. Biomass products such as rubber, latex, corn oil, castor oil, jojoba oil have been converted to high quality fuel with this catalyst system[139]. Among other transformations, para-directing aromatic conversions, octane enhancement by post reforming, shape selective cracking, have been reported[140-142].

Table 1.4[123] summarises important industrial applications of shape selective catalysts.

1.8 SCOPE OF THE PRESENT WORK

EU-1, a medium pore, high-silica, zeolite is composed of unidimensional non-interpenetrating 10-ring channels with large side pockets. The presence of 10-ring channels, characteristic of medium pore zeolites together with large side pockets, makes this zeolite interesting from the point of view of shape selective catalysis.

The objective of the present investigation was the synthesis and characterisation of high silica EU-1 zeolites, wherein the SiO_2/Al_2O_3 is greater than 120, using a mixture of benzyldimethylamine (BDMA) and benzyl chloride as the templating agents. The scope of the present study includes the following aspects:

1. Hydrothermal synthesis of high silica EU-1 zeolite with different Si/Al ratios and isomorphous substitution of Fe^{+3} in place of Al^{+3}, in the EU-1 framework.

Table 1.4. INDUSTRIAL PROCESSES BASED ON SHAPE SELECTIVE ZEOLITES*

Process	Objective	Major chemical process characterisation
Selectoforming	Octane number is increased in gasoline LPG production	Selective n-paraffin cracking
M-forming	High yield, Octane number increase in gasoline	cracking depending on degree of branching aromatic alkylation and cracking fragments
Dewaxing	Light fuel from heavy fuel oil, Lube oil with low temperature pour point	cracking of high molecular weight, n-monomethyl paraffins
Xylene isomerisation	High yield of p-xylene product	High throughput, long cycle life, suppression of side reaction
Ethyl benzene	High yield of EB eliminating $AlCl_3$ handling	
Toluene disproportionation	Benzene and xylenes from toluene	
Methanol to gasoline	Methanol (from coal or natural gas) conversion to high grade gasoline	Synthesis of hydrocarbons only, restricted to gasoline range (C_4 to C_{10}) including aromatics

*. Ref. 123

2. The use of a mixture of benzyldimethylamine and benzyl chloride in-situ as well as dibenzyldimethylammonium chloride $(DBDM)^+$ during hydrothermal synthesis of zeolite EU-1.

3. Understanding of the mechanism of EU-1 nucleation and crystallization during hydrothermal synthesis.

4. Evaluation of the sorption characteristics of EU-1 using various thermodynamic equations for isotherms and discussion of the physical state of the sorbed phases.

5. Charactersization of the shape selective catalytic properties of zeolite EU-1 in reactions of aromatic hydrocarbons and comparision of the data with those obtained using other medium pore zeolites such as ZSM-5, -22, -23, -48, for the same reactions.

CHAPTER 2

SYNTHESIS OF EU-1 ZEOLITES

CONTENTS

2.1 INTRODUCTION

Zeolites are usually prepared by using aqueous solutions of appropriate compositions at relatively low temperatures, in the range of 298 to 473 K. Under these conditions, the nature of the actual product is determined by the composition of the reaction mixture, temperature, reaction period, etc,. The synthesis conditions of important zeolites using systems such as Na_2O - Al_2O_3 - SiO_2 - H_2O have been reviewed[143-145] in detail. Because of lack of thermodynamic equilibrium there is infinite scope for modifying the reactants and physical conditions to produce new zeolites or to modify the chemical composition (SiO_2/Al_2O_3 ratio) and physical properties such as size and shape of the crystals. Reaction diagrams are often used to record the product of the synthesis[76].

Typical synthesis utilize highly unstable reactants, such as "young" co-precipitated gels, and an aqueous solution containing an alkali hydroxide at high pH. Under such conditions, the zeolite should inherit structural units, such as rings of linked AlO_4 or SiO_4 tetrahedra, with associated cations and water molecules.

A number of studies[11] have shown that the co-precipitated gel undergoes an ageing in which the bulk physical nature, and consequently intimate atomic linkages, change. After this ageing process, which presumably produces the appropriate structural units or building blocks, nucleation and growth of the zeolite is accomplished from the aqueous phases. Usually, the ageing

process is carried out at a lower temperature (298 K) than that of the crystallisation (373-573 K).

Reactions with smaller changes of entropy favour zeolites with high disorder. These zeolites with wide pores and consequent disorder among the water molecules and exchangeable cations are closer in structural properties and entropy to the highly disordered gels, and tend to form initially in preference to the compact zeolites. With increasing temperature of the synthesis, the more compact zeolites are formed because of the greater reaction rates towards true equilibrium. The yields of zeolites depend on the source of the raw materials. Changing the source of SiO_2 from sodium silicate to colloidal silica produces marked variations in the products, even for the same bulk composition and temperature.

Since it is difficult to observe the detailed atomic movement during the gel formation and crystallisation of zeolites, all theories are mostly speculative, but data on hydrated cations occurring in the zeolite structure and incorporation of various elements like phosphorous, by simultaneous co-precipitation of all components into intermediate gel, support the theories of structural inheritance during zeolite crystallisation.

2.2 SYSTEM FOR CRYSTALLISATION OF ZEOLITE EU-1

The hydrothermal syntheses of high-silica zeolites in the presence of organic cations have been extensively studied during

the last 20 years. High-silica zeolites (SiO_2/Al_2O_3 > 20) are usually prepared from systems containing sources of silica, alumina, an aqueous base and an organic molecule such as a quaternary ammonium compound or an amine. Zeolite EU-1 is a high-silica zeolite and its synthesis was first reported in 1981[18]. It has been synthesised using penta- or hexamethonium cations[18,47,146,147] or dibenzyl-dimethyl ammonium ions[148] as the templating agents. Detailed kinetic studies of the nucleation and crystallisation of EU-1 from systems containing dicationic methonium ions are reported[47,146,147]. There are many intriguing features in the synthesis of EU-1, using templates with such diverse cross-sections and charge densities as penta/hexmethonium and dibenzyl dimethylammonium cations (the former carries a charge of +2 while the latter is singly charged). Dodwell et al.[147] reported that while EU-1 crystallized from SiO_2/Al_2O_3 ratios of 120 and lower, mixtures of EU-1 and EU-2(identical to ZSM-48) crystallized from ratios between 120 and 240, and pure EU-2 crystallized from ratio 240 and higher when using systems containing dicationic hexamethonium ions. Casci et al.[146] also reported similar results when using dicationic methonium ions as templates. In fact, they reported[146] that the formation of mixtures of EU-1 and EU-2 even at a SiO_2/Al_2O_3 ratio of 120. The system for crystallisation of EU-1 zeolite is,

$$M_{2/n}O\text{-}Q\text{-}Al_2O_3\text{-}SiO_2\text{-}H_2O$$

where M is the alkali metal cation of valence n. Q is either

monovalent or divalent N-containing organic cation such as a quaternary ammonium compound or an amine.

Zeolite EU-1 is conventionally formed as an aluminosilicate. The composition can be prepared by utilizing materials which supply the appropriate oxides. Such compositions include for an aluminosilicate, sodium aluminate/ aluminium salts/ alumina, sodium silicate/ silica hydrosol/ silica gel/ silicic acid, sodium hydroxide and quaternary ammonium compounds / amines.

In this chapter, factors influencing the synthesis of high silica EU-1 zeolite using mixed benzyldimethyl amine (BDMA) and benzyl chloride as templating molecule have been investigated. The kinetic features of the crystallisation process, such as the influence of time, temperature, ageing of the precursor species, etc., are also studied. A synthesis procedure for the isomorphous substitution of Fe^{+3} in place of Al^{+3} in the zeolite framework is also described.

2.3. EXPERIMENTAL

2.3.1. SYNTHESIS OF ZEOLITE Al-EU-1 SYSTEM

Synthesis runs were carried out for the Al-EU-1 system at various temperatures, in a 250 ml capacity stainless steel autoclave(Fig 2.1) without stirring, under autogeneous pressure.

PROCEDURE

A basic solution was prepared by dissolving appropriate amounts of sodium aluminate (CP gr. 43.6 % Al_2O_3, 39.0 % Na_2O)

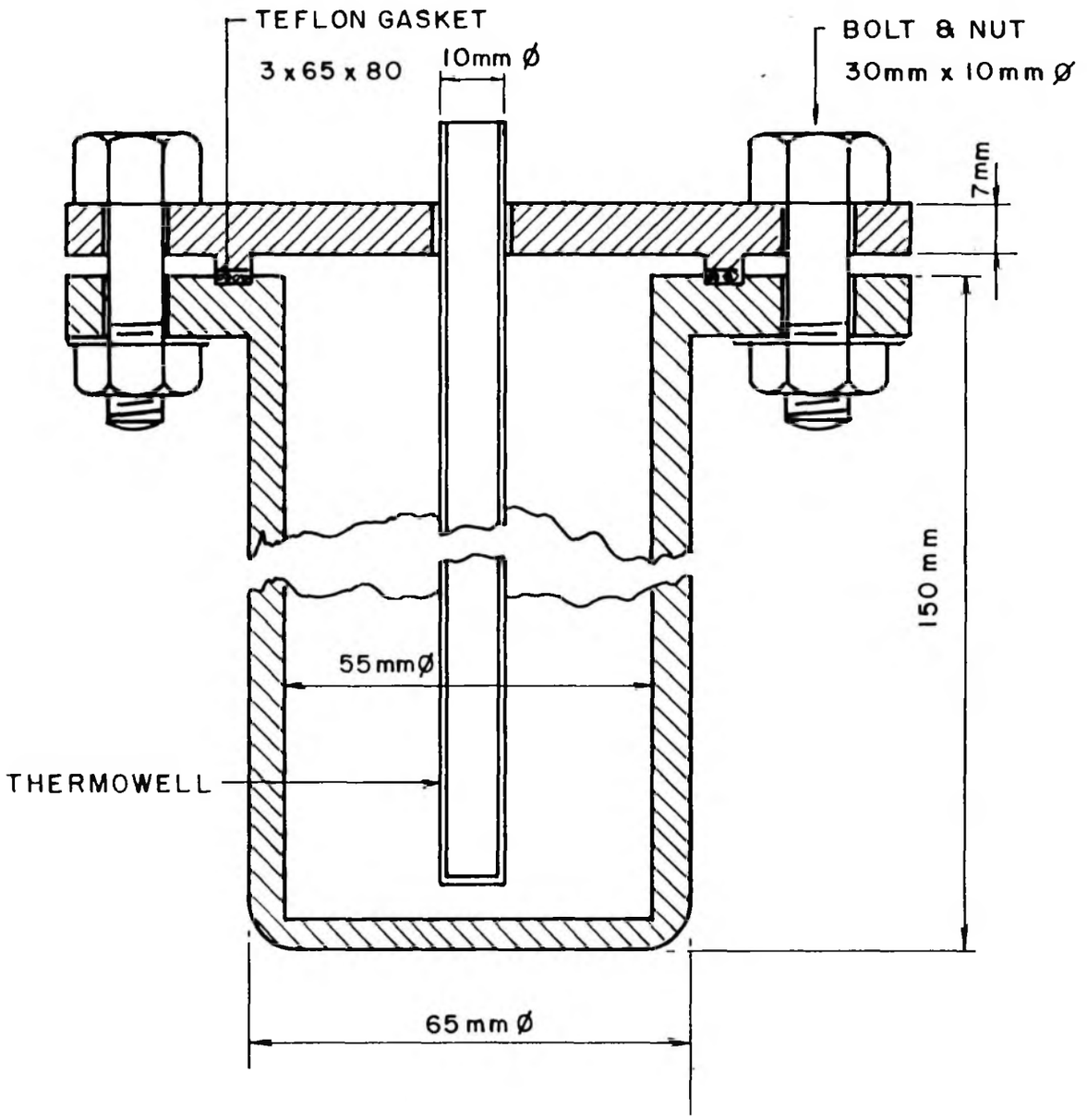

FIG. 2.1. STAINLESS-STEEL (316) AUTOCLAVE WITH TEFLON-GASKET FOR HYDROTHERMAL SYNTHESIS.

and sodium hydroxide (AR gr., 97 %) in a known quantity of distilled water. This basic solution is then added to a silica slurry (Microsil II, Leuchtstoffwerk, 95 % SiO_2) in a known quantity of distilled water. The semi-viscous gel so obtained was stirred for one hour at ambient temperature,and then equimolar quantities of liquid benzyldimethylamine(BDMA) and benzyl chloride (Fluka, 99 %) were added. This starting gel mixture (pH > 13 in all cases) was transferred to a 250 ml autoclave and heated at a controlled temperature in an air oven.

When the required temperature was attained (measured by chromel-alumel thermocouple inserted in a thermowell of the autoclave) the time was noted as the zeroeth hour. On the termination of the reaction, the autoclaves were quenched in cold-water to stop the crystallisation process. The solid products were separated by filtration, washed and dried in the air oven at 398 K.

2.3.2. FERRISILICATE ANALOG OF ZEOLITE EU-1 (Fe-EU-1)

Synthesis runs were carried out for the iron analog (Fe-EU-1) systems of different SiO_2/Fe_2O_3 ratios at constant temperature in a 250 ml capacity stainless steel autoclaves under autogeneous pressure. The crystallisations were carried out in autoclaves attached to a horizontally fitted rotating (50-60 rpm) assembly and heated to various temperatures in an electrical oven.

PROCEDURE

Two separate solutions of silicate and iron nitrate [$Fe(NO_3)_3.9H_2O$] were made by adding appropriate amounts of sodium silicate (SiO_2 28.0 %, Na_2O 8.4 % and H_2O 63.6 %) and iron nitrate (AR, BDH) to a known volume of distilled water. The iron-nitrate solution is acidified(upto 0.1 pH) with a known amount of 98 % sulphuric acid. Both the aqueous solutions were mixed under stirring, by adding the silicate solution, dropwise, to the acidified iron nitrate solution. An aqueous solution of hexamethonium bromide was prepared by taking appropriate amounts of solid hexamethonium bromide (HM-Br, Aldrich) in a known volume of distilled water. This HM-Br solution was then added to the above mixture while stirring.

The final gel mix was continuously stirred for half an hour at room temperature before charging it into the stainless steel autoclave. The autoclave was then heated in the electric oven. When the reaction (crystallisation) was terminated the solid crystalline product was separated and treated in an analogous manner to the Al-EU-1 system for further studies.

2.4. CHARACTERIZATION

2.4.1. X-RAY DIFFRACTION

The synthesized samples obtained at different time of crystallisation for Al-EU-1 system as well as various SiO_2/Fe_2O_3 ratio samples of Fe-EU-1 system were analysed by the X-ray powder diffraction method for quantitative phase identification. A

Philips X-ray diffractometer, (Model PW 1730, Ni filtered CuK_{α} radiation (1.5405 A^{o}) was used for the analysis of the samples. The degree of the crystallinity of the samples was estimated by measuring the total intensity of the characteristic diffraction peaks occurring at 2θ values between 18-24°, 100 % crystallinity being arbitrarily assigned to the most crystalline material obtained during the kinetic study.

$$\% \text{ crystallisation} = \frac{\text{Peak area between } 2\theta=18\text{-}24^{o} \text{ of the product}}{\text{Peak area between } 2\theta=18\text{-}24^{o} \text{ of the selected 100 \% crystalline sample}} \times 100$$

2.4.2. INFRARED SPECTROSCOPY

The ir-spectra were recorded in the frequency range 200-1300 cm^{-1} on a PYE UNICAM SP-300 spectrophotometer using KBr pellets and/or nujol mulls of the sample. For quantitative phase identification, a selected reference sample was used and percent crystallisation was calculated from the area under the band at 572 cm^{-1}. The extent of crystallization was estimated using the formula[149].

$$\% \text{ crystallization} = \frac{\text{Peak area of the band at } 572 \text{ cm}^{-1} \text{ of the product}}{\text{Peak area of the band at } 572 \text{ cm}^{-1} \text{ of the selected 100 \% crystalline sample}} \times 100$$

KCN was used as an internal standard.

2.4.3. THERMAL ANALYSIS

Simultaneous TG-DTA-DTG analysis of intermediate as well as fully crystalline phases were performed on an automatic derivatograph (Netsch, Model STA 490). The thermograms of the samples were recorded under the following conditions.

Weight of the sample -- 50 mg

Heating rate -- 10 K min^{-1}

Sensitivity:

TG -- 25 mg

DTA -- 0.1 mV

DTG -- 0.2 mV

Atmosphere -- Flowing air

Preheated and finely powdered alumina was used as a reference material.

2.4.4. SCANNING ELECTRON MICROSCOPY

The morphology of Al and Fe-EU-1 zeolites and representative intermediate phases was investigated using scanning electron microscope, (Sterioscan Model 150 Cambridge, U.K.). The samples were dusted on aluminium pegs and coated with an Au-Pd evaporated film.

2.4.5. CHEMICAL ANALYSIS

A known quantity of zeolite sample was heated to a high temperature in a platinum crucible for 6 hours to constant weight. This ignited solid powder was treated with 25 % hydrofluoric acid and evaporated to dryness. The HF treatment was repeated three times. From the loss in weight silica was estimated. The residue was fused in potassium pyrosulfate and dissolved in hot water. This solution was used for the estimation of sodium,aluminium and iron by atomic absorption spectroscopy. The results are tabulated for both -Al and Fe-EU-1 system in Table 3.1., chapter III.

2.4.6. ^{13}C-CP MASNMR

The ^{13}C-CP MASNMR of the as synthesised form of the zeolite was recorded with a Bruker MSL-300 NMR spectrometer at 298 K. The chemical shifts were given in ppm with respect to external tetramethylsilane. The contact time was 3 ms and the pulse delay was 3 seconds. 600-8000 FIDs were accumulated before Fourier transformation. For reasons of experimental convenience the

spinning frequency was kept at 2.5-2.8 KHz.

2.4.7. ELECTRON PARAMAGNETIC RESONANCE SPECTROSCOPY (EPR)

The EPR spectra of polycrystalline Fe-EU-1 samples were recorded on Brucker E.R. 100D spectrometer, at room temperature (298 K). The spectrometer was operated at X-band microwave frequencyy (9.6 GHz) and calibrated with diphenyl picryl hydrazine (DPPH).

2.4.8. X-RAY PHOTOELECTRON SPECTROSCOPY

The XPS spectra of Fe-EU-1 samples were recorded on an ESCA-3-MK-II Vacuum Generator (VG) spectrometer. The exciting radiation was MgK_{α} with an energy of 1253.6 eV. The spectral resolution of the analyzer was 1.0 eV. The spectra were recorded at room temperature under a vacuum of 10^{-8} to 10^{-9} torr. A binding energy of 284.4 eV for C_{1s}(carbon) level was used as an internal standard for all samples. The accuracy of binding energy as determined with respect to this standard value was within $\pm$ 0.2 eV.

2.5. RESULTS AND DISCUSSION

The synthesis runs were carried out using equimolar mixtures of benzyldimethylamine (BDMA) and benzyl chloride in case of Al-EU-1 and hexamethonium bromide for Fe-EU-1 system as the templating agents. The molar compositions of the reaction mixture used for synthesis are given in Table 2.1.

Table 2.1. COMPOSITION OF THE REACTION MIXTURES

SiO_2/Al_2O_3 (SiO_2/Fe_2O_3)	Q^+/SiO_2* (R^+/SiO_2)**	Na_2O/SiO_2	OH^-/H_2O
70	0.0935	0.058	0.011
(60)	(0.103)	(0.299)	(0.008)
150	0.0935	0.058	0.011
(100)	(0.103)	(0.299)	(0.008)
300	0.0935	0.058	0.011
(140)	(0.103)	(0.299)	(0.008)
600	0.0935	0.058	0.011

* Q^+= Dibenzyldimethylammonium cation $(DBDM)^+$.

** R^+= Hexamethonium cation.

Bracketed numbers refer to the Fe-EU-1 system.

TABLE 2.2. XRD PATTERN OF AS-SYNTHESISED EU-1.

Al-EU-1		Fe-EU-1	
d(A^o)	I/I_o %	d (A^o)	I/I_o %
11.04	30.6	11.12	34.0
10.15	16.3	10.18	26.0
9.70	10.0	9.75	13.0
7.66	7.0	7.70	9.4
6.85	6.0	6.90	8.6
5.78	7.0	5.80	10.8
5.60	7.0	5.65	10.8
4.64	36.7	4.70	41.3
4.30	100.0	4.39	100.0
3.99	61.0	4.00	65.0
3.81	35.0	3.82	42.3
3.68	28.0	3.70	32.6
3.43	16.3	3.45	30.0
3.36	22.4	3.40	25.3
3.28	44.0	3.30	41.3
3.24	24.0	3.28	28.9
3.14	10.0	3.18	13.0
3.08	8.0	3.10	10.0
2.95	10.0	2.95	11.6
2.69	6.0	2.71	8.6
2.64	5.0	2.66	7.2
2.62	5.0	2.62	7.2
2.53	11.5	2.55	13.0
2.40	10.0	2.40	10.1
2.31	6.0	2.33	8.7
2.29	4.0	2.30	7.2

The X-ray diffraction pattern of the crystalline products is shown in Fig 2.2. The peak height I and the position of the X-ray diffraction peak as a function of 2θ, where θ is the Bragg angle were read from the spectrometer chart. From these, following observations were made, 1) the relative intensities (I/I_o X 100), in which I and I_o are the heights of the strongest line or peak of the sample and the reference, respectively and 2) d the observed interplanar spacings in A^o, corresponding to recorded lines. The values of interplanar spacings (d values) and

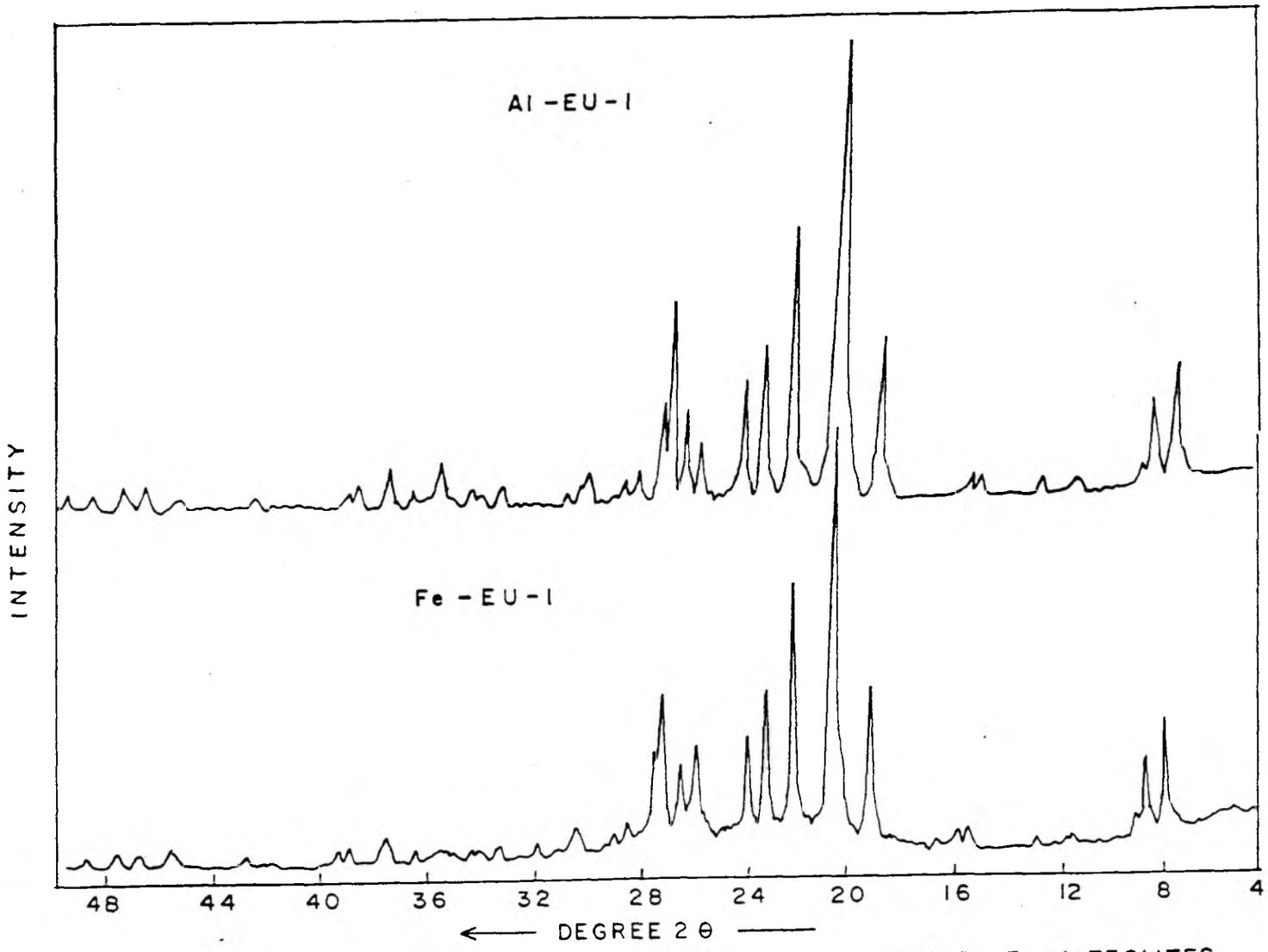

FIG. 2·2 X-RAY DIFFRACTION PATTERNS OF THE AS-SYNTHESISED EU-1 ZEOLITES

relative intensities derived from X- ray diffraction pattern for both the systems are given in Table 2.2. Both the d values and relative intensities were found to be similiar to those of the reported[146] for the Al-EU-1 system. However, in case of Fe-EU-1 system a significant shift in the interplanar (d A^{o}) spacings towards higher values have been observed. The observed shift in d (A^{o}) is consistent with the lattice expansion when Al^{+3} is replaced by Fe^{+3} in the framework[67].

2.5.1. KINETICS OF CRYSTALLISATION

The kinetics of crystallisation of zeolite Al-EU-1 was investigated in the temperature range 373-423 K, using BDMA and benzyl chloride, in-situ, as the source of organic cations. The crystallisation curves are illustrated in Fig 2.3a. In a typical example, the reactive aluminosilicate hydrogels having the molar composition,

17.5 Na_2O : 28.0 Q^+ : Al_2O_3 : 300 SiO_2 : 3200 H_2O

were used, where Q^+, represents dibenzyldimethyl ammonium, $(DBDM)^+$ formed in-situ. Fig 2.3a represents the crystallisation curves at 373 K, 398 K and 423 K for the same batch composition without hydrogel predigestion. Three different temperatures gave s-shaped growth curves, characterstic of nucleation and crystallisation stages. The curves show that the rate of zeolite crystallisation significantly depends on the temperature and indicates that during the zeolite crystallisation, the reaction temperature strongly influences the kinetics of the process.

Increasing the temperature of zeolite crystallisation, raises the solubility of the solid aluminosilicate phase and hence the composition of the liquid phase in such heterogeneous systems has a beneficial effect on crystallisation. The crystallisation curves exhibit a sigmoid nature, characteristic of the process involving two distinct stages, namely:

a) an induction period when nuclei are formed, and

b) a crystal growth period when nuclei grow into crystals.

The induction period may be defined as the time required for providing the condition for the nuclei formation rather than the time which is necessary for the growth of nuclei to a critical size[75].

Assuming that the formation of nuclei during the induction period is an energetically activated process and since nucleation is the rate determining step during the induction period, the apparent energy of activation for nucleation E_n was calculated from the temperature dependence of the rate of nucleation. The rate of nucleation has been assumed to be inversely proportional to the induction period. Temperature dependance of the rate of nucleation was expressed by an Arrhenius-type equation and the apparent activation energy for nucleation was calculated from

$$\frac{d \ln (1/\theta)}{d\ (1/T)} = \frac{-E_n}{R} \qquad \text{----------(1)}$$

where θ is the induction period, that is, the time on the crystallisation curve where conversion to the crystalline phase starts, T is the temperature (absolute) of synthesis and R the gas constant.

Similarly, E_c, the apparent activation energy for crystal growth was calculated from the temperature dependence of the rate of crystallisation and was obtained from the inflexion point on the crystallisation curves where the extent of crystallisation is 50 %. The rate equation may be represented as

$$\frac{d \ln (K)}{d (1/T)} = \frac{-E_c}{R} \qquad \text{---------- (2)}$$

where K is the point on the crystallisation (in hours), where 50 % crystallisation is complete, T the temperature (in degrees Kelvin) and R, the gas constant. Arrhenius plots of the rates of nucleation and crystallisation are shown in Fig 2.3b. The apparent activation energies for both nucleation (E_n= 26.1 kJ mole^{-1}) and crystallisation (E_n = 22.1 kJ mole^{-1}) in zeolite EU-1 formation were evaluated from the straight-line plots. Literature values of 95.4 kJ mole^{-1}, for the formation of EU-1[146] and 78.0 kJ mole^{-1}, and 45.0 kJ mole^{-1} for nucleation and crystallisation[147], respectively, reported for the systems using dipositive methonium ions as templates are substantially higher than those observed in this study. Again, Dodwell et al.[147], using hexamethonium cation as the template in the

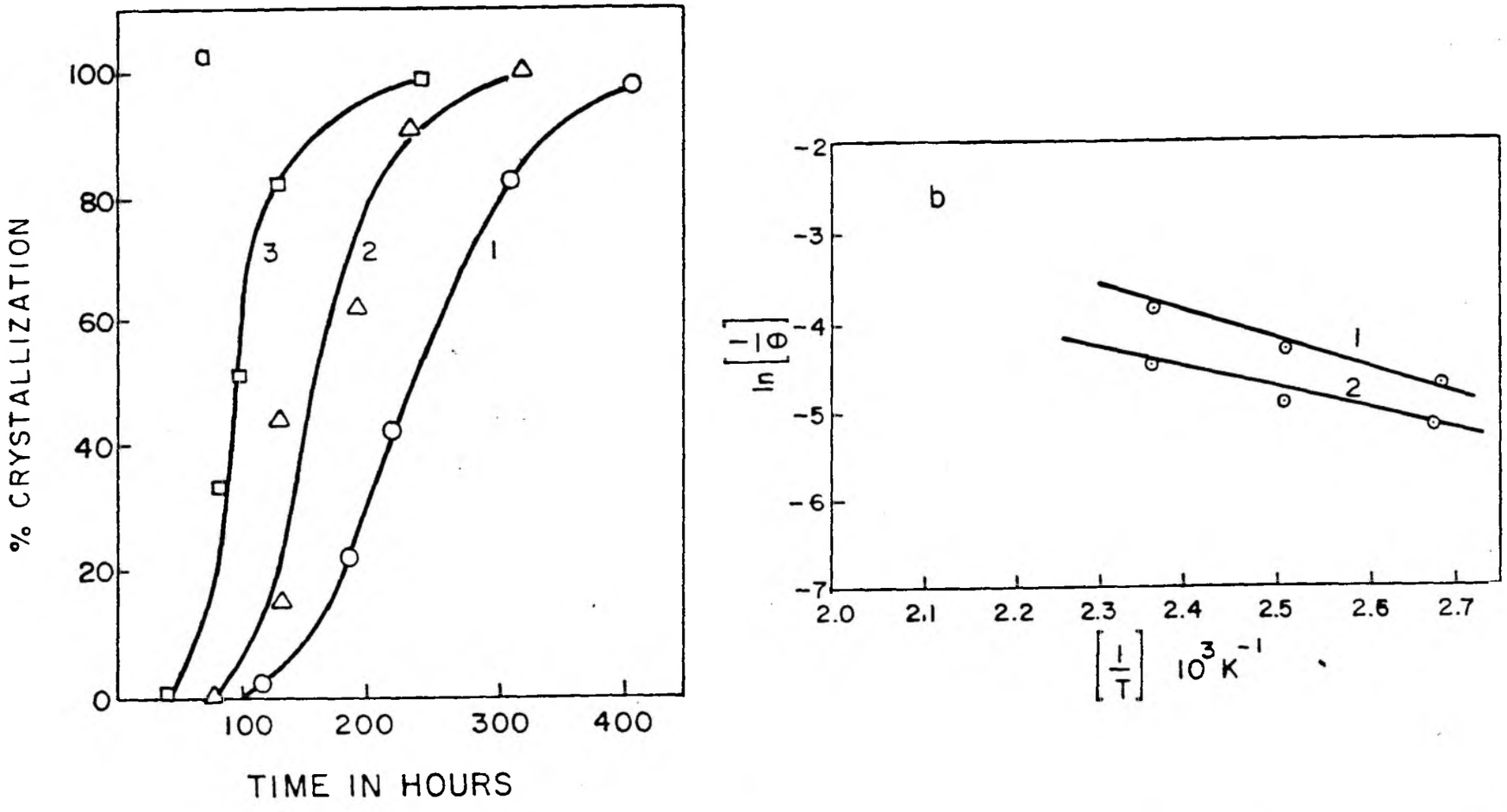

FIG. 2.3. a) CRYSTALLIZATION CURVES FOR THE ZEOLITE EU-1 AT 373, 398 AND 423 K (CURVES 1–3, RESPECTIVELY) b) ARRHENIUS PLOTS FOR (1) NUCLEATION AND (2) CRYSTALLIZATION.

synthesis of EU-1 of SiO_2/Al_2O_3 = 60, reported activation energies for crystallization and nucleation of 10.9 and 18.9 k Cal $mole^{-1}$, respectively. These diverse values underline the crucial role of the organic template and the Si/Al ratio in the kinetics of zeolite formation.

BDMA and benzyl chloride are believed to produce the halide salt of dibenzyldimethylammonium($DBDM^+$) during the hydrothermal synthesis, the latter functioning as the template in the nucleation and growth of zeolite EU-1 crystals. The ^{13}C-CP/MASNMR spectra of the as-synthesised form of EU-1 confirmed the formation of $DBDM^+$ in the zeolite (Fig 2.4). In Fig 2.4, the narrow peak around 48 ppm is due to $N-CH_3$ groups while the broad peaks at 68-73 and 130-135 ppm are assigned to the $-CH_2-$ and aromatic carbons respectively. While the similar values of the chemical shifts in curves A and B confirm the formation of $DBDM^+$ cation in the zeolite cavities, the broader line widths in curve B are indicative of the interaction of the template atoms with the intracrystalline electrostatic field.

A few trials were conducted utilising the same gel composition containing BDMA and benzyl chloride at higher synthesis temperatures i.e. at 453 K and above. The objective was to accelerate the crystallisation and reduce the synthesis time. However, it was not possible to obtain the pure EU-1 phase. The products were either amorphous or crystalline, dense phases (like quartz and crystobalite).

To check if the kinetics of zeolite formation in this system

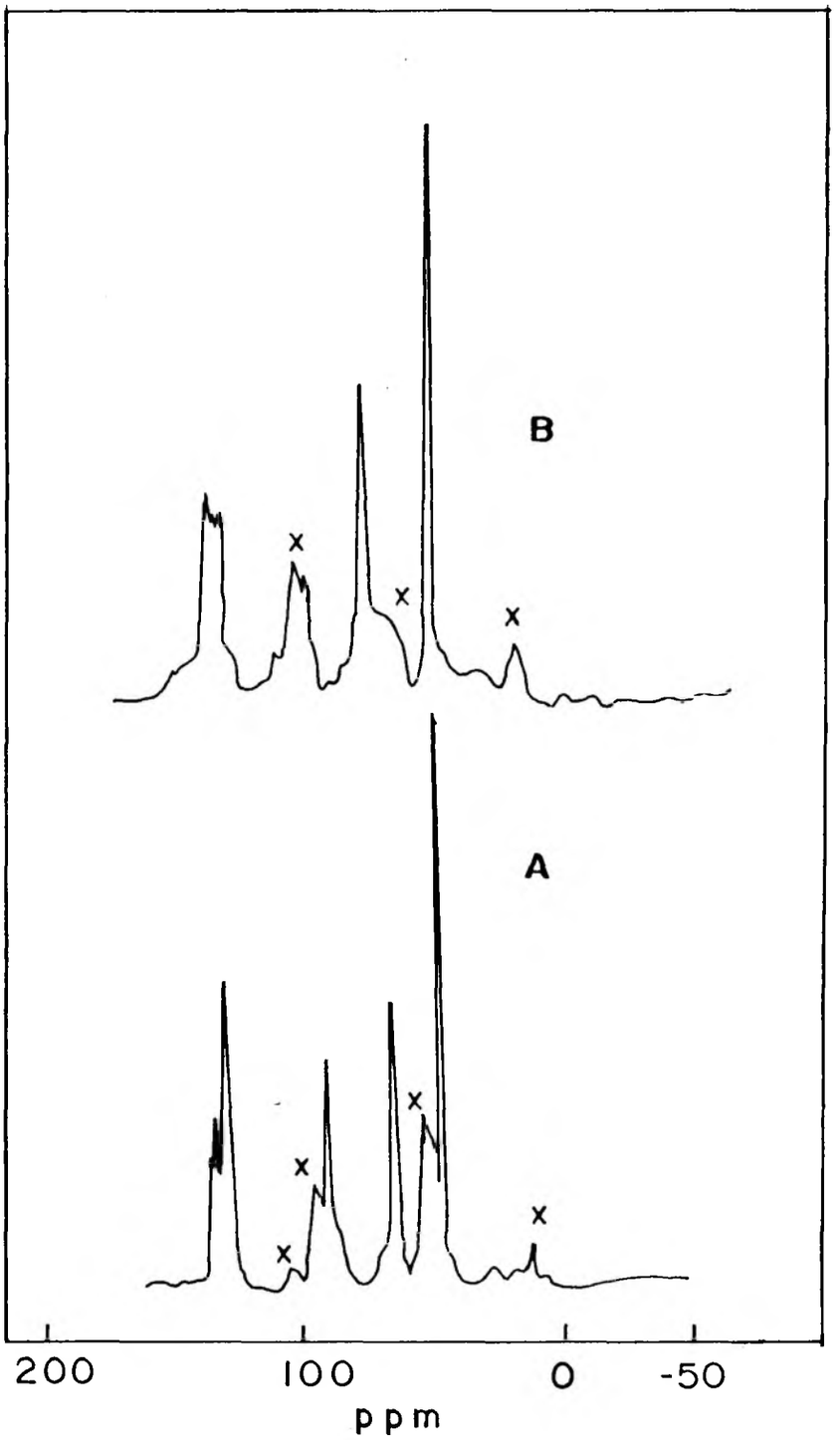

FIG. 2·4 : C^{13}- CP / MAS NMR SPECTRA OF (A) DIBENZYL DIMETHYL AMMONIUM CHLORIDE AND (B) AS-SYNTHESISED EU-1, THE SIGNALS MARKED ARE DUE TO SPINNING SIDE BANDS.

confirms the above general picture, the data of Fig 2.3a were fitted to the Avarami-Erofeev equation[150],

$$\ln [1/1-\alpha] = (kt)^m \text{ --------(3)}$$

where α and t are fractional conversion and time, respectively, and k and m are the constants. The results are shown in Fig 2.5 and values of k and m, obtained at 373, 398 and 423 K using a mixture of dimethylbenzylamine and benzyl chloride as the templating agents are given in Table 2.3.

Table 2.3.

Synthesis temp.(K)	10^2 k	m
373	3.69	4.0
398	5.56	3.68
423	8.74	3.33

From the good fit of the data, it is concluded that the kinetics of the crystallisation process can be described, at least mathematically, by the Avarami-Erofeev equation involving nucleation and growth of crystalline zeolite EU-1 phase.

2.5.2. INFLUENCE OF LOW TEMPERATURE AGEING

In order to obtain the pure EU-1 phase at higher crystallization temperatures (eg. above 453 K) a modified process involving the low temperature ageing of the gel was followed. The method comprises maintaining the reactive aluminosilicate in closed autoclaves at 398 K, for upto one or two days. The

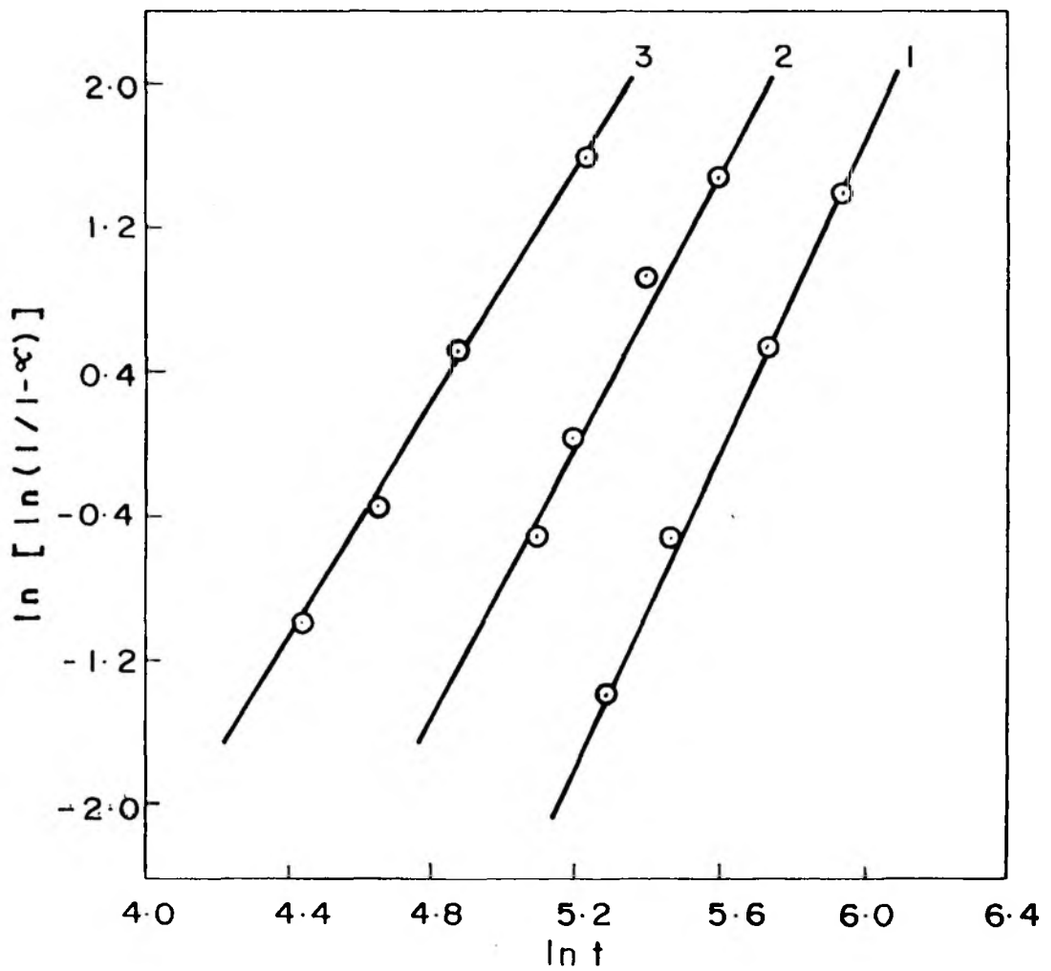

FIG. 2.5 FIT OF EXPERIMENTAL DATA TO AVARAMI - EROFEEV EQUATION AT (1) 373 K (2) 398 K (3) 423 K FOR CRYSTALLIZATION OF EU-1 WITH $SiO_2 / Al_2O_3 = 283$

temperature of the autoclave was then raised gradually, at a constant rate of heating (approximately 1 deg. min^{-1}), to 453 K or above. The growth curves obtained using this method for the same gel composition as above in the temperature range 453-473 K, are illustrated in Fig 2.6(A). It can be seen that this procedure significantly reduced the time needed to obtain highly crystalline material (compare Figures 2.3a and 2.6(A)). In addition, EU-1 crystals could be obtained without any unwanted contribution of dense phases. However, the morphology of EU-1 crystallites obtained by this method is different (scanning electron photomicrographs shown in Fig 2.7). The low temperature synthesis method produces fairly large crystallites (10 μm) having well defined cuboid shape in contrast to those obtained by ageing of the gel at low temperature (5 μm). The latter exhibits inter-layer growth developing into spherulitic shape.

It is probable that the low temperature ageing of the gel promotes the reaction between the benzyldimethylamine and the benzyl chloride to produce the template, dibenzyldimethylammonium cation. Once this template cation is produced in sufficient quantity in the hydrogel, the rate of crystallisation of EU-1 is enhanced in the higher temperature synthesis step. In order to check this hypothesis, two batches were prepared. In the first one, the dibenzyldimethylammonium chloride salt itself was added to the aluminosilicate hydrogel. In the second experiment, a mixture of the dimethylbenzylamine and benzyl chloride was added (Fig 2.6(B)). When the salt is added, even though the induction

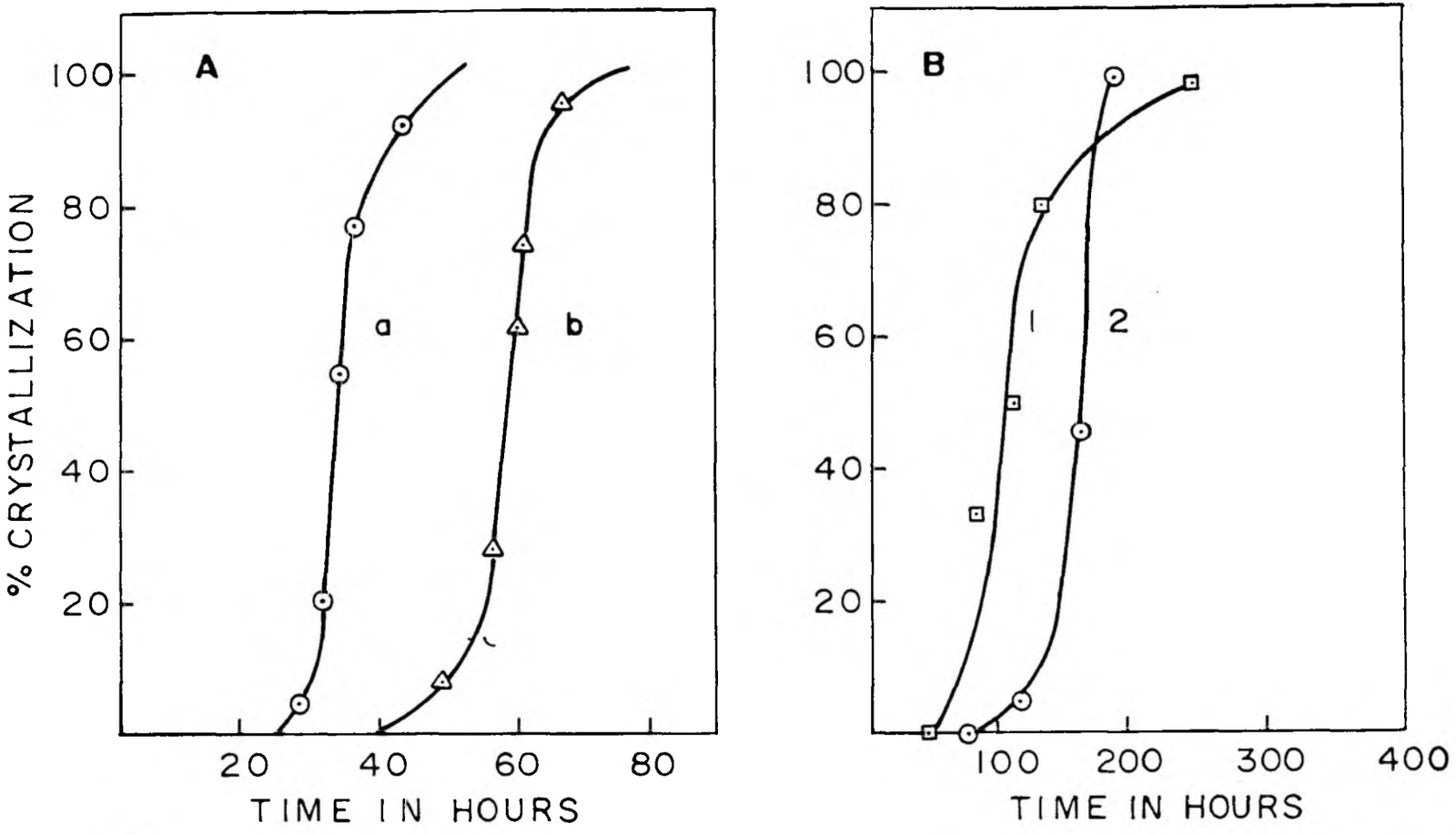

FIG 2·6. **A**) CRYSTALLIZATION CURVES FOR THE GEL PREPARED BY THE LOW TEMP. AGEING METHOD AT(a) 473 K AND(b) 453 K. **B**) INFLUENCE OF ADDING PRE SYNTHESISED TEMPLATES ON CRYSTALLISATION KINETICS (1) MIXTURE OF DIMETHYL BENZYL AMINE AND BENZYL CHLORIDE, (2) PRE SYNTHESISED DIMETHYL DIBENZYL AMMONIUM CHLORIDE SALT, AT 423 K.

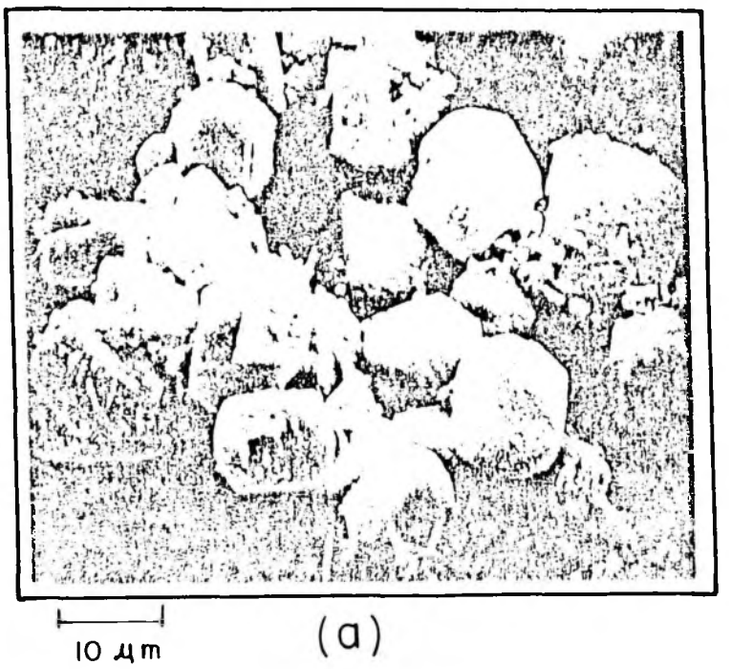

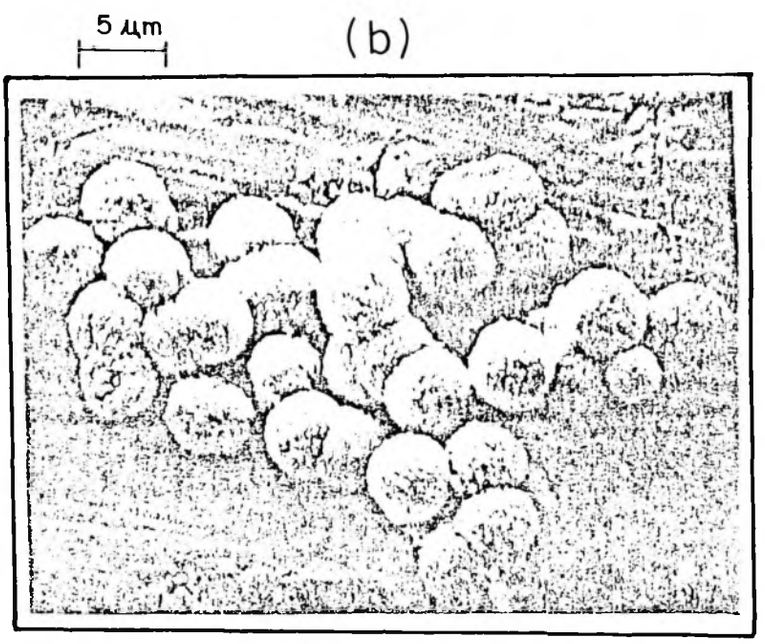

FIG. 2.7 SCANNING ELECTRON MICROGRAPHS OF EU-1 OBTAINED BY (a) THE NORMAL SYNTHESIS AND (b) THE LOW TEMPERATURE AGEING METHOD.

period is longer, the rate of crystallisation is faster. The shorter induction period observed (curve 1, Fig 2.6(b)) in the presence of a mixture of amine and benzyl chloride may be related to the mineralising action of the amine in solubilising the silica.

2.5.3. EFFECT OF SiO_2/Al_2O_3 RATIO ON THE KINETICS OF CRYSTALLISATION OF EU-1

Changing the aluminium content in the reaction mixture at 423 K shows that both the induction period as well as crystal growth strongly depend on SiO_2/Al_2O_3 ratios. Fig 2.8 illustrates the crystallisation curves at 423 K. It can be seen that the crystallisation period for EU-1 phase varies inversely with the SiO_2/Al_2O_3 ratio in the reation mixture, and it can be formed in a fairly broad range. Ghamami and Sand [151] also observed the lower rates of crystallisation at lower SiO_2/Al_2O_3 values in the ZSM-5 system. These results have been explained by the observation that a higher concentration of aluminate species in the gel or in the solution "blocks" a larger amount of silica monomers which are needed for nucleation. A smaller number of nuclei are formed resulting ultimately in lower growth rate of ZSM-5 zeolites. As growth occurs and Al gets incorporated, extra framework cations (Na^+ or organic) must be included in the zeolite. Such a requirement can also slow down the process relative to crystallisation from silicate species only. In our synthesis of EU-1 at SiO_2/Al_2O_3 below 70 or greater than 600,

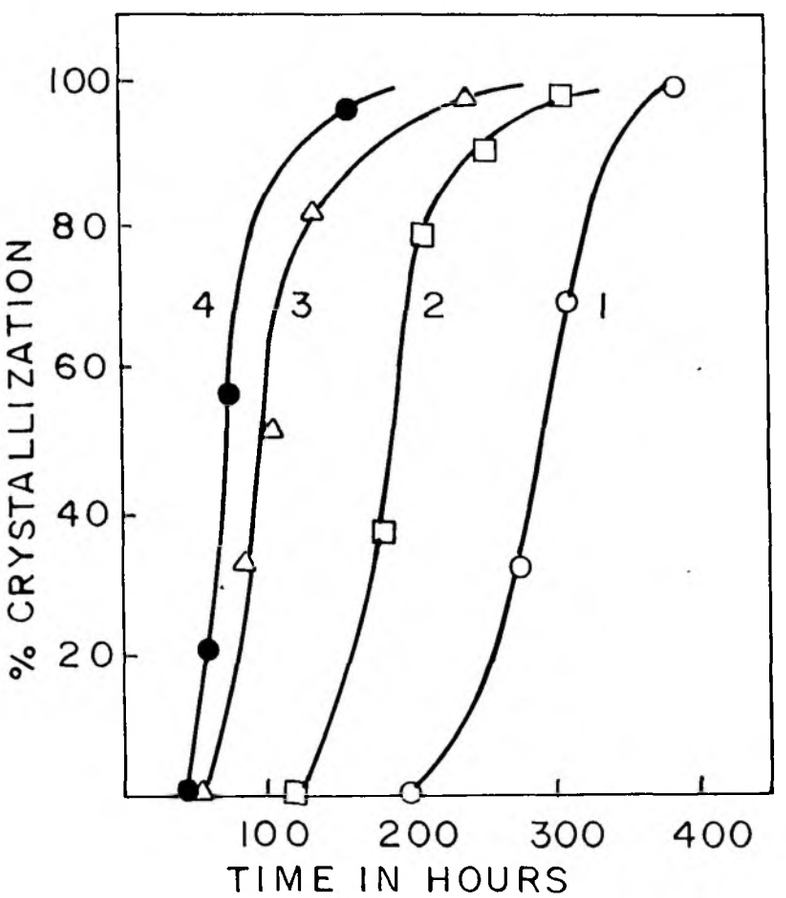

FIG. 2.8 INFLUENCE OF SiO_2/Al_2O_3 RATIO ON THE CRYSTALLISATION OF EU-1, AT 423 K. CURVES 1 AND 4 REFER TO SiO_2/Al_2O_3 MOLAR RATIOS OF 150, 250, 300 AND 600 RESPECTIVELY.

only amorphous matter was obtained.

2.5.4. EFFECT OF $(OH)^-/SiO_2$ RATIO

An increase in the $(OH)^-/SiO_2$ ratio from 0.1 to 0.15 enhances both the nucleation and crystallisation rates (Fig 2.9a). Hydrated silica was the only phase obtained outside this range. The experiments in Fig 2.9a were carried out without any low temperature ageing of the hydrogel. Under our synthesis conditions, pure EU-1 could be obtained only in a narrow range of values of $(OH)^-/SiO_2$ (0.1 - 0.15).

In the range of concentration of $(OH)^-$ of interest an increase in OH^- ions increased both the induction period and the rate of crystallisation. Now, during the synthesis reactions, the amorphous aluminosilicate gel formed initially dissolves under the influence of OH^- ions into smaller hydroxylated Al, Si and aluminosilicate species. OH^- ions accelerate this process. In the next stage, these dissolved species, in the presence of templates, like the quaternary ammonium ions, condense to form nuclei which grow into zeolite crystals. OH^- ions, when present in excess, inhibit this nucleation and crystal growth process. An optimum OH^- ion concentration, sufficient to maintain enough dissolved hydroxy species but not in such excess as to inhibit the subsequent nucleation and crystal growth, is desirable.

2.5.5. INFLUENCE OF TEMPLATE CONCENTRATION

Crystallisation of zeolite is a nucleation controlled process occuring from a molecularly inhomogeneous, aqueous aluminosilicate gel. The product is strongly dependent on the cation distribution in these mixtures. The addition of quaternary ammonium cation to a reaction mixture can induce the following effects as:

i) a different zeolite structure is formed,

ii) a zeolite crystallizes where the reaction mixture would otherwise remains amorphous indefinitely,

iii) the same zeolite is formed as without quaternary ammonium cations, but it possesses an altered chemical composition.

Unless crystallisation is markedly accelerated, only (i) and (ii) represent "template effects" attributable to the quaternary cations; (i) is by far the more common of the two effects. In the case of highly silicious molecular sieves a true "templating" or clathration mechanism pervades wherein the alkyl ammonium cations form complexes with silica via hydrogen bonding interactions. These complexes template or cause replication of the structure via a stereo-specific hydrogen bonding interaction of the quaternary ammonium cations with the framework oxygen[52a,105,152]. The concept of cation templating in zeolite synthesis has been discussed by Flanigen[153], and summarized and further developed by Rollman[154]. Thus, the concept of templating is the phenomenon occurring during either the gelation or the nucleation process whereby the organic molecule organizes

oxide tetrahedra into a particular geometric topology around itself and thus provides the initial building block for a particular structure type. Such an important role is often referred to as the structure directing role.

The nature of pentasil zeolites synthesised in specific conditions by using various tetraalkyl ammonium cations $(TAA)^+$ or corresponding trialkylamine (TAA) precursors was investigated by Gabelica et al.[155] ZSM-8, ZSM-5, ZSM-11 zeolites were obtained using tetraethyl ammonium $(TEA)^+$, tetrapropyl ammonium $(TPA)^+$ and tetrabutyl ammonium $(TBA)^+$ bromide, respectively, demonstrating the structure directing role of $(TAA)^+$ cations. EU-1, EU-2, EU-4, ZSM-23 and ZSM-39 zeolites from systems containing a range of bis-quaternary ammonium compounds of general formula $[(CH_3)_3N(CH_2)_XN(CH_3)_3]^{+2}$ were reported[47]. Zeolite EU-1 has been synthesised using penta- or hexamethonium cations[18,47,146,147] or dibenzyldimethyl ammonium[148] ions as the templating agents.

Fig 2.9b shows the influence of the concentration of the template (dibenzyldimethyl ammonium, Q^+) on the kinetics of the crystallisation of EU-1 zeolite for the reaction mixture with different Q^+/SiO_2 ratios. Below a value of (Q^+/SiO_2) of 0.046 only an amorphous phase or hydrated silica was observed. Above this value, increasing the concentration of the template enhanced the rates of both nucleation and crystallisation (Fig 2.9b). Low temperature digestion of the hydrogel was not carried out in the experiments of Fig 2.9b. Since the formation of zeolite takes

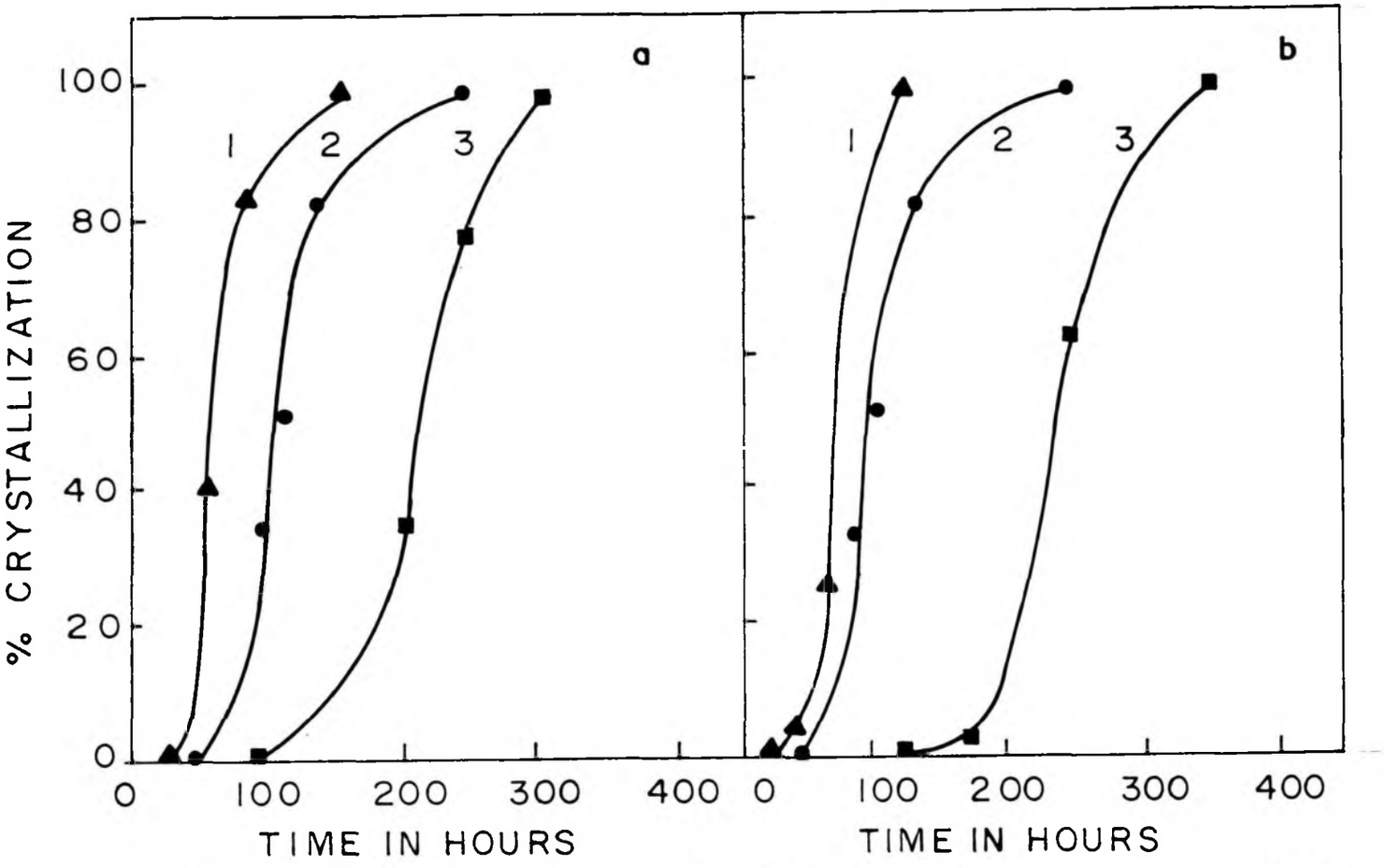

FIG. 2·9 (a) INFLUENCE OF $(OH^-)/SiO_2$ ON CRYSTALLISATION KINETICS. CURVES 1-3 REFERS TO $(OH^-)/SiO_2$ VALUES OF 0·15, 0·116, 0·11 RESPECTIVELY.
(b) INFLUENCE OF TEMPLATE CONCENTRATION, Q^+/SiO_2 = 0·135, 0·093 AND 0·046 CURVES 1-3 RESPECTIVELY AT 423 K.

place around the organic template[152], at higher concentration of organic template which provides large number of species to form nuclei, the rate of nucleation as well as the rate of crystallisation is enhanced.

2.5.6. INFRARED SPECTROSCOPY

The structure of the zeolite phase formed from the aluminosilicate was studied by infrared technique. The IR spectra in the framework region (200-1300 cm^{-1}) for a series of Al-EU-1 zeolite prepared at different synthesis time are shown in Fig 2.10. The spectra were recorded using nujol-mull technique with KCN as internal standered (reference peak at 2200 cm^{-1}). All the samples showed strong absorption band in the 1000-1200 cm^{-1} region, assigned to internal vibration of $Si(Al)O_4$ tetrahedra, which are also observed in silica and quartz[156]. Many of the other bands observed for EU-1 in the present study are similar to those in pentasil zeolites[45], especially, in the region 500-650 cm^{-1}. Bands in this region are due to vibrations related to external linkages between tetrahedra and are sensitive to the framework structure and to the presence of some secondary building unit and building block polyhedra such as double ring and large pore openings. Thus the bands at 590 and 620 cm^{-1} (Fig 2.10) are identical to those observed[45] in ZSM-5 at 590 and 620 cm^{-1}, respectively. The additional strong band at 572 cm^{-1} in EU-1 was also observed by Casci[157]. Jacobs and Martens[158] assign IR absorption bands in this region to double rings in high

silica zeolite frameworks. ZSM-12, beta, ZSM-5 and ZSM-11 exhibit this absorption at 575, 575, 570 and 570 cm^{-1}, respectively[158]. The second "finger print" region for external linkage frequencies which are sensitive to topology and building units in the zeolite framework occurs in the 300-400 cm^{-1} region. We do not observe any band in this region (Fig 2.10). Bands in this region are prominent in those structures which have cubic unit cell symmetry and decrease in prominence as the symmetry decreases[157]. The absence of absorption in this region is consistent with the orthorhombic symmetry[71] of the unit cell of EU-1. The variation in crystallinity evaluated by both X-ray diffraction and IR technique for EU-1 zeolite prepared at different synthesis times, is represented in Fig 2.11a. The absorbance of the skeletal vibration at 572 cm^{-1} was used to estimate IR crystallinity using a highly crystalline (X-ray) sample as 100 % standard. Both IR and X-ray crystallinity plots (Fig 2.11a) are sigmoid in nature indicating that nucleation and crystal growth occurs successively. The lower value of crystallinity obtained by XRD is attributed to its inability to "see" crystals smaller than 5 nm[149]. Further, the linear correlation between the two values of crystallinity is also in accordance with the above picture (Fig 2.11b). In a recent study, Jacobs et al.[149] showed that although the XRD pattern of the sample was characteristic of an amorphous material, the IR spectra show the material to be ZSM-5 zeolite with crystallite size less than 5 nm[149].

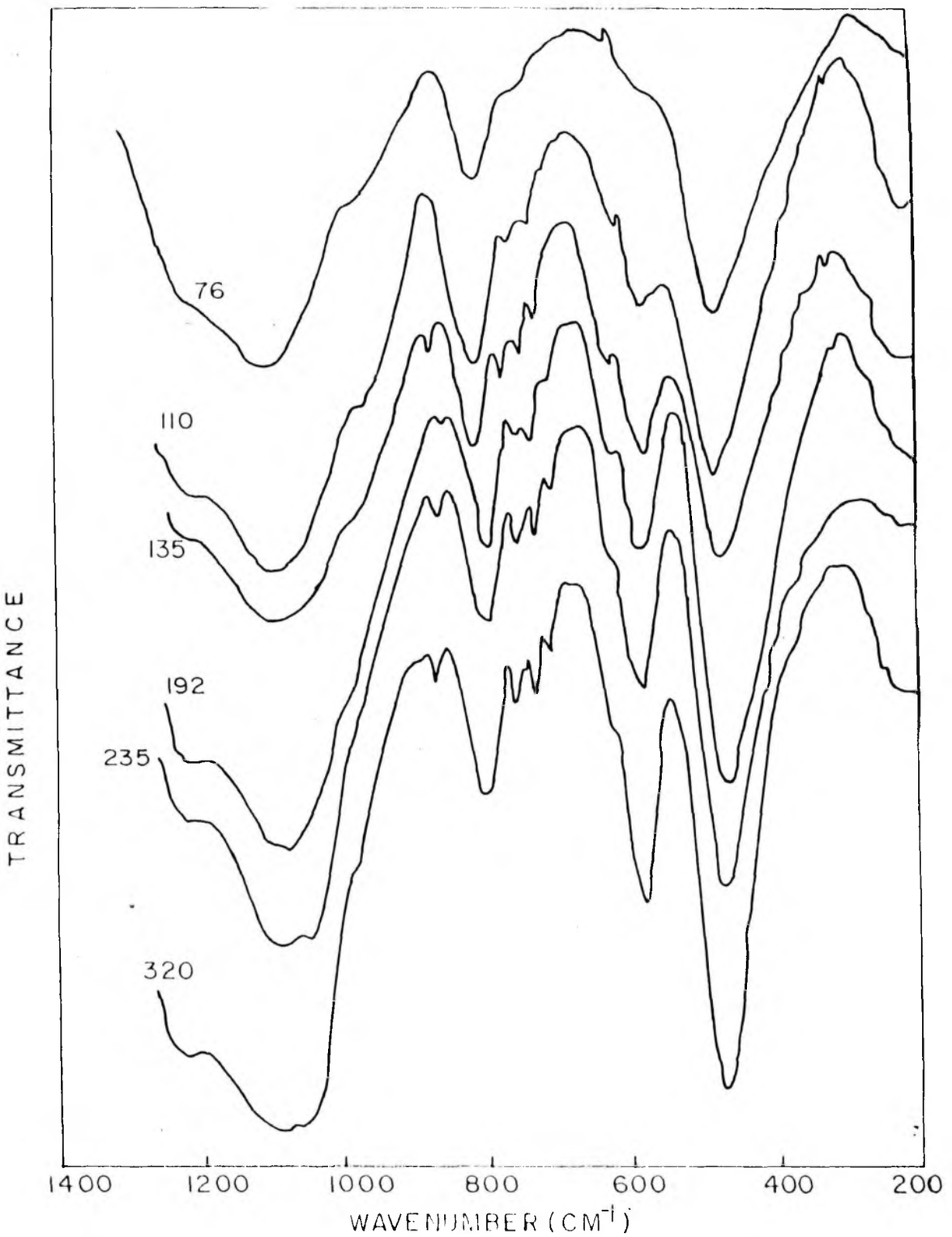

FIG. 2-10. IR SPECTRA OF Al-EU-IZFOLITES SYNTHESIZED AT T = 398 K, NUMBERS INDICATE SYNTHESIS TIME IN HOURS.

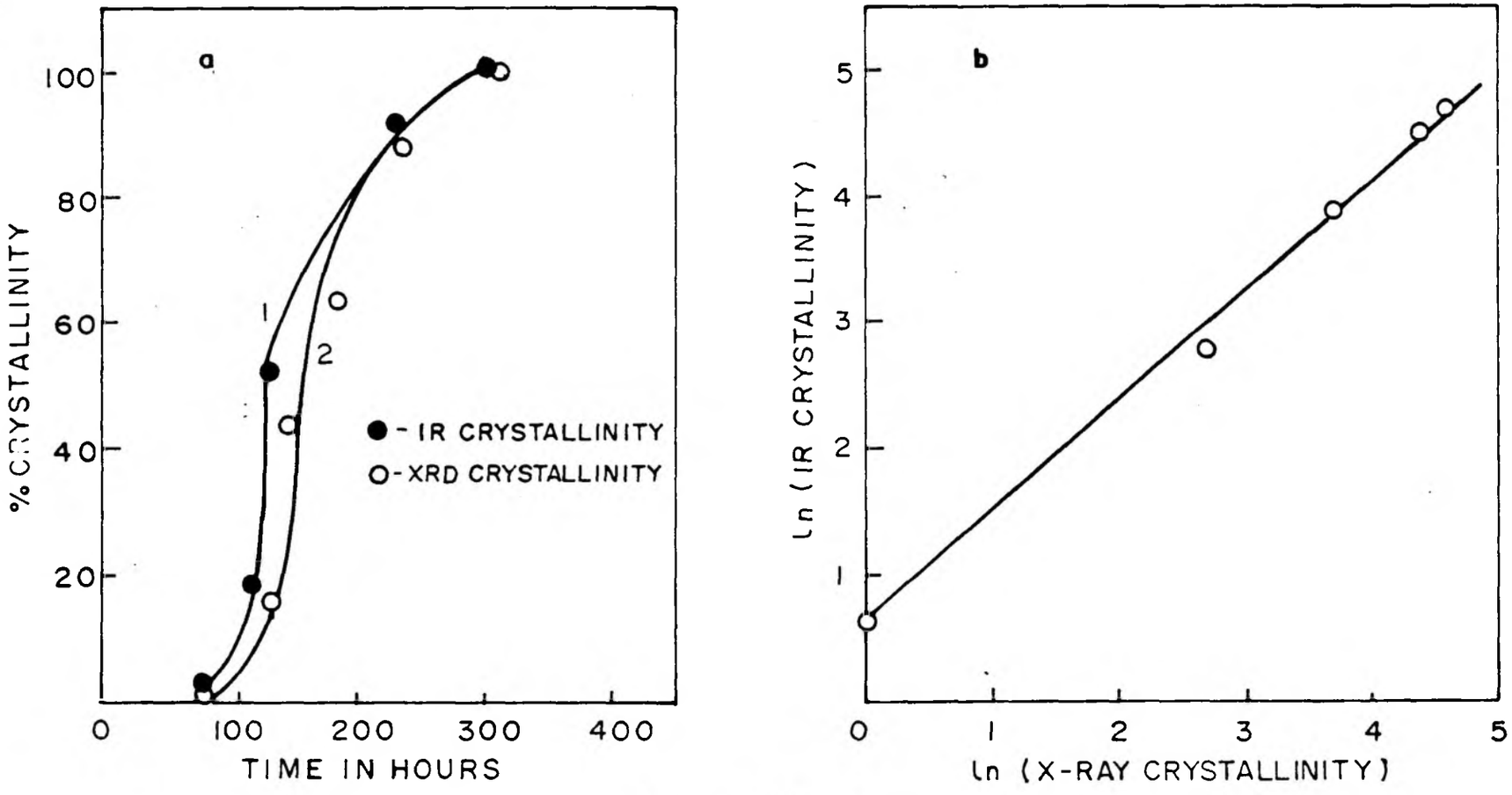

FIG. 2·11 a). CHANGE IN CRYSTALLINITY OF EU-1 WITH SYNTHESIS TIME ESTIMATED BY IR (CURVE 1) AND X-RAY DIFFRACTION (CURVE 2)
b) RELATION BETWEEN THE CRYSTALLINITY EVALUATED FROM IR AND X-RAY DIFFRACTION.

2.5.7. THERMAL ANALYSIS

The as-synthesised zeolite Al-EU-1 samples were studied by thermogravimetry. Both the weight loss and magnitude of the corresponding thermal effects are used to characterize the thermal changes. The DTA/TG patterns for amorphous and fully crystalline EU-1 zeolites are shown in Fig 2.12. The TG curve shows three distinct zones of weight loss at 353-473 473-723 and 723-1108 K, while DTA exhibits an endotherm and the two exotherms respectively. The first stage is a relatively small endothermic weight loss due to the dehydration of physically adsorbed and occluded water. The exothermic effects with maxima around 673 and 950 K are due to the oxidative decomposition of the organic template occluded in the zeolite framework. These exothermic transformations were also observed by Chao[159] and Bibby [160] et al. curve 1 indicates that the pure salt, dibenzyldimethyl ammonium chloride melts around 473 K. The higher temperature of decomposition of the organic template in the zeolite (curve 2) may be due to the decomposition of the quaternary ammonium compounds or protonated amine held in the zeolite pores[151]. The small exotherm around 1375 K is due to the collapse of the zeolite lattice and is not accompanied by any weight loss. The material partially loses its crystallinity.

The representative thermoanalytical curves for EU-1 are shown in Fig 2.13. It may be seen that the amorphous zeolite phase has a continuous weight loss in the temperature range 353-1108 K. The observed weight loss in the temperature range 353 to

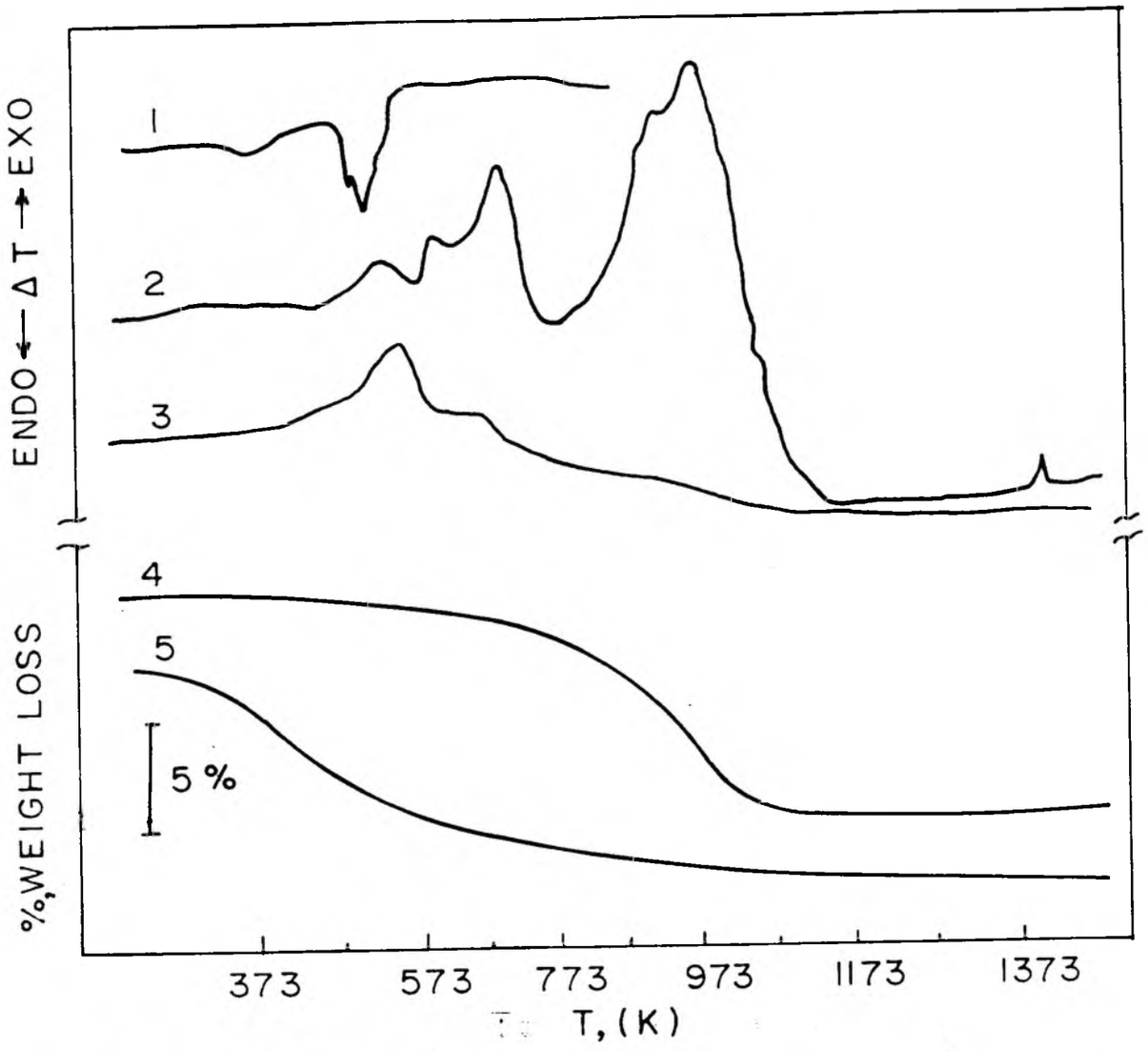

FIG.2·12. THERMO ANALYTICAL CURVES 1) DTA OF PURE DIMETHYL DIBENZYL AMMONIUM CHLORIDE. 2 AND 4, DTA, TG FOR 100% AI-EU-1 AND 3 AND 5 FOR AMORPHOUS MATERIAL RESPECTIVELY

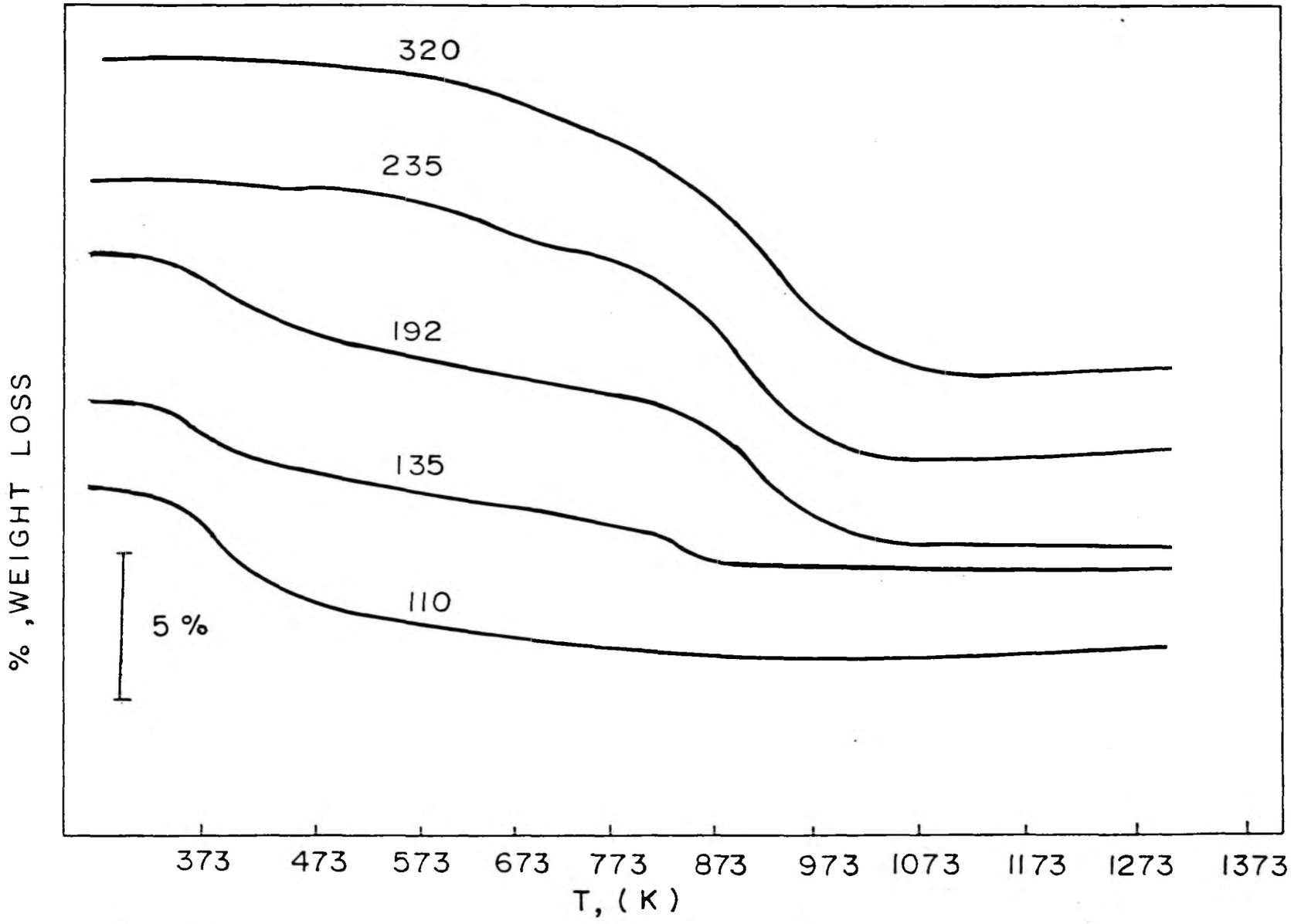

FIG. 2-13. TG CURVES FOR INTERMEDIATE PHASES, NUMBERS INDICATE SYNTHESIS TIME IN HOURS.

473 K is due to dehydration of physically adsorbed and occluded water. No major weight loss was observed above 473 K, for the amorphous materials. Table 2.4 summarizes the quantitative data for dehydration and decomposition of EU-1 zeolites.

The weight loss corresponding to decomposition of organic cation as a function of crystallinity, measured by X-ray diffraction, is plotted in Fig 2.14. Linear relations are observed, which do not pass through the origin. This may be due to the fact that the nuclei of EU-1 are probably present in amorphous gel which are not detected by X-ray diffraction on account of their smaller size (< 5 nm). From the weight loss due to decomposition of organic compound, it has been estimated that about four $DBDM^{+}$ cations are present per unit cell.

TABLE 2.4.

LOSS IN WEIGHT UPON DEHYDRATION AND DECOMPOSITION IN Al-EU-1 ZEOLITES.

% X-ray crystallinity	% Weight loss upon dehydration	% Weight loss upon decomposition
7.5	2.88	3.08
44.0	2.08	5.80
62.0	1.78	7.95
92.0	0.62	10.56
100.0	0.50	11.03

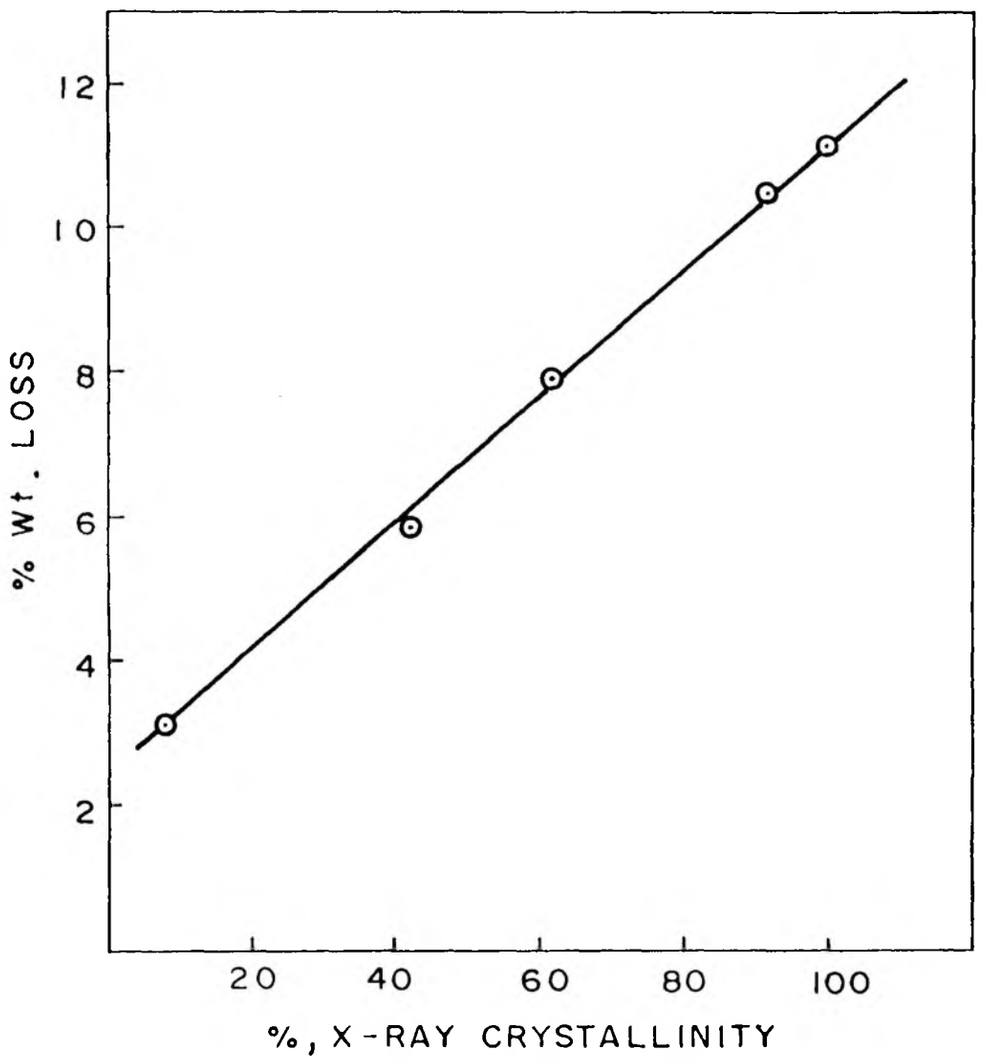

FIG. 2.14. CORRELATION BETWEEN THE WEIGHT LOSS FOR DECOMPOSITION OF $DBDM^+$ CATIONS AND X-RAY CRYSTALLINITY FOR AI-EU-1 ZEOLITE.

2.5.8. SCANNING ELECTRON MICROSCOPY

The scanning electron micrographs of EU-1 zeolites and representative phases for $DBDM^+$ synthesis system (SiO_2/Al_2O_3= 283, OH^-/H_2O = 1.1 X 10^{-2}, T = 398 K) are illustrated in Fig. 2.15. An amorphous phase is detected after 3 days (Fig. 2.15 a). Figure 2.15(b) indicates that after 7 days, both amorphous and crystalline phases coexist. However, at longer crystallisation time, the presence of crystalline aggregates (Fig 2.15c), as well as well-defined crystals are observed for 100 percent crystalline samples (Fig. 2.15d). The morphology of the crystalline Al-EU-1 product shows cuboid shape, having an inhomogeneous size distribution between 3-6 μm. However, hexamethonium salt in Fe-EU-1 system shows the marked change in the morphology (Fig 15e and 15f).

Using hexamethoniumbromide in the Al-EU-1 system Casci et al.[146] observed ellipsoidal 0.5 to 4.0μm long crystals whereas Dodwell et al.[147] reported a tenfold increase in crystal size using ammonia and hexamethoniumbromide in the gel system. The inhomogeneous size distribution with significant difference in crystal morphology observed in our samples can be attributed to the role of $DBDM^+$ cations and silica source used.

2.5.9. MECHANISM OF ZEOLITE CRYSTALLISATION

In 1937 Morey and Ingerson[161] proposed a mechanism for zeolite crystallisation involving the formation of a solid amorphous precursor which is followed by a solution

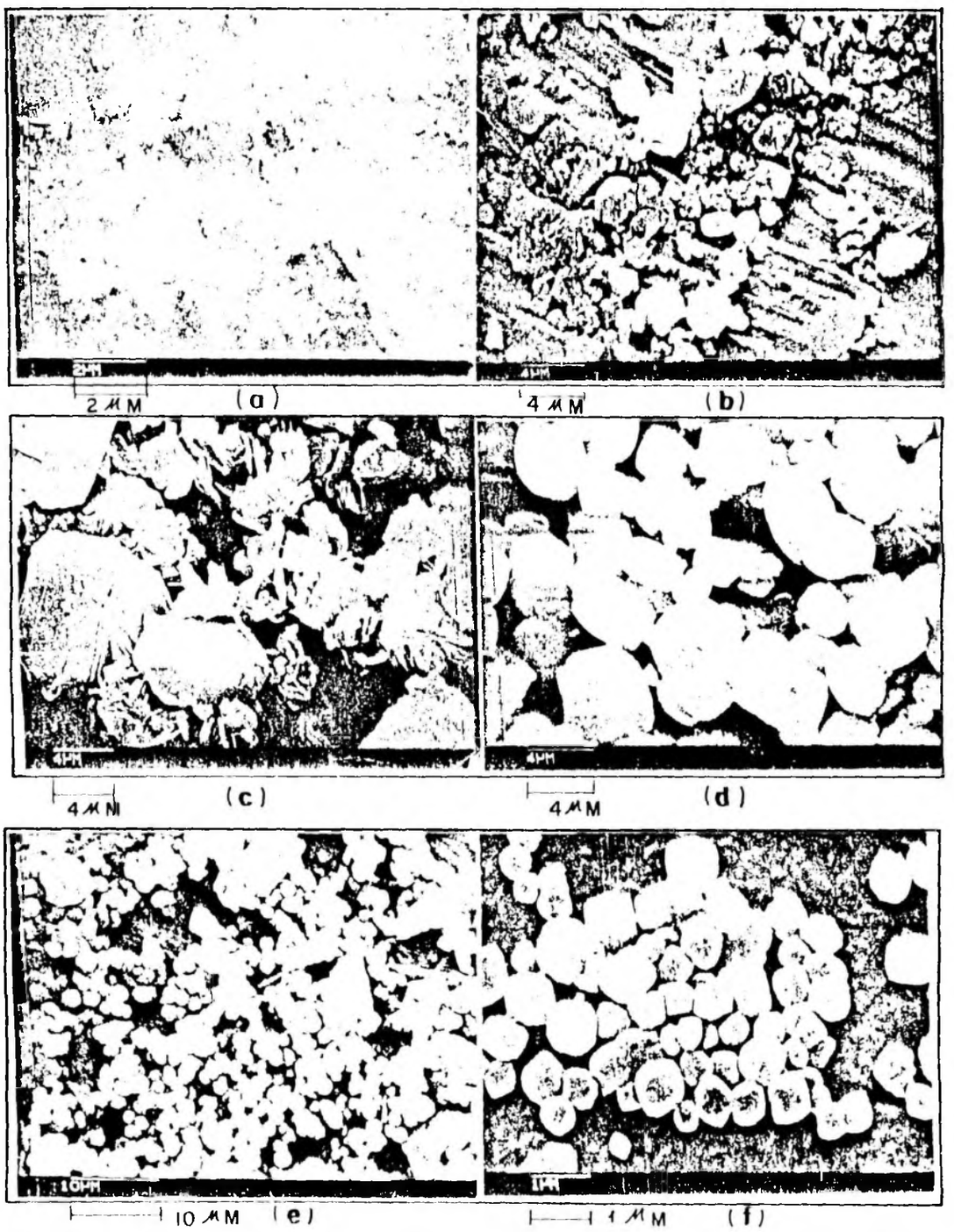

FIG. 2.15. SCANNING ELECTRON MICROGRAPHS OF EU-1 ZEOLITES (a) AMORPHOUS, (b) 40 %, (c) 65 % AND (d) 100 % CRYSTALLINE PHASES OF -Al-EU-1 (SiO_2/Al_2O_3=283) (e) AND (f) REFERS 100 % CRYSTALLINE Fe-EU-1 (SiO_2/Fe_2O_3=48)

crystallisation mechanism. Investigations of the mechanisms involved in zeolite crystallisation have received extensive attention from many investigators over the past 25 years[9,17,26,162-173]. However, many ambiguities still exist concerning the mechanism of crystallisation including those concerning the autocatalytic kinetics of the crystallisation process, the effect of alkalinity on the rate of crystallisation, the specific nature of the induction period, the effect of seeding on reaction rate, and the effect of clathrating or templating cations[9,17,26,165,172-176]. Two mecanisms of crystallisation of zeolites have been proposed. One supports the concept that zeolite crystallisation occurs in the liquid phase. The second postulates that zeolite crystallisation occur predominantly in the solid phase of the gel through an ordering of the aluminosilicate network. Khatami and Flanigen[26] observed the crystallisation of zeolite X in the absence of a liquid phase. Culfaz and Sand[177] proposed a mechanism wherein nucleation occurs at the solid liquid interface. In this mechanism it is proposed that nucleation, mass transfer of species by surface diffusion, and zeolite crystallisation occure in a boundary layer at the solid liquid interface. Support of this surface nucleation mechanism was given by Kerr[178] through the epitaxial growth which he observed in the co-crystallisation of zeolite L, offretite and erionite. The main supporting evidence suggesting that zeolites form without the participation of the liquid phase are those experiments wherein zeolite

formation occurred subsequent to the removal of a considerable part of the liquid phase. Equilibrium between solid and liquid phases of gels is, however, independent of the volume of solution[172]. Removal of a substantial quantity of the liquid phase will not lead to a change in the equilibrium and should not, therefore, have influence on the crystallisation processes of such gels[172]. Even in situations where zeolites were found to crystallize from physically dry, free-flowing powders[26] it is conceivable that the condensation polymerization reaction itself contributed sufficient water to the system to produce a new aqueous boundary layer. The formation of zeolites at this boundary layer is consistent with the mechanism proposed by Culfaz and Sand[177].

2.6. FERRISILICATE ANALOG OF EU-1 SYSTEM

All samples of the Fe-EU-1 zeolites synthesised by the methods described under section 2.3.2 and Table 2.1 are white and highly crystalline based on X-ray diffraction and n-hexane adsorption studies.

2.6. PHYSICO-CHEMICAL CHARACTERIZATION

2.6.1. THERMAL ANALYSIS

The DTA and TG curves for Fe-EU-1 (as-synthesised form, SiO_2/Fe_2O_3 = 48) are shown in Fig 2.16. DTA shows endothermic peak in the temperature range 298 to 473 K, and exothermic peaks in the temperature range 533 K to 884 K. The endothermic peak is

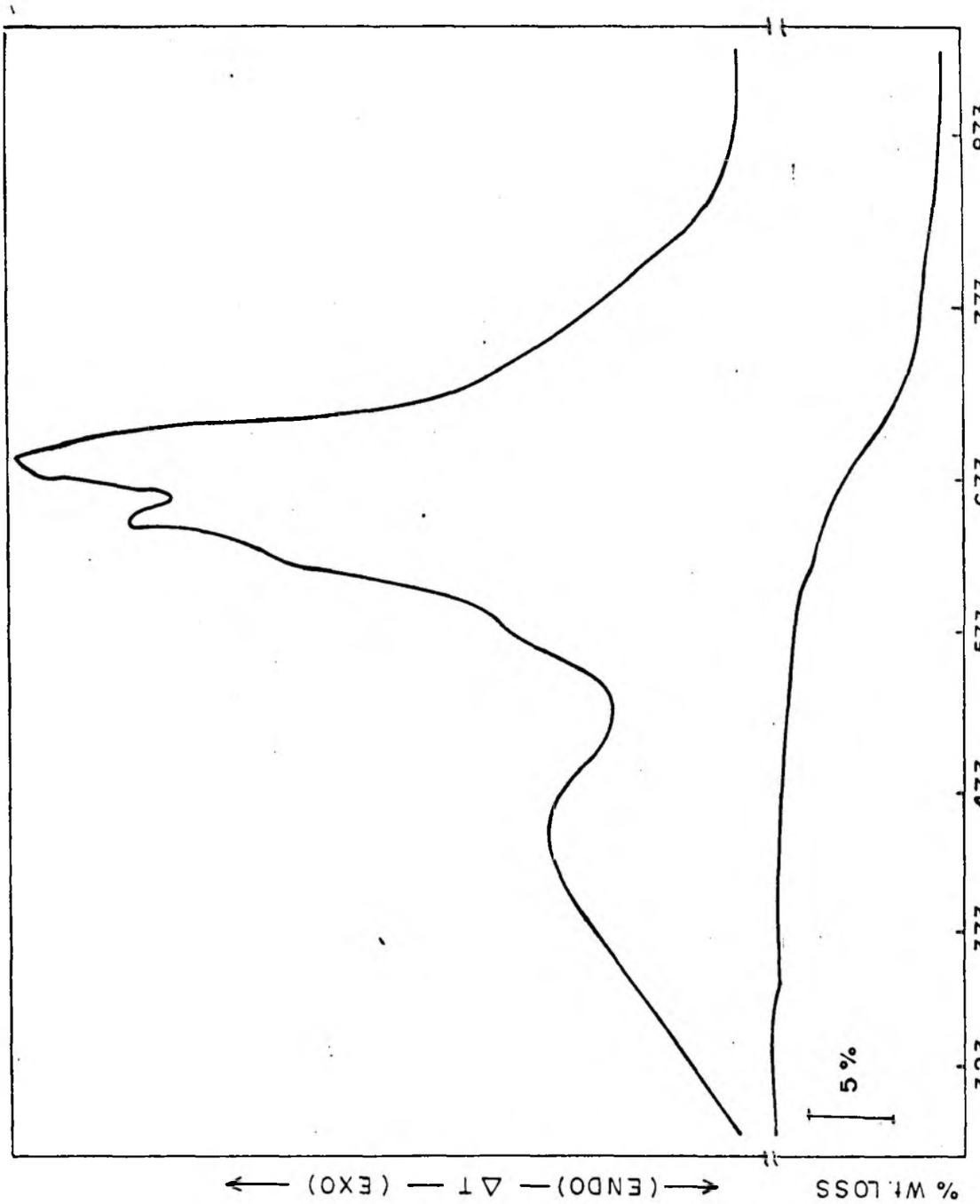

FIG. 2·16. DTA/TG THERMOGRAMS OF Fe-EU-1.

due to the dehydration of physically sorbed or occluded water within the zeolitic framework, while the exothermic peak is due to the decomposition of hexamethonium cations. For more iron-rich samples (SiO_2/Fe_2O_3 = 48 and 78), upon calcination it is observed that iron is being partly removed from the framework: The samples develop an off white colour.

2.6.2. INFRARED SPECTROSCOPY

The infrared spectra of ferrisilicates in the mid-infrared region (1300-200 cm^{-1}) were used to establish substitution of Fe^{+3} ions in the zeolite framework. The ir spectra of ferrisilicate, silicalite and a sample containing 4.0 % Fe_2O_3 impregnated on silicalite, are shown in Fig 2.17. The last sample was prepared by adding an aqueous solution of $Fe(NO_3)_3$ to silicalite, followed by drying and calcination.

The most intense absorption band which occurs at around 1100 cm^{-1} is related to the asymmetric stretching vibrations of T-O bond. This band is shifted to lower frequency for ferrisilicate (Fe-EU-1) as compared to silicalite and 4 % Fe_2O_3 impregnated silicalite samples. The shift in frequency can be explained on the basis of T-O bond distances. Substitution of Al for Si in the framework causes a shift to lower frequency owing to longer Al-O bond distance (1.75 A^o) as compared to Si-O bond distance (1.60 A^o). A substitution of phosphorous in the zeolite framework[87] shifts the main asymmetric stretching vibration band towards higher frequency because of shorter tetrahedral P-O bond distance (1.54 A^o). On substitution of iron in the zeolite framework, due

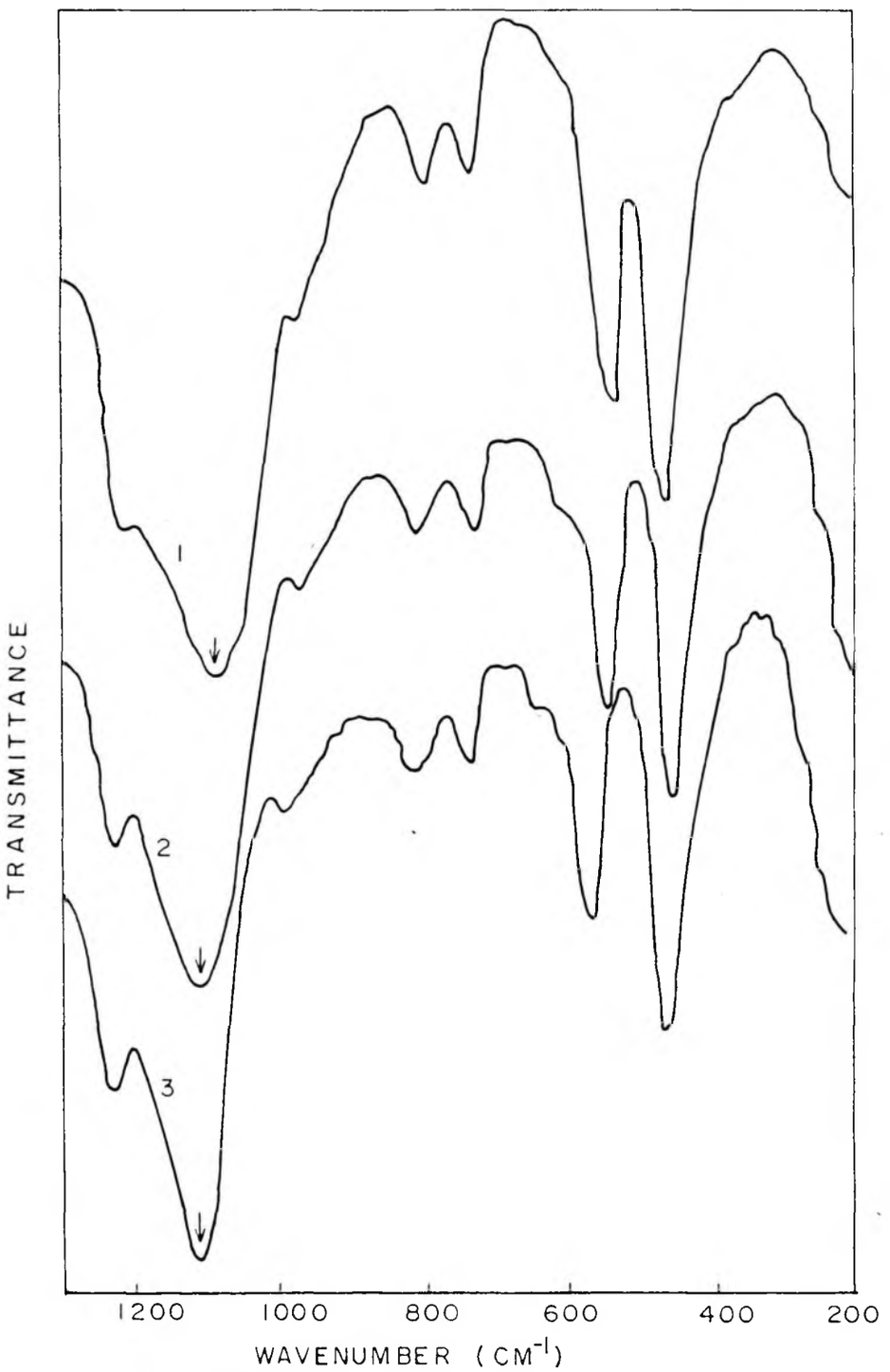

FIG. 2·17. INFRARED SPECTRA OF 1) Fe-EU-1
2) Fe_2O_3 + SILICALITE 3) SILICALITE

to the longer Fe-O bond distance (1.97 A^{o}) the 1100 cm^{-1} band should shift towards the lower frequency as indeed seen in Fig. 2.17. This is also consistent with previously reported for Fe-ZSM-5 zeolites[46].

2.6.3. ELECTRON PARAMAGNETIC RESONANCE SPECTROSCOPY

The EPR spectroscopic study reveal that the Fe^{+3} ions which are incorporated into the zeolite during the synthesis may exist[179,180] in the following forms:

i) As exchangeable cations

ii) as hydroxides/oxides in the pores of the zeolite

or iii) in the zeolite lattice framework positions.

To identify the position of Fe^{+3} ions in ferrisilicate,(Fe-EU-1) the EPR spectra of Fe-EU-1 samples were recorded (Fig 2.18).

In X-band e.s.r. studies the signal at g=2.0 has been assigned[179] to the Fe^{+3} hexacoordinated complexes located at the cationic sites of the original hydrated zeolites. The signal at g=2.3 was assigned[179,181] to iron oxides and hydroxide, which did not belong to the structure of zeolite itself. The signal at g_{eff}=4.3 is attributed to the Fe^{+3} ions in distorted tetrahedral environment[179,181-183].

2.6.4. X-RAY PHOTOELECTRON SPECTROSCOPY (XPS)

The XPS spectra for zeolite Fe-EU-1 samples were recorded with a Vacuum Generators, model ESCA-3-MK-II instrument. MgK_{α} radiation was used. A slit width of 4 mm and analyser energy of 50 eV was employed.

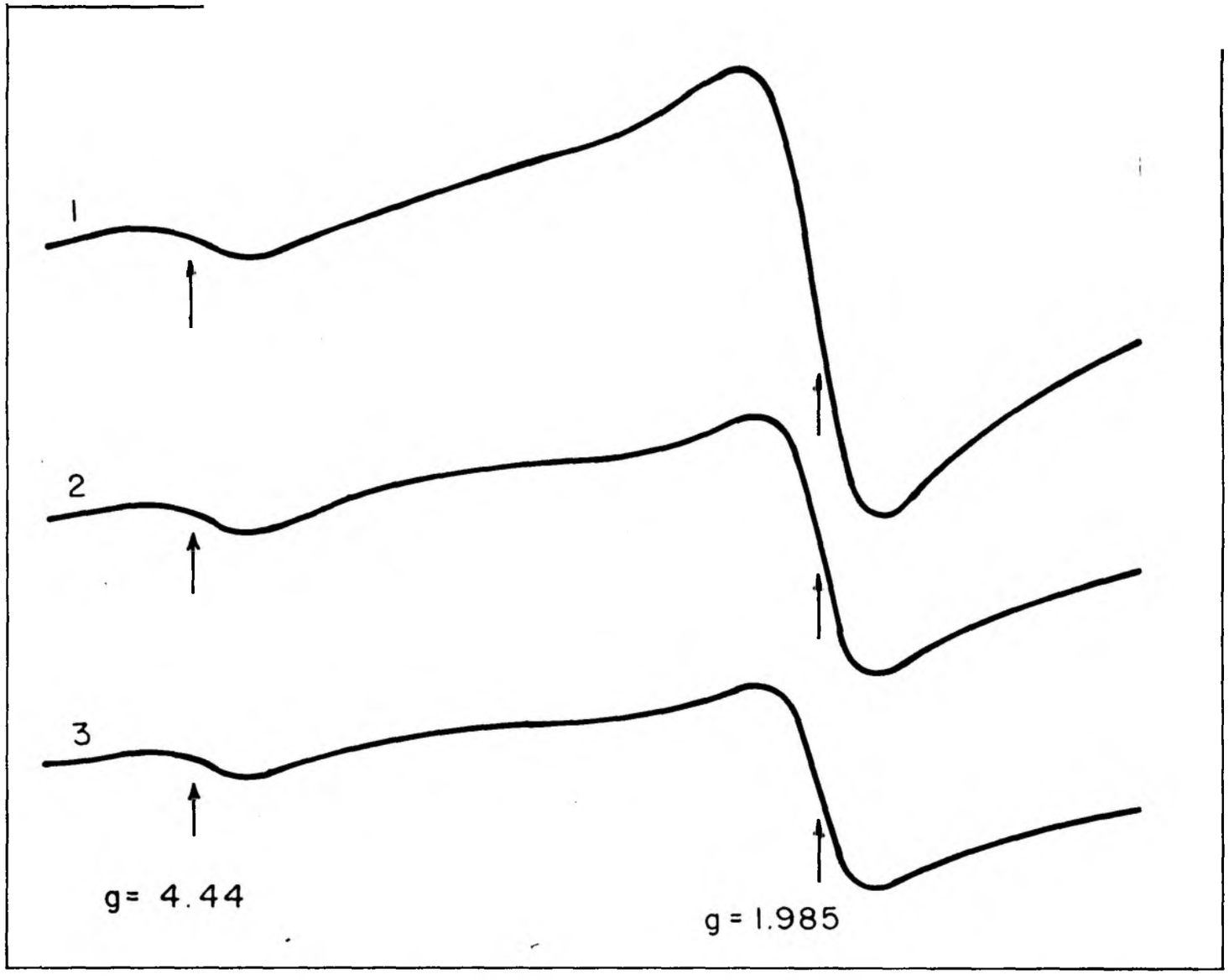

FIG. 2.18. EPR SPECTRA OF AS-SYNTHESISED Fe-EU-1 ZEOLITES WITH SiO_2/Fe_2O_3 RATIO (1) 48 (2) 78 AND (3 7, AT 298 K.

It was shown[46] that the ferric ions in iron analog of pentasil zeolites are in the trivalent state Fig 2.19 illustrates the XPS spectra of iron and oxygen in Fe-EU-1 and in the sample of silicalite containing Fe_2O_3.

The binding energy of $Fe_{2p\ 3/2}$ level in both the samples (value of 103.3 eV for Si_{2p} level as the internal standard) were 711.6 eV for Fe-EU-1 and 711.0 eV for Fe_2O_3 belonging to silicalite indicating that Fe ions are in the trivalent oxidation state in both the materials. A $2p_{3/2}$--$2p_{1/2}$ splitting of 14.0 eV was also observed for both of these materials. However, only one O_{1s} peak (zeolite lattice oxygen) is observed for Fe-EU-1 while two peaks at 531.5 eV and 529.0 eV are exhibited by 4.0 % Fe_2O_3 impregnated silicalite sample. The peak at 531.5 eV corresponds to the zeolite lattice oxygen, the other peak is due to the oxygen associated with the occluded Fe_2O_3 phase. Stencel et al.[184], for a sample of ZSM-5 containing Fe_2O_3, have also observed two O_{1s} peaks at 532 eV and 529 eV corresponding to oxygen ions in the zeolite lattice and Fe_2O_3, respectively.

2.7. SUMMARY

The experimental procedures for synthesizing -Al and -Fe analogs of EU-1 framework zeolites have been described in detail. EU-1 has been synthesised using Dibenzyldimethylammonium chloride as the template. Bis quaternaryammonium compound, hexamethonium bromide $(CH_3)_3N$-$(CH_2)_6$-$N(CH_3)_3$ Br_2, has been used for the synthesis of the ferrisilicate analog of EU-1 zeolite. The

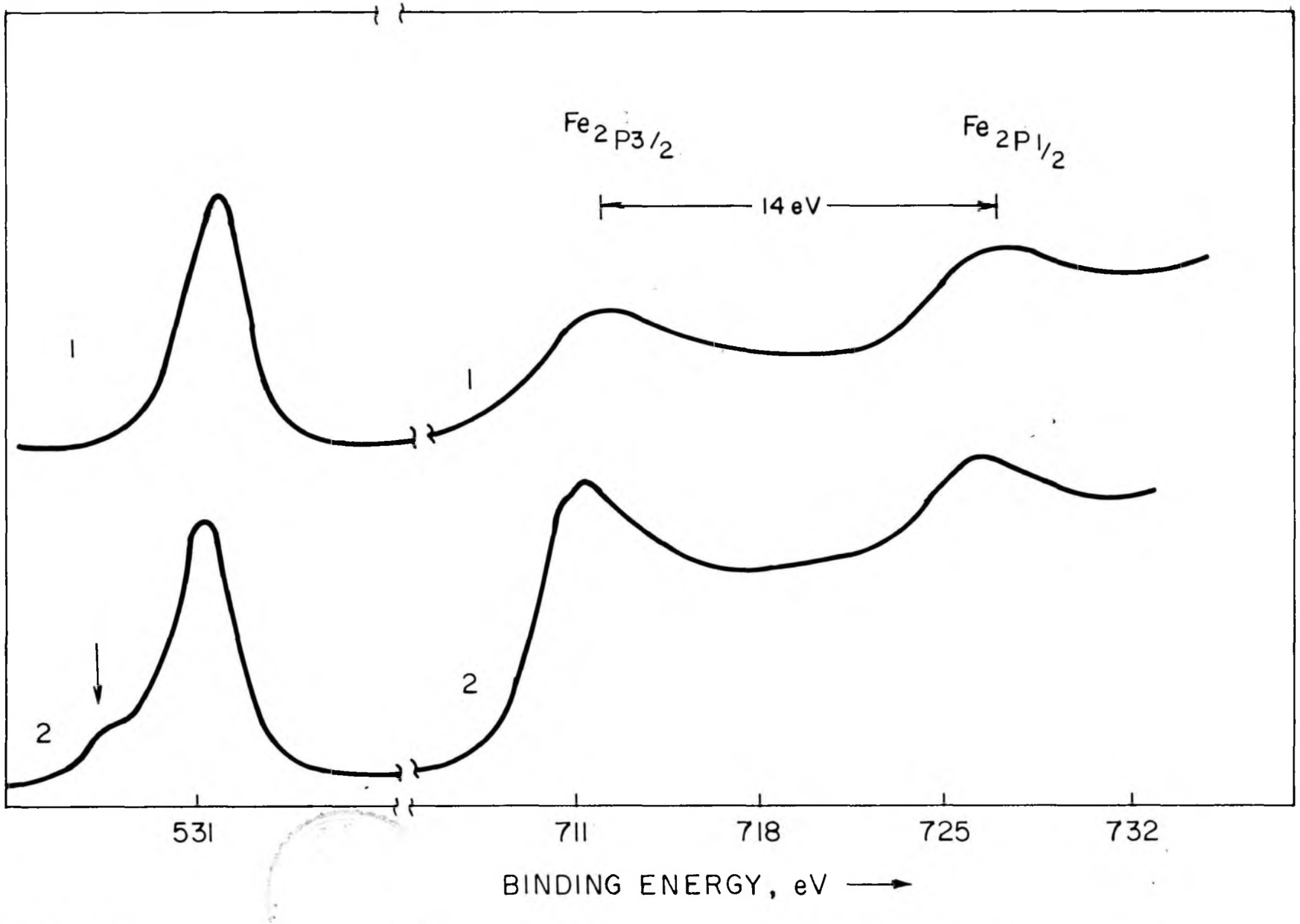

FIG.2.19. XPS SPECTRA OF 1)Fe-EU-1 2) Fe_2O_3+ SILICALITE.

crystallization kinetics of -Al analog of EU-1 zeolites has been investigated utilizing the following molar composition: 17.0 Na_2O : 18.0 Q^+ : Al_2O_3 : 300 SiO_2 : 3200 H_2O of the hydrogels at 373, 398 and 423 K. From the kinetic data apparent activation energies for nucleation(En) as well as crystal growth (Ec) have been determined by applying Arrhenius type equations. The values of En = 26.1 kJ $mole^{-1}$ and Ec = 22.1 kJ, $mole^{-1}$, so obtained have been compared with the reported values. The kinetics data has been further fitted to Avarami-Erofeev, $\ln(1/1-\alpha) = (kt)^m$, equation. The good fit of the data for Avarami-Eurofeev equation suggests that the process of crystallization involves nucleation and subsequent growth of the crystalline EU-1 phase. A modified process involving the low temperature ageing of the gel has been described to achieve pure EU-1 phase at elevated temperatures. Influence of SiO_2/Al_2O_3, OH^-/SiO_2 ratio and the concentration of the templating species on the crystallization kinetics have been studied and discussed.

Synthesis runs for varying SiO_2/Fe_2O_3 ratios of ferrisilicate analog of EU-1 zeolite have also been described.

X-ray diffraction studies of both the analogs revealed that the samples were highly crystalline without the presence of any amorphous impurities. A marked shift in the interplanar spacings (d A^o) towards the higher values for ferrisilicate analogs has been found indicative of lattice expansion when Al^{+3} replaced by Fe^{+3} in the framework.

Infrared framework vibrations of both the analogs have been studied in the 200-1300 cm^{-1} region. The absorbance at 572 cm^{-1} has been utilized to estimate the crystallinity of the products. The IR crystallinity of both the analogs correlate with that obtained from XRD studies. The IR crystallinity values are higher than those from XRD. In the case of ferrisilicate analog, a shift towards the lower frequency in Si-O asymmetric stretching vibration (1100 cm^{-1}) has been explained on the basis of bond distances.

Thermoanalytical studies in a flow of air for both the analogs in the as-synthesized form has been studied and discussed. Two exotherms in DTA have been found to be characteristic for both -Al and -Fe analogs. These have been assigned to the oxidative decomposition of the templating species occluded during the hydrothermal syntheses. Both the analogs of EU-1 phase are stable upto 1273 K without any crystal structure breakdown.

Morphological studies of both the analogs have been described employing scanning electron microscope. The -Al analogs have been found to crystallise with cuboid shape (3-6 μm) whereas -Fe analogs have a near spherical growth ($\simeq$ 1 μm).

X-ray photoelectron spectroscopy and electron paramagnetic resonance studies have been utilized to characterize the Fe^{+3} species in EU-1 framework. Analysis of the results indicate that Fe^{+3} ions are in tetrahedral positins in the lattice framework of EU-1.

CHAPTER 3

PHYSICO-CHEMICAL CHARACTERIZATION OF EU-1 ZEOLITES

CONTENTS

3.1. INTRODUCTION

The adsorption and catalytic properties of zeolites are modified to a considerable extent by replacement of Na^+ with hydrogen or multivalent ions[185]. The variations of the physico-chemical properties of exchanged zeolites are generally determined by the measurement of sorption, thermal and diffusional properties[185,186]. The nitrogen adsorption isotherm for a pure zeolite is quite characteristic and is distinguishable from that of amorphous materials. Johnson[187] used the nitrogen adsorption isotherm of a thermally treated zeolite containing catalyst to estimate the quantity of zeolite in the catalyst. The sorption of nitrogen, not only gives a measure of the surface accessible to molecules comparable in size with nitrogen, but also the surface area of the samples[188]. From the sorption capacities for water, n-hexane and cyclohexane, the modifications in the pore structure have been determined and the available total void volume has been evaluated. The modifications in the crystal structure are studied by X-ray diffraction[189] and infrared spectroscopy[86].

The thermal stability of the zeolite structure can be determined from the DTA curves. The high temperature exotherm is often used to determine the thermal stability of the samples. Thus, the framework distortion caused by ion exchange and steam treatment has been evaluated from the sorption of nitrogen, water and other suitable hydrocarbons[190], in addition to the X-ray and ir data of the samples. The EU-1 zeolites, in protonated

form or modified by introduction of Ni and Pt, are being used as catalyst in shape selective reactions of hydrocarbons[191]. The zeolite EU-1 possesses high thermal and hydrothermal stability. In this chapter we report changes in the structural parameters studied by X-ray and ir techniques, alongwith the sorption of nitrogen, water, n-butylamine and paraffinic hydrocarbons. The acidity of EU-1 zeolites with varying SiO_2/M_2O_3 (M= Al^{+3} or Fe^{+3}) ratios is also reported in this chapter.

3.2. EXPERIMENTAL

3.2.1 PREPARATION OF PROTONATED (H^+) EU-1 ZEOLITES.

The EU-1 zeolite samples in the as-synthesized form contain occluded and stabilized quaternary ammonium ions and are designated as EU-1 (C/N). The organic cations which occupy the channels in the zeolite crystals are removed by heating the sample in a muffle furnace at 823 K for about 24 hours. The final calcination temperature is attained at a linear heating rate of 2.5 K min^{-1}. The product is cooled to room temperature and kept over saturated NH_4Cl solution for a week. The samples are designated as Na-EU-1.

In order to obtain NH_4-EU-1, the zeolite samples were exchanged at 95°C under reflux condition with 5M solution of NH_4Cl at a liquid to solid ratio of 15. The samples were filtered, washed with hot water and dried at 393 K overnight. The same procedure was repeated twice to obtain maximum degree of exchange.

The acidic or protonated forms (H-EU-1) were obtained by air calcination of NH_4-EU-1 samples at 823 K for 10 hours. The heating rate was 2.5 K min^{-1}. Then the samples were cooled to room temperature and kept in a desiccator over saturated ammonium chloride solution for a week.

3.2.2. X-RAY DIFFRACTION

The X-ray diffraction patterns were recorded to ascertain the purity in the samples and to detect the structural changes if any, of zeolites after ion-exchange and calcination at different temperatures. The X-ray diffraction patterns of zeolite samples were recorded on a Philps PW 1730 X-ray diffractometer using nickel filtered CuK_α radiation λ= 1.5405 A°.

3.2.3. THERMAL ANALYSIS

The thermo-analytical curves were recorded on an automatic derivatograph (Netzsch, Model STA 490). The thermograms of the samples were recorded under the following conditions.

weight of the sample	50 mg
heating rate	10 K min^{-1}
sensitivity:	
TG	25 mg
DTA	0.1 mV
DTG	0.2 mV
Atmosphere	Flowing air

Preheated and finely powdered alumina was used as a reference material.

3.2.4. THERMAL AND STEAM STABILITY

The zeolite samples were heated in a muffle furnace to the desired temperature, at a heating rate of 2.5 K min^{-1} for 5-6 hours, then the samples were cooled to room temperature and kept in the desiccator over saturated ammonium chloride solution.

Steam treatment was carried out by heating the zeolite samples at a heating rate 2.5 K min^{-1} to the desired temperature in flowing steam, at atmospheric pressure, for about 5-7 hours. After steam treatment, the samples were cooled and kept over saturated ammonium chloride solution in a desiccator for a week and then these samples were subjected to X-ray diffraction studies.

3.2.5. NITROGEN ADSORPTION

A conventional all glass BET unit was used for the measurement of nitrogen adsorption and consists of three burettes B_1 B_2 and B_3 (B_3 is not shown in Fig 3.1), a manometer M and a sample bulb S. High vacuum systems consisting of a two stage rotary pump, mercury diffusion pump, a Mcleod gauge, and a series of liquid nitrogen cold traps, were used for degassing the sample.

The volumes of the burette bulbs were precalibrated with mercury before joining to the adsorption system. The burettes

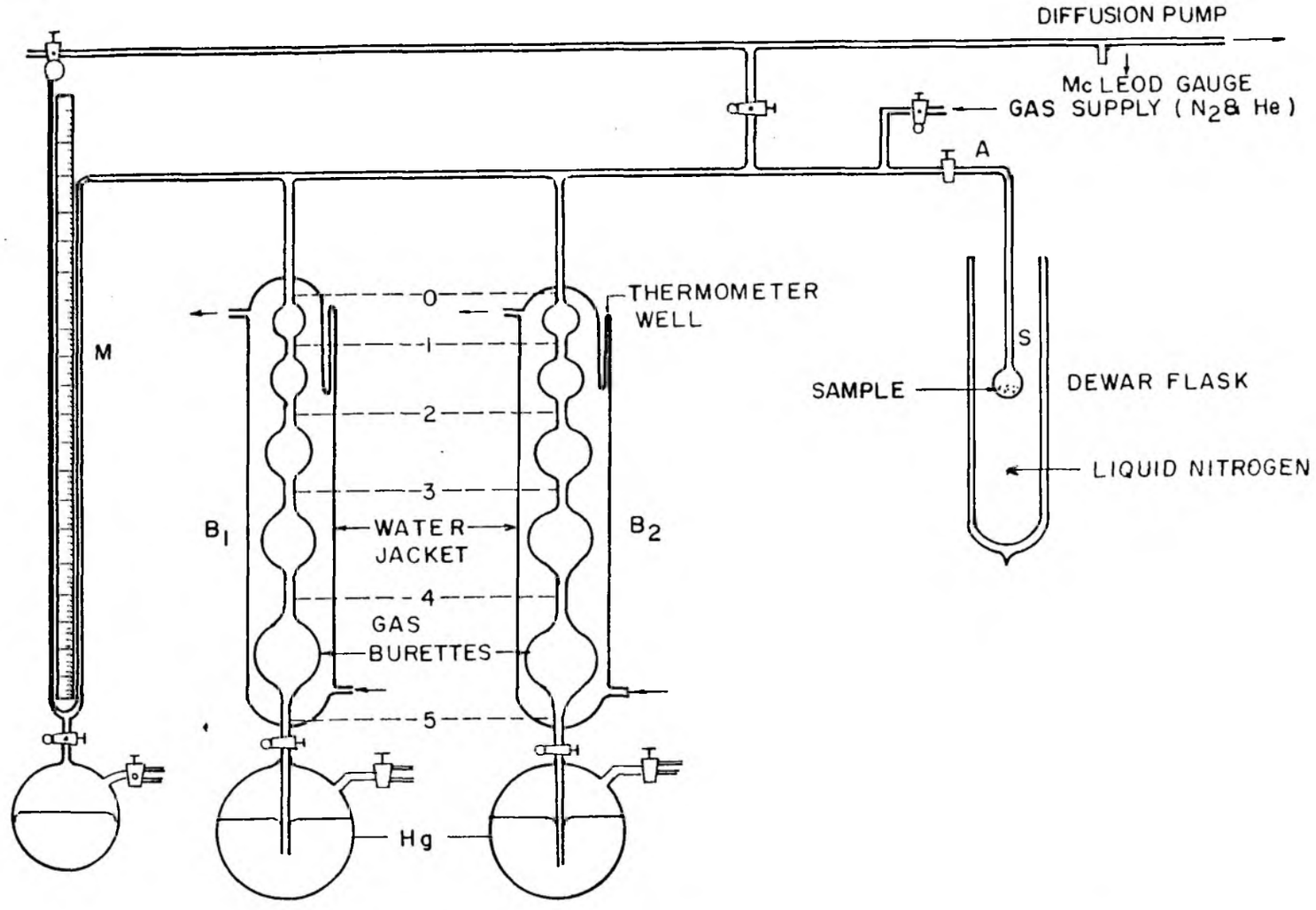

FIG. 3.1. GAS ADSORPTION UNIT FOR THE MEASUREMENTS OF BET SURFACE AREA.

B_1, B_2 were immersed in water jackets provided with a thermowell for temperature measurements. The dead space volume in the system was determined by using spectrally pure helium supplied by British oxygen Co.,(U.K). About 0.2 to 0.3 gms of hydrated sample weighed in the sample bulb was activated by increasing temperature slowly in steps under continuous pumping. The sample was activated at 673 K by evacuation to about 10^{-6} torr for a period of 6 hours. The sample was cooled and the dead-space volume was determined by using helium at liquid nitrogen temperature. After pumping the helium gas, a dose of nitrogen was admitted and calibrated. The sample was exposed to N_2 gas at 78 K. The adsorption was measured at different equilibrium pressures. The adsorption measurements were continued by admitting consequent calibrated doses, until a sufficient number of points were obtained. The reversibility was checked by carrying out desorption measurements.

The volume of gas adsorbed at STP was estimated as follows.

$$V_{ads} = V_1 - V_2 - V_3(1+\alpha P/760) \quad \text{--------> (4)}$$

where V_1, V_2, V_3 are the volumes of gas taken, remaining in the system, and in the bulb, respectively. α is the correction for the non-ideality of nitrogen at 78 K. The applicability of the Langmuir or the BET isotherm equations for the estimation of surface area was checked by using the following relations.

$$P/P_oV = 1/bV_m + P/V_mP_o \quad \text{----------> (5)}$$

$$P/V_{ads}(P_o-P) = 1/V_mC + (C-1)/V_mC \text{ X } P/P_o \quad \text{---> (6)}$$

where $C = e^{(E-E_o)/RT}$ is constant and depends on the sorbate-

sorbent system, V_m is the monolayer volume, P_o is the saturation vapour pressure of nitrogen at 78 K, P is equilibrium pressure, and b is a constant.

The void volume of the zeolite sample was determined from the Dubinin s plots of log(a) Vs $(\log P_s/P)^2$.

The equation used was

$$\log(a) = C-D\ (\log P_s/P)^2 \quad \text{----------> (7)}$$

where C and D are constants, P is equilibrium pressure and P_s is saturation pressure.

3.2.6. SORPTION AND DIFFUSION STUDIES

The sorption and diffusion measurements for hydrocarbons in the micropores of EU-1 zeolites were conducted on a McBain type gravimetric unit (Fig 3.2). A sensitive silica spring was used for the measurement of weight changes. The zeolite sample, about 50 mgs, was pressed into a pellet and weighed into an aluminum bucket which was attached to a silica spring. The assembly was evacuated by means of a two-stage rotary pump and a mercury diffusion pump to a vacuum of 10^{-6} torr. The sample was activated at 673 K by continuous pumping till a constant weight was obtained. After the zeolite sample had reached a constant weight, the temperature of the sample was lowered to the desired value. To study the equilibrium sorption and the rate of adsorption, the sorbate was admitted to the sample at constant temperature and pressure; and the weight gain was recorded with a cathetometer (accuracy ± 0.01mm) as a function of time. After

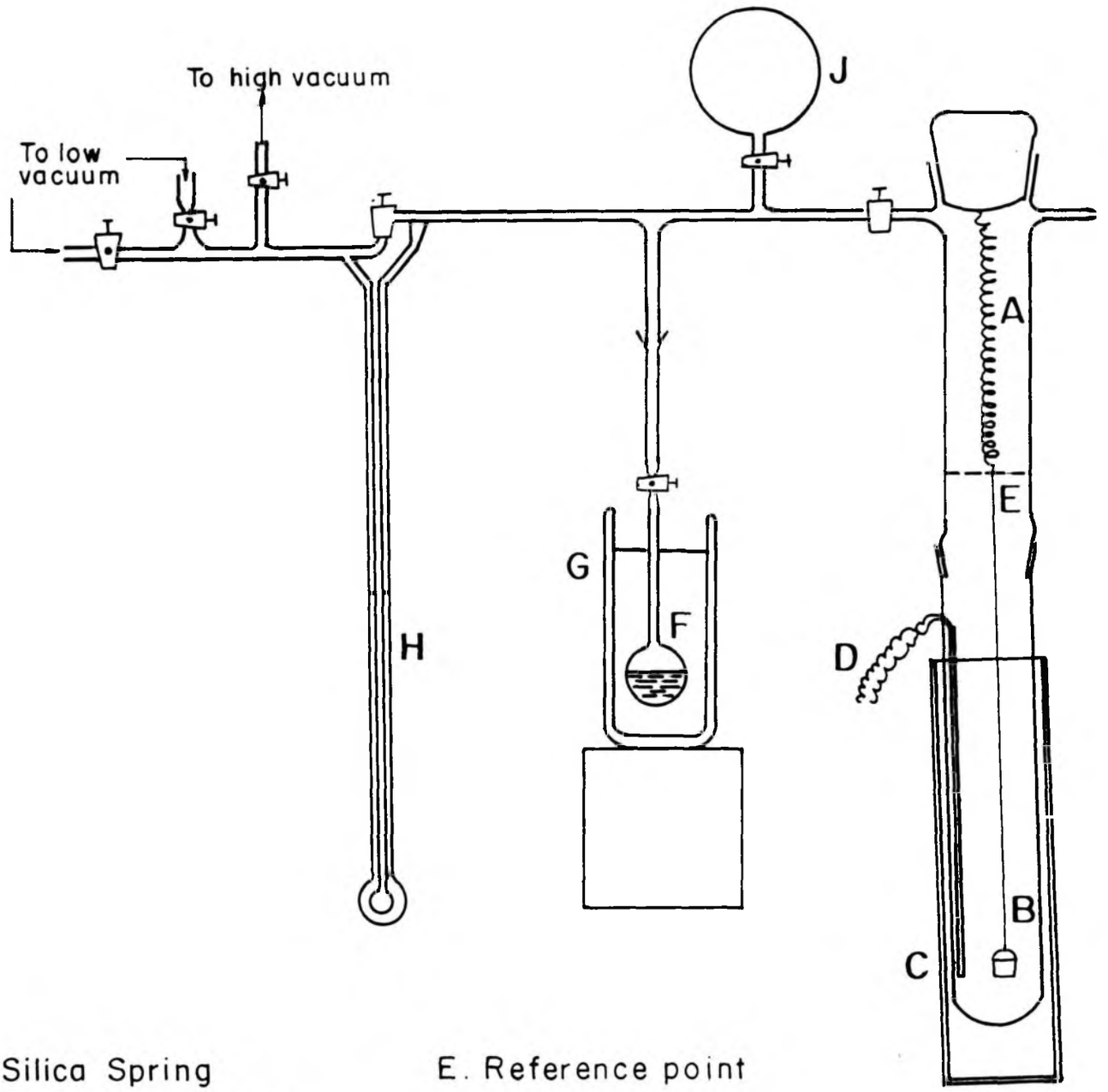

A. Silica Spring
B. Aluminium Bucket
C. Furnace or Thermostat
D. Thermocouple
E. Reference point
F. Liquid bulb
G. Thermostat
J. Gas Reservior
H. Manometer

FIG. 3.2. GRAVIMETRIC ADSORPTION UNIT.

recording the equilibrium sorption, the catalyst was evacuated and heated to 673 K at 10^{-6} torr and used for the next measurement.

3.2.7. ISOTHERMS OF n-BUTYLAMINE

The isotherms for the sorption of n-butylamine were measured upto a pressure of 80 torr in the temperature range of 298-423 K by the gravimetric method using a calibrated silica spring balance. The sample (50 mg) in the form of a pellet, was activated under high vacuum (~ 10^{-6} torr) at 673 K for 10 h to a constant weight and cooled to the required temperature for the isotherm studies. The adsorbate liquid bulb was rendered air-free and was separately thermostated. The pressure of the adsorbate was measured accurately with a cathetometer. The amount sorbed was estimated from changes in the weight of the sample after equilibrium was obtained. The adsorption isotherms were obtained by progressive increase of vapour pressure and noting the extent of adsorption.

3.2.8. TEMPERATURE PROGRAMMED DESORPTION OF AMMONIA (TPD)

The acidity of catalyst samples was measured by a temperature programmed desorption technique. The experimental set-up of TPD of NH_3 is shown schematically in Fig 3.3. 0.4 g of zeolite catalyst sample (10-20 mesh) was taken in a micro reactor connected to an on-line gas chromatograph (SHIMADZU, GC-R1A Model).

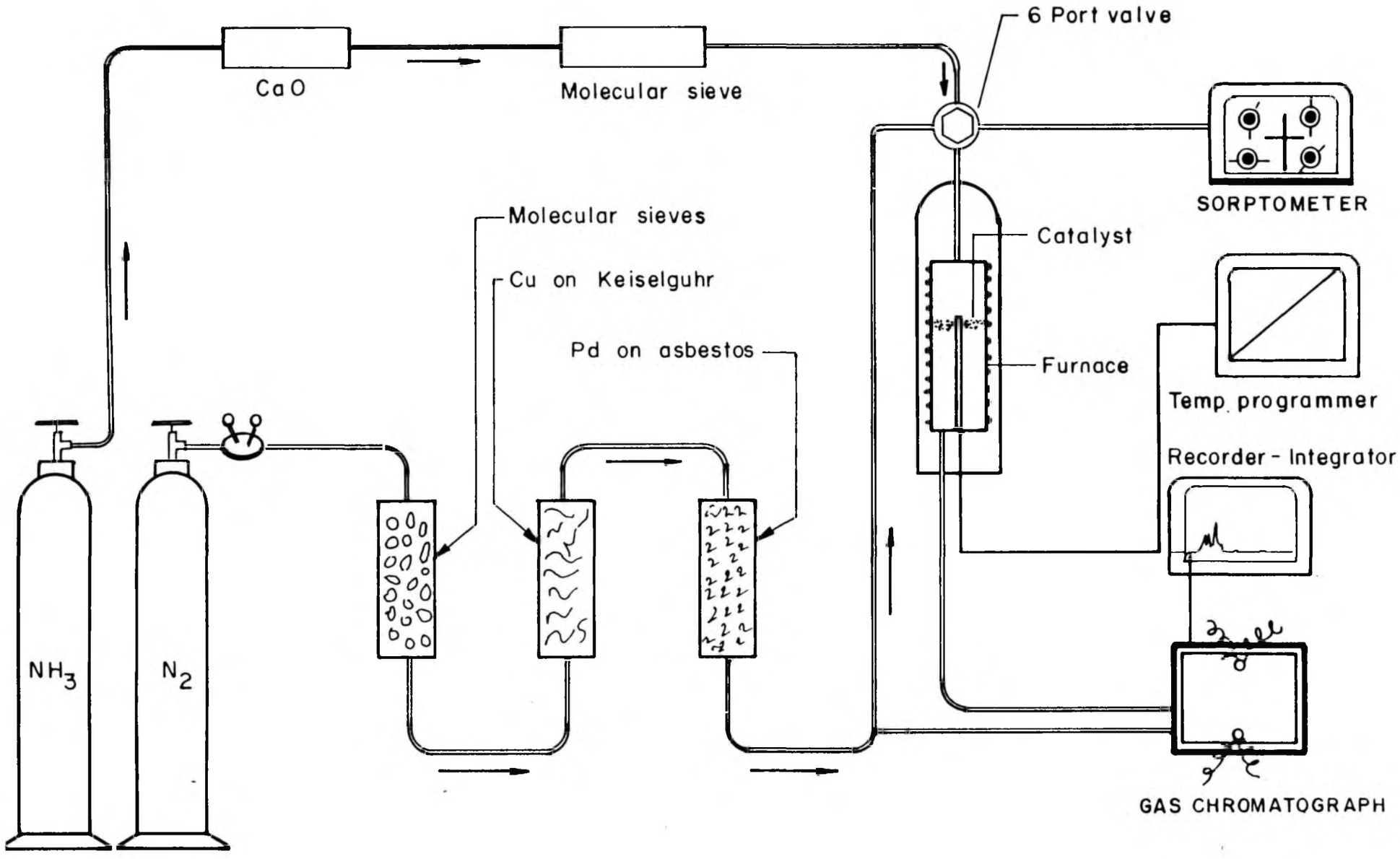

FIG.3.3. SCHEMATIC DIAGRAM OF TPD UNIT.

The catalyst sample(protonated form) was initially heated to 673 K at a rate of 10 K min^{-1} in a flow of purified and dry N_2 gas, and then coupled to a sorptometer for evacuation. It was activated under vacuum at 673 K for 2 hours, and cooled to 523 K. A calibrated volume of NH_3 (RCF, 99.5 %) was then admitted to the sample. The sample was cooled further to 298 K. The equilibrium sorption of NH_3 was determined at 298 K, and 200 mm vapour pressure. The loosely adsorbed NH_3 was evacuated at the same temperature. Equilibrium sorption of NH_3 was once again determined at the same temperature and pressure. The difference between the first and the second equilibrium sorption was taken as the chemisorbed ammonia.

The sample was then coupled to the on-line G.C. after allowing sufficient time to stabilize the G.C. The sample was heated at a linear rate of 10 K min^{-1} with carrier gas flow of 60 ml, min^{-1} and the TPD spectrum was obtained on the integrator.

3.2.9. INFRARED SPECTROSCOPY

The IR spectra of zeolite samples were recorded in the frequency range of 200-1300 cm^{-1} using KBr pellets or nujol mull technique on a PYE UNICAM SP-300 spectrophotometer.

3.2.10. SOLID STATE MASNMR SPECTROSCOPY

The high resolution MASNMR (magic angle spinning) spectra for ^{29}Si were obtained at room temperature on a BRUKER MSL-300 spectrometer, operating in Fourier transform mode, using "one

cycle" type measurements. A 90^{o} pulse with 3 seconds delay-time was used for ^{29}Si nuclei and chemical shifts (δ) in ppm were measured with respect to tetramethylsilane (TMS) as an external reference. The rotor (sample holder) was spun at a rate of 4.0 KHz.

^{27}Al MAS-NMR spectra were obtained using a 45^{o} pulse with 1 second delay-time. Chemical shifts in ppm were measured with respect to aqueous (0.1N) $AlCl_3$ as an external standard.

3.3. RESULTS AND DISCUSSION

3.3.1. X-RAY DIFFRACTION

The unit cell compositions of the Al-EU-1 and Fe-EU-1 zeolites determined by AAS and ICP techniques are given in Table 3.1.

TABLE 3.1

Unit cell composition of anhydrous Na-Al-EU-1 zeolites

1. $Na_{1.28}H_{0.63}[(SiO_2)_{110.09}(AlO_2)_{1.91}]$
2. $Na_{1.06}H_{0.17}[(SiO_2)_{110.76}(AlO_2)_{1.23}]$
3. $Na_{0.78}[(SiO_2)_{111.22}(AlO_2)_{0.78}]$
4. $Na_{0.41}[(SiO_2)_{111.58}(AlO_2)_{0.41}]$

Unit cell composition of anhydrous Na-Fe-EU-1 zeolites

1. $Na_{5.00}[(SiO_2)_{106.93}(FeO_2)_{5.06}]$
2. $Na_{2.78}[(SiO_2)_{109.22}(FeO_2)_{2.78}]$
3. $Na_{1.87}[(SiO_2)_{110.13}(FeO_2)_{1.87}]$

The X-ray diffraction patterns of zeolite samples of as synthesized (C/N), Na, NH_4^+ and H^+ forms are shown in Fig 3.4. The first sample was synthesized using $DBDM^+$ as the organic template. The XRD pattern and "d" values for these samples are in good agreement with the reported data[146].

The most intense peak is observed at $2\theta = 20.6^{\circ}$. The intensity of the low angle peak at $2\theta = 7.9^{\circ}$ and 8.8° were found to increase when the samples were converted to sodium form. The increase in intensity was due to the removal of organic cations which are present in the intracrystalline voids. Similar results have been reported earlier for EU-1[146] and pentasil zeolites[45]. On further conversion to the ammonium and hydrogen form, the intensity of these two peaks further increased. The intensity changes have been explained[78] as due to the removal of extra framework organic and inorganic species incorporated into the structural voids during synthesis of the zeolite.

Fig 3.5 shows the X-ray diffraction patterns of Na-EU-1 zeolites with varying SiO_2/Al_2O_3 ratios. All EU-1 samples exhibit similar X-ray diffraction patterns except some minor changes in the relative intensity of the peaks at $2\theta = 7.9^{\circ}$ and 8.8°. With increase in the SiO_2/Al_2O_3 ratio, the increase in the intensity of the two peaks is observed.

It has been reported[192] that lattice parameters of the crystals vary as the impurities are incorporated which produce changes in peak positions and intensities in the XRD pattern. In

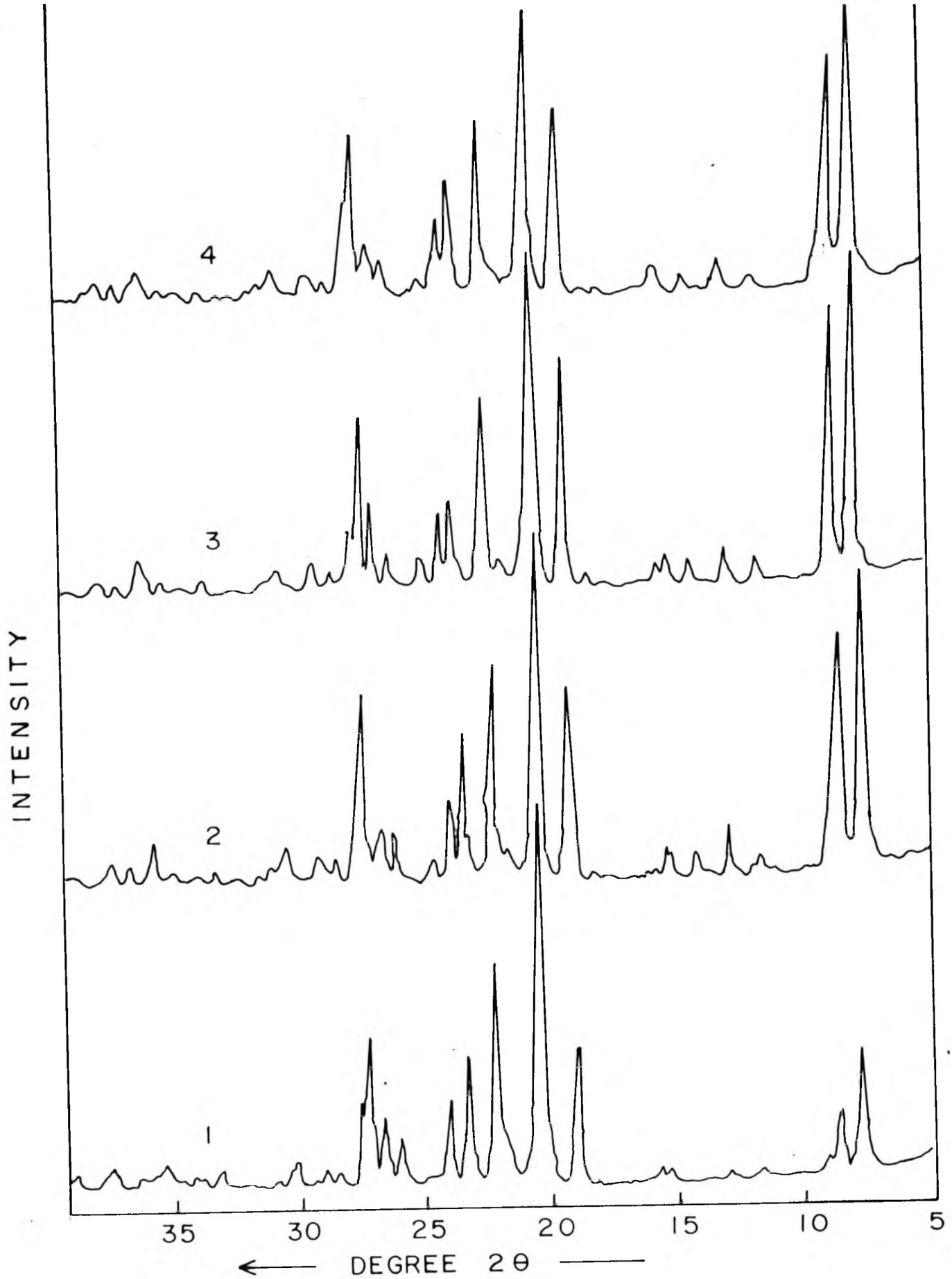

FIG.3·4. X-RAY DIFFRACTION PROFILES OF Al-EU-1 ZEOLITES 1) EU-1(C/N), 2) Na-EU-1, 3) N[illegible]-EU-1 4) H-EU-1

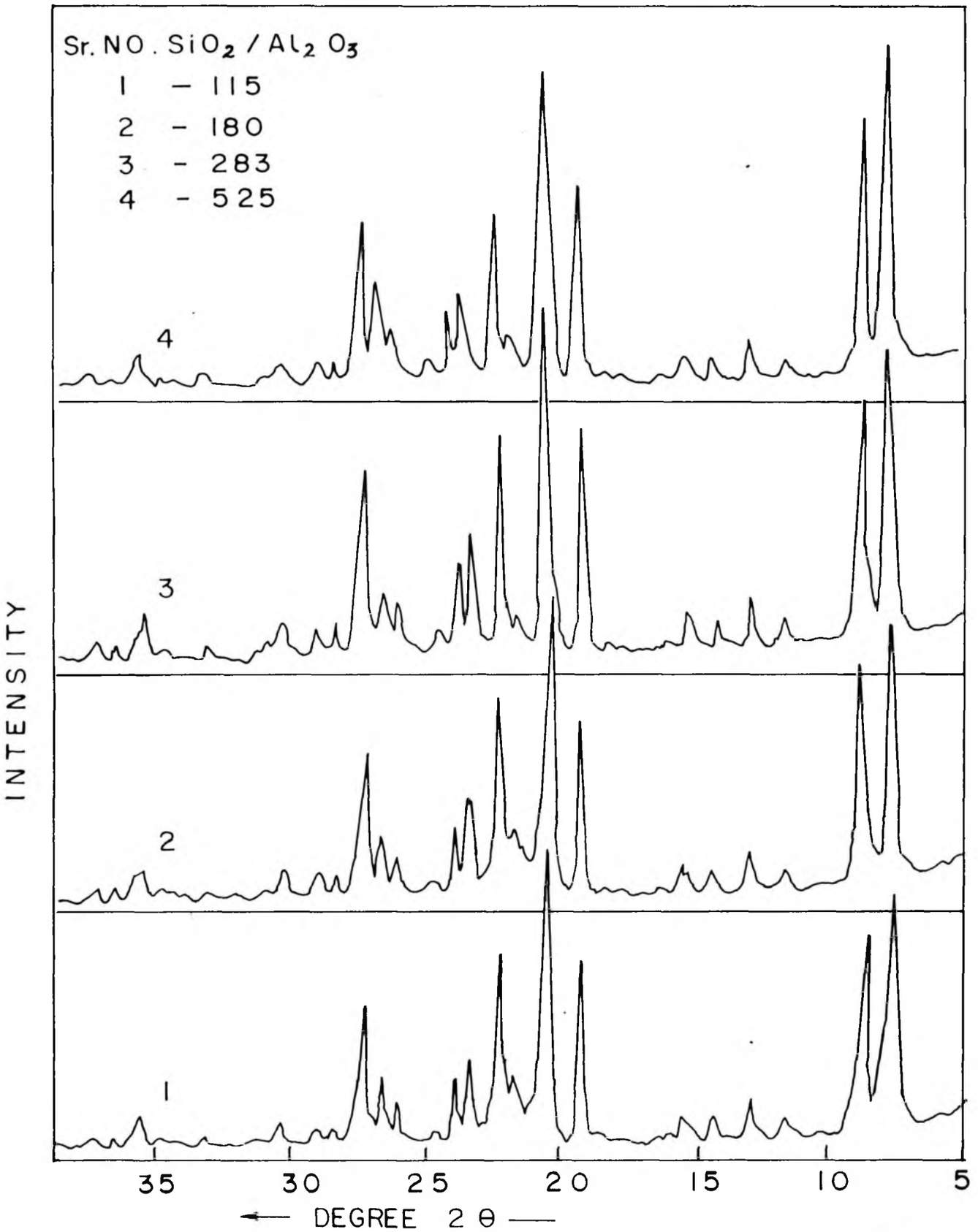

FIG. 3.5 X-RAY DIFFRACTION PROFILES OF Na-EU-1 ZEOLITES.

the case of zeolites, lattice parameters vary with the degree of Al^{+3} substitution for Si^{+4}. Similar observations have been made by Bibby et al.[79] who found that the broadening of the peaks results from the inhomogeneous distribution of Al within individual crystals.

The loss in crystallinity, estimated from the decrease in X-ray diffraction peak area in the range of $2\theta = 18\text{-}24^{o}$ for EU-1 samples calcined at different temperatures for a fixed period of time (5 hours), is shown in Fig 3.6. The sample calcined at 823 K is considered as 100 % crystalline. It was observed that sample Na-EU-1(180), Na-EU-1(283), and Na-EU-1(525) (the numbers in the bracket refer to SiO_2/Al_2O_3 ratios) calcined at 1273 K for 5 hours did not show any major loss in crystallinity, while the zeolite Na-EU-1 (115), shows about 25 % loss in crystallinity under the same conditions. This indicates that the higher the silica content in the zeolite framework, the more stable is the crystalline structure. Further, the thermal stability of Na-EU-1 zeolites with SiO_2/Al_2O_3 ratios of 115, 180, 283 and 525 was examined by calcining the samples in air at 1373 K for 5 hours. The first three samples were converted to cristobalite at 1373 K. The last sample (SiO_2/Al_2O_3 = 525) showed no structural transformation upto 1373 K. These results further confirmed the dependence of the structural stability on the SiO_2/Al_2O_3 ratios in the EU-1 zeolites (Fig 3.6).

The X-ray diffraction patterns of H-EU-1 (283) zeolite calcined in the temperature range of 573 to 773 K in the presence

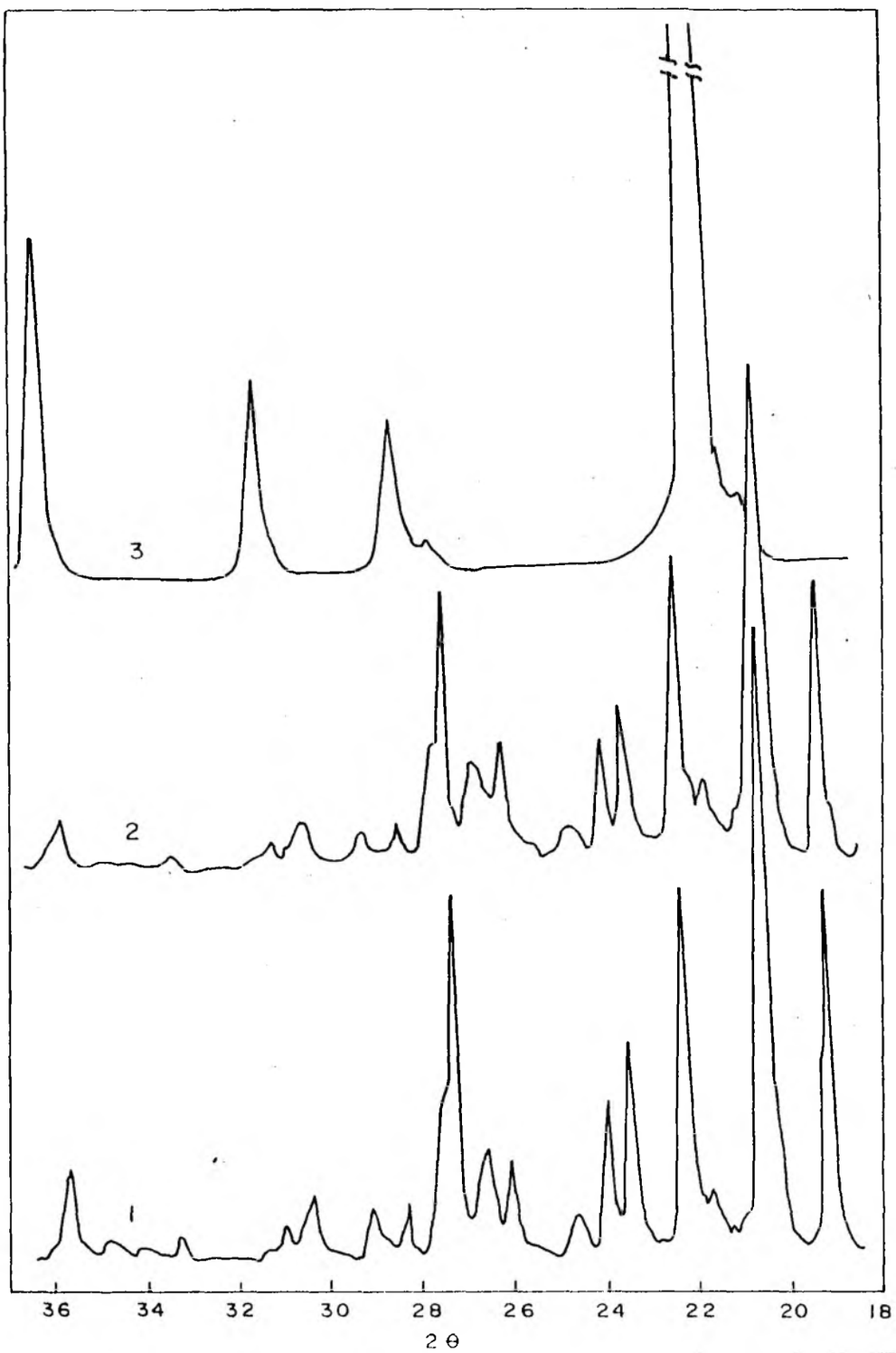

FIG.3.6: X-RAY DIFRACTION PROFILES FOR THERMALLY TREATED EU-1 ZEOLITES 1) 100 % CRYSTALLINITY (823 K), 2) 75 % CRYSTALLINITY (1273 K), 3) CRISTOBALITE (1373 K).

of steam are shown in Fig 3.7. It can be seen that the crystallinity of the steam treated sample is within ±10 % of that of the original zeolite. It has been observed that with the increase in the temperature of the steam treatment the intensity of the peaks at $2\theta = 7.9^{o}$ and 8.8^{o}, increased.

Such an increase in intensity has been attributed to the dealumination of zeolites at elevated temperatures[107].

3.3.2. THERMAL ANALYSIS

Fig 3.8 shows DTA and TG curves for as-synthesized (C/N), and for the Na^{+}, NH_4^{+} and H^{+} forms of EU-1 zeolites. The structural collapse of the zeolite crystals is accompanied by liberation of heat. Consequently, the position of this exothermic peak has often been considered as a measure of thermal stability. It is seen from the Fig 3.8 that the samples in the C/N, Na^{+},NH_4 and H^{+} forms do not exhibit such exothermic peaks upto 1273 K indicating high thermal stability of the EU-1 framework.

As described in chapter II, all the above mentioned forms of EU-1 zeolites show a relatively small endothermic peaks in the temperature 298 to 473 K due to the removal of physically sorbed and occluded water. On the other hand, the as-synthesized EU-1 (C/N) form and NH_4-EU-1 form show an exothermic peak in the temperature range 473-1108 K due to the oxidative decomposition of the organic template and NH_4^{+} ions.

Both the Bronsted and Lewis acid sites, exist in zeolites. The former are protons attached to the lattice oxygen atoms,

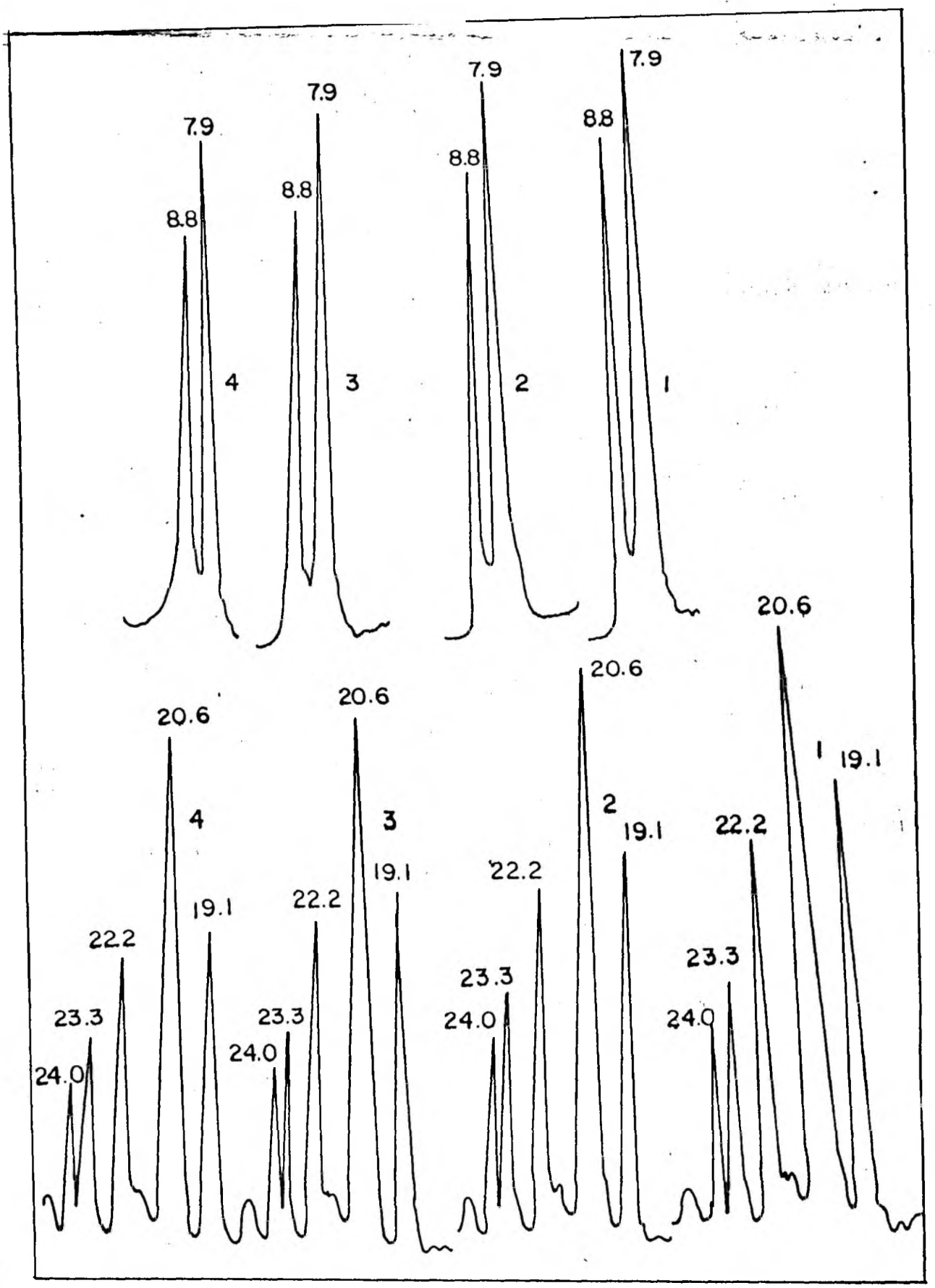

FIG: 3·7 XRD PATTERNS OF STEAM TREATED SAMPLES AT 1) 500 °C, 2) 400 °C, 3) 300 °C, 4) NIL.
$SiO_2/Al_2O_3 = 283$

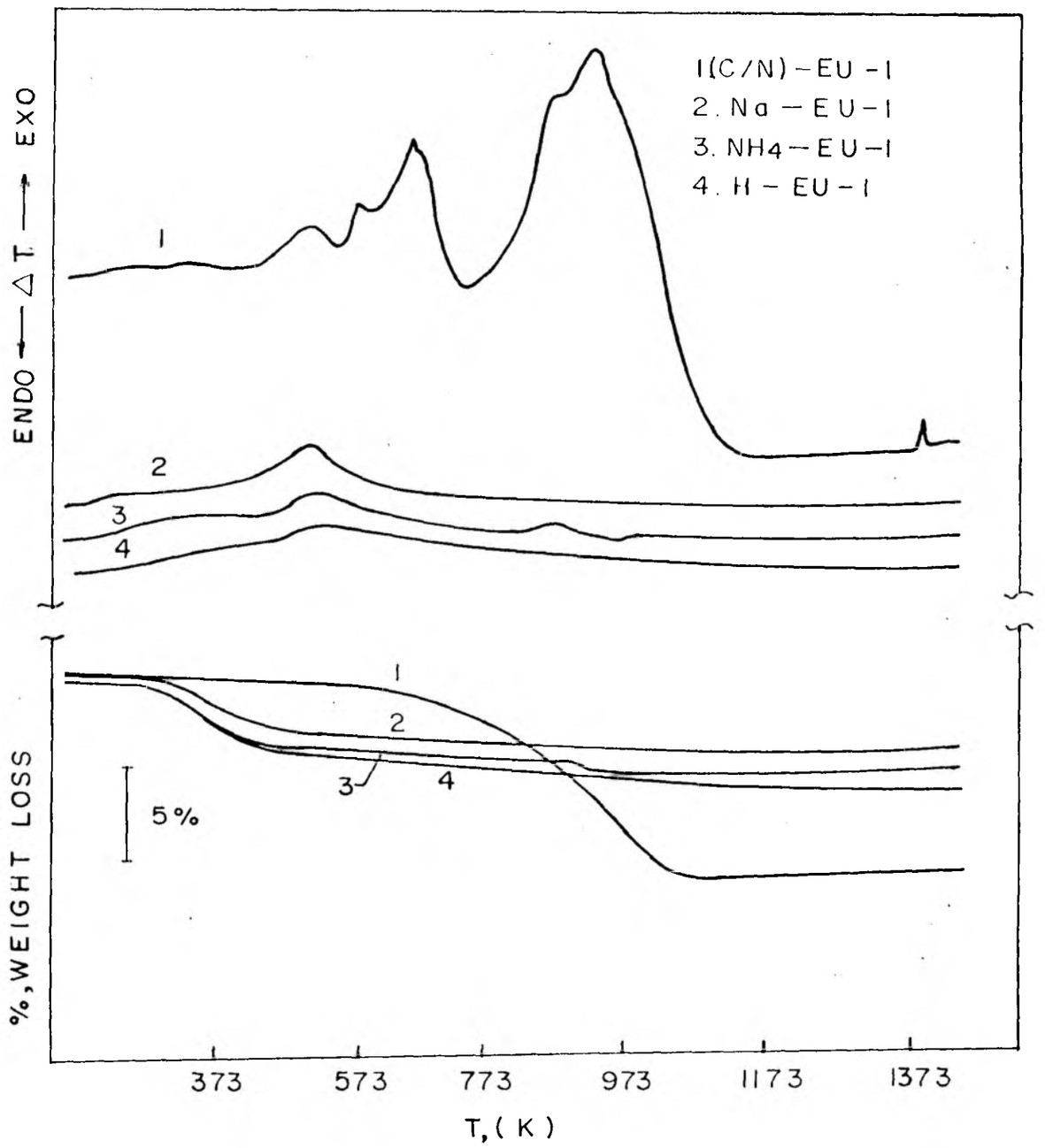

FIG. 3·8. DTA AND TG CURVES FOR DIFFERENT FORMS OF Al-EU-1 ZEOLITES.

while the latter can be the charge compensating cations or trigonal aluminum atoms at the oxygen deficient sites or cation positions. The protons can be introduced into the zeolite by ammonium exchange and subsequently deammoniation, as well as by hydrolysis of cations or reduction of cations to a lower valency state.

At higher temperatures, dehydroxylation of the zeolite takes place. During the dehydroxylation process, the Bronsted acid sites are converted to Lewis acid sites. The dehydroxylation process in case of zeolite is generally assumed to occur according to the following equation.

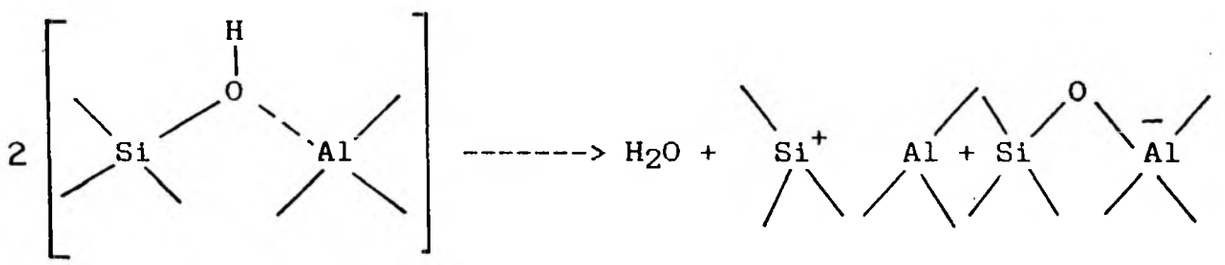

For applications in catalysis, it is desirable that the organic moiety be removed at a temperature lower than 773 K. To check this feasibility, the following experiments were done (Fig 3.9). The as-synthesized sample was first heated in a separate furnace in flowing air (heating rate = 10 K min^{-1}). When the temperature reached 723 K, a part of it (50 mg) was removed and its DTA pattern was recorded (curve a, Fig 3.9). The pattern is similar to curve 1 of Fig 3.8. The remaining sample in the furnace was maintained at 723 K for 9 h, at which time a second

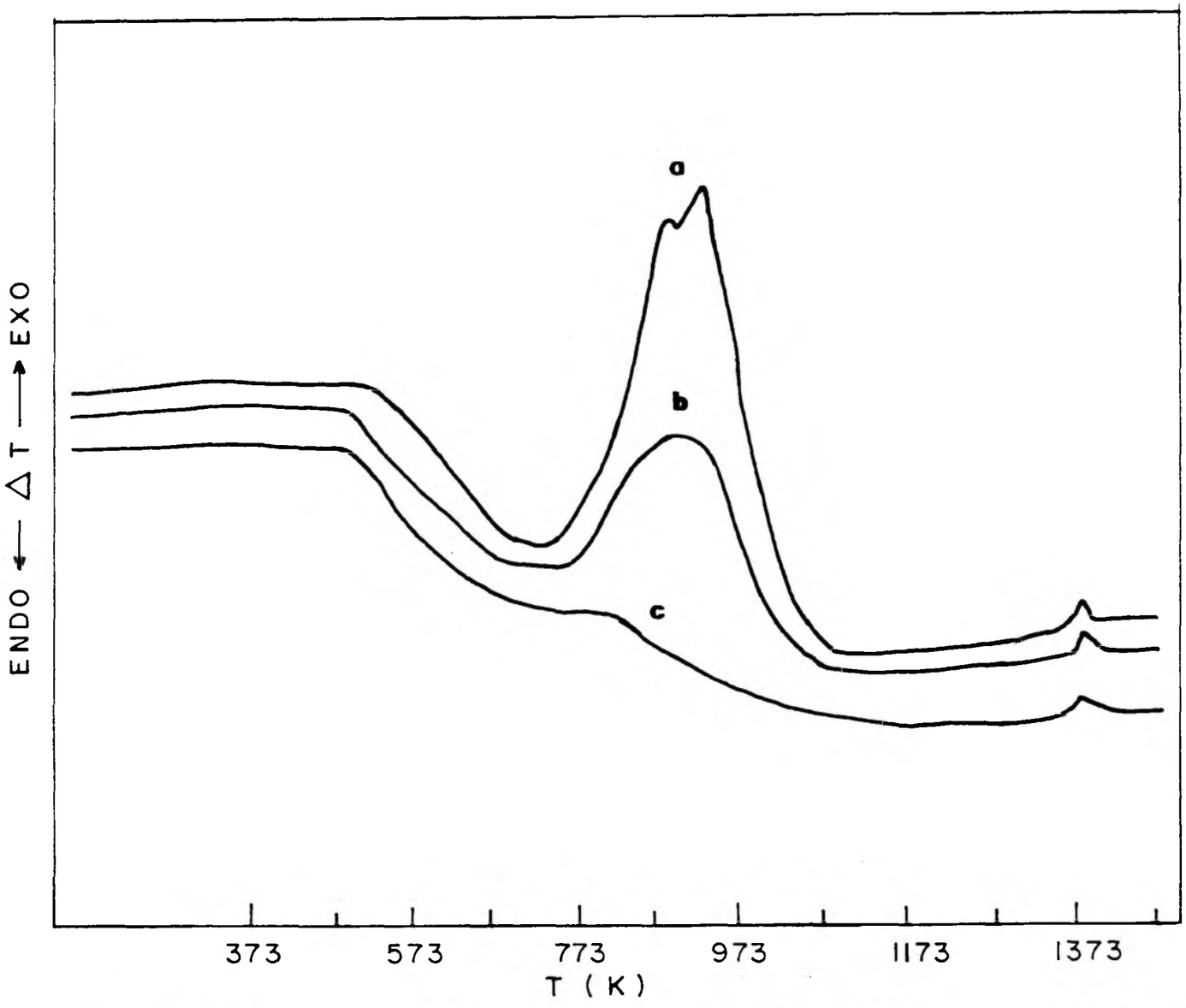

FIG. 3·9· DTA CURVES OF EU-1 PREHEATED AT 723 K FOR VARIOUS INTERVALS, t: (a) t = 0h, (b) t = 9 h, (c) t = 24 h

sample was removed and its DTA curve recorded (curve b Fig 3.9) A third sample was removed after another 15 h at 723 K, and its DTA pattern (curve c) is also shown in Fig 3.9. It is seen that calcination in flowing air at 723 K for 24 h is adequate to remove the organic template from the as-synthesized EU-1 zeolite.

3.3.3.NITROGEN ADSORPTION

Nitrogen adsorption isotherms for Al-Na-EU-1 zeolites with varying crystallinity (estimated from XRD data) are shown in Fig 3.10a. The isotherms exhibit different behaviour for samples with low and high crystallinity. For highly crystalline samples, a very rapid uptake at low relative pressure followed by a flat region at increased relative pressure was observed, while for low crystalline zeolites slow and sluggish uptake with increased relative pressure was observed. Fig 3.10 b shows a plot of the amount of nitrogen sorbed at P/P_o = 0.5 (in cc per g of zeolite) Vs X-ray crystallinity. A straight line plot with positive intercept is obtained.

The values of BET surface area for various Na-EU-1 zeolites synthesized at different synthesis time and the 100 % crystalline samples with different SiO_2/M_2O_3 (M= Al^{+3} or Fe^{+3}) ratios are given in Table 3.2 and 3.3. The surface area is found to decrease with the increase in Si/M ratio. This may be a consequence of either larger crystallites obtained with higher Si/M ratio or of the occlusion of the amorphous matter.

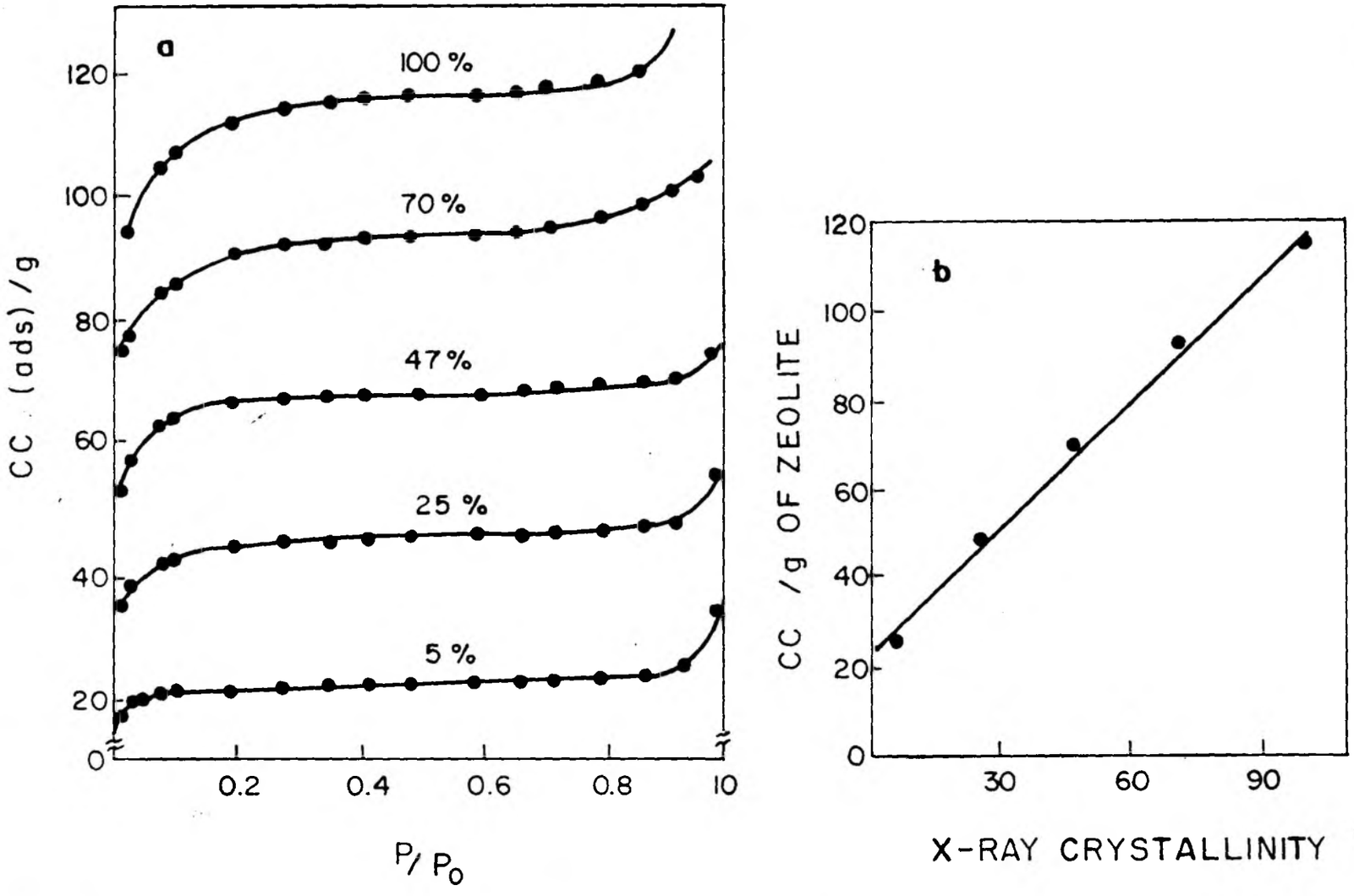

FIG. 3·10 (a) NITROGEN ADSORPTION ISOTHERMS OF Na-Al-EU-1 SAMPLES OF DIFFERENT CRYSTALLINITY. (b) RELATION BETWEEN AMOUNT OF NITROGEN ADSORBED Vs X-RAY CRYSTALLINITY (P / Po = 0.5)

Table 3.2 Effect of synthesis time on surface area and void volume of Al-EU-1 zeolites*.

Synthesis time (hrs)	Surface area (m^2/g)		Void volume (cc/g)
	BET	Langmuir	
50	60	83	0.021
78	190	260	0.067
100	250	295	0.088
120	310	408	0.110
200	348	470	0.123

*. SiO_2/Al_2O_3 = 283, Na_2O/SiO_2 = 0.058, OH^-/H_2O = 0.011, T=423 K.

Table 3.3 Surface area and void volumes for 100 % crystalline Na-EU-1 zeolites*.

Sample	Surface area (m^2/g)		Void volume (cc/g)
	BET	Langmuir	
Na-EU-1 (115)(48)	385,400	485,512	0.135, 0.139
Na-EU-1 (180)(78)	379,390	480,507	0.133, 0.136
Na-EU-1 (283)(117)	348,378	470,488	0.123, 0.132
Na-EU-1 (525)	290	420	0.102

*. Bracketed figures indicate SiO_2/Al_2O_3 ratio.
Underlined numbers indicate data for Fe-EU-1.

3.3.4. SORPTION PROPERTIES

The sorption of water, n-hexane and cyclohexane in EU-1 zeolites of different SiO_2/M_2O_3 ratios(M=Al^{+3} or Fe^{+3}) are given in Table 3.4.

The values in Table 3.4 are comparable with those reported by Casci et al.[146] (6.9, 9.5 and 1.1 wt% for H_2O and n-hexane and cyclohexane, respectively). The salient features of the Table 3.4 include almost constant adsorption capacities for n-hexane and cyclohexane, irrespective of SiO_2/M_2O_3 ratio. The amount of uptake of water decreases with an increase in SiO_2/M_2O_3 ratio. Uptake of water is indicative of the relative hydrophobicity/hydrophilicity of the zeolite and is dependent on the SiO_2/M_2O_3 ratios. In case of Fe-EU-1 the water uptake values are nearly twice than that of the Al-EU-1 analogs due to the lower SiO_2/Fe_2O_3 values. The equilibrium sorption of the comparatively larger molecules of cyclohexane (molecular diameter = 0.62 nm) is only 1.9 %.

3.3.5. ADSORPTION ISOTHERMS OF n-BUTYLAMINE

Fig 3.11 shows family of the isotherms of n-butylamine(n-BA) sorption in EU-1 zeolites with different Si/Al ratios. Most of the isotherms exhibit type I (Langmuir type). Almost 75% of the total sorption takes place over a very narrow range of relative pressures. Initially the basic n-BA molecules interact with the sorption centres of higher strength (usually acidic hydroxyls in this case) and volume filling phenomenon may be operative.

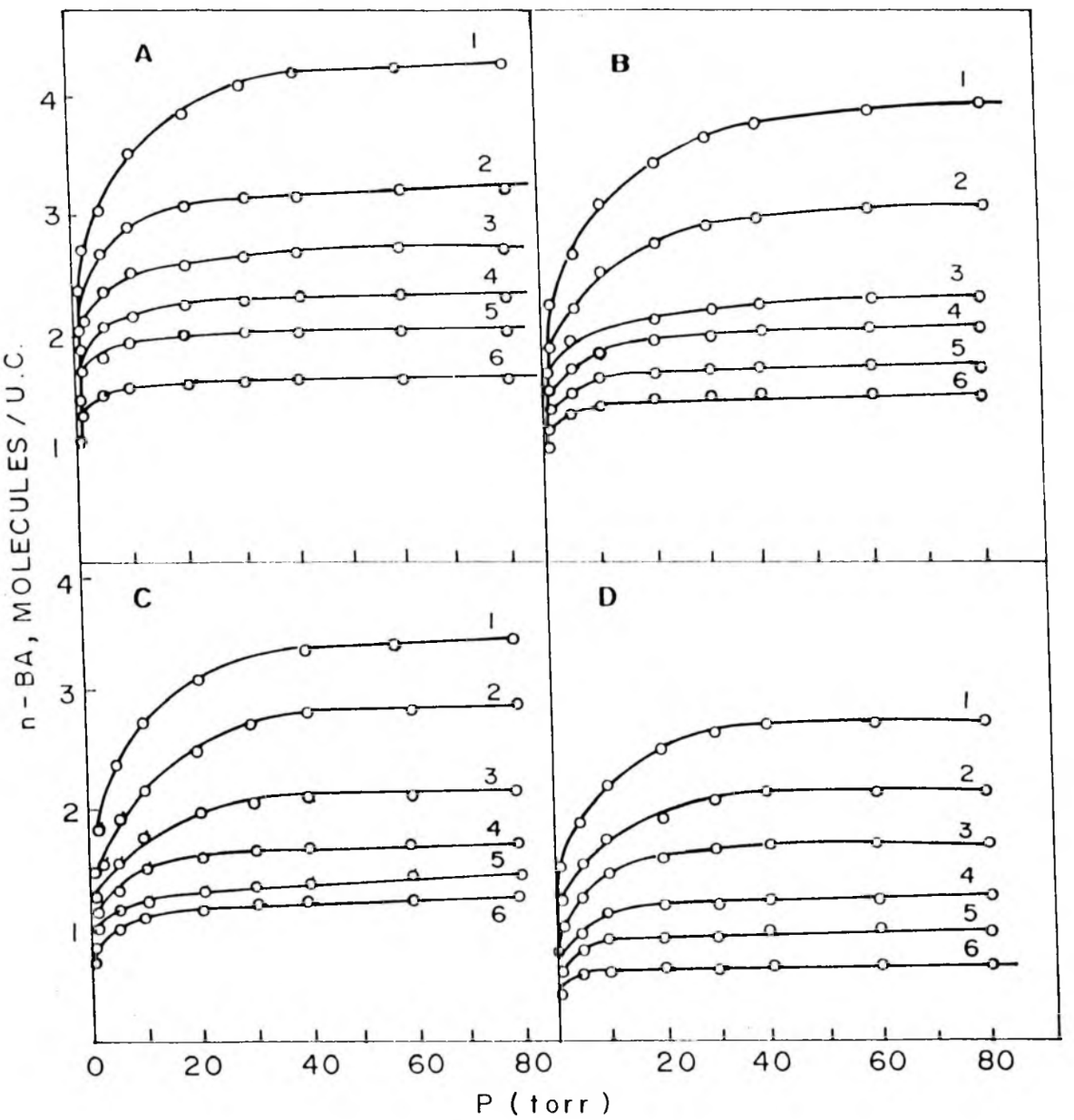

FIG. 3·11 n-BA SORPTION ISOTHERMS FOR EU-1 ZEOLITES WITH SiO_2/Al_2O_3 RATIO (A) 115, (B) 180, (C) 283 AND (D) 525 AT 1) 298 K, 2) 323 K, 3) 348 K 4) 373 K, 5) 398 K AND 6) 423 K.

Sorption isotherms show that the equilibrium sorption capacity (molecules/U.C) decreases continuously with the increase in SiO_2/Al_2O_3 of the zeolite. The existence of large side pockets in the framework of EU-1 zeolite, apparently, does not seems to affect the nature of the isotherms. Fig 3.12 shows a systematic hyperbolic decrease in sorption capacity with increase in the SiO_2/Al_2O_3 ratio in EU-1 zeolites over the entire temperature range between 298-423 K of the isotherm.

Table 3.4 Influence of SiO_2/M_2O_3 ratio the sorption properties of Na-EU-1 zeolites.

Sample (R)[a]	Amount adsorbed (g/100 g of zeolite)					
	Al-EU-1			Fe-EU-1		
	H_2O	n-C_6H_{14}	C_6H_{12}	H_2O	n-C_6H_{14}	C_6H_{12}
115 (48)	5.89	8.23	1.56	10.5	8.82	1.87
180 (78)	5.02	8.20	1.72	9.0	8.79	1.92
283(117)	4.52	8.47	1.90	7.8	8.90	1.82
525	3.95	8.11	1.88	--	--	--

[a]. SiO_2/M_2O_3 ratio (M = Al^{+3} or Fe^{+3})

bracketed figures are Fe samples

P/P_o = 0.8 at 298 K.

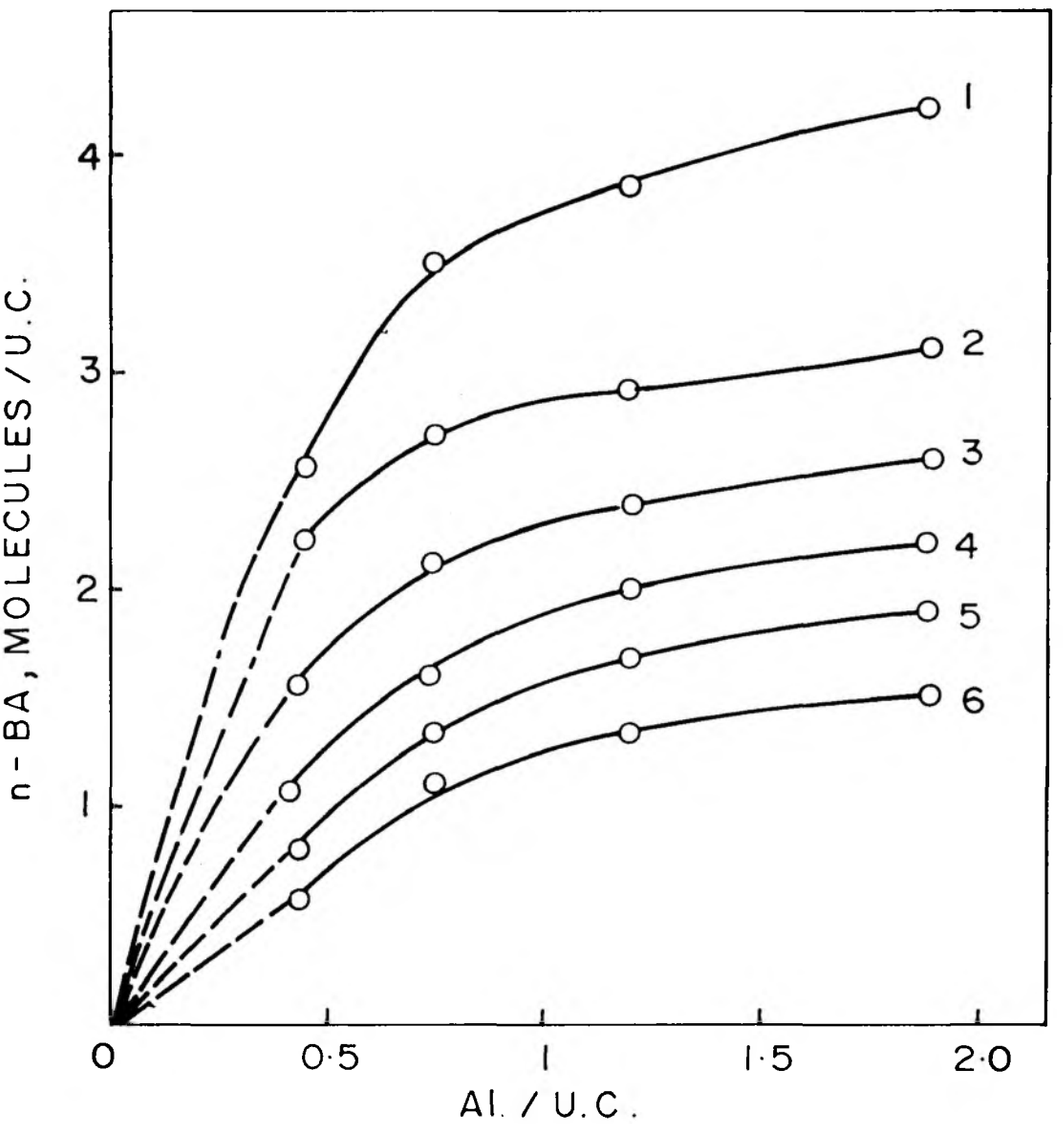

FIG. 3.12. SORPTION CAPACITY AS A FUNCTION OF Al/U.C AT (1) 298 K, (2) 323 K, (3) 348 K, (4) 373 K, (5) 398 K AND (6) 423 K.

3.3.6. APPLICATION OF ISOTHERM EQUATIONS

3.3.6(A). DUBININ ISOTHERM EQUATION

An analysis of the sorption data in terms of various isotherm equations always yields useful information. An attempt is made here to the apply Polanyi"s Potential theory modified by Dubinin and Radushkevich[193] for the n-BA sorption over the entire temperature range (298-423 K) in zeolites EU-1 with silica to alumina ratio ranging from 115-525. The Dubinin-Radushkevich equation is expressed as

$$\text{Log } W = \text{Log } W_o - B/2.303\,\beta^2[T \text{ Log } P_o/P]^2 \quad \text{-------> (8)}$$

where W is the amount sorbed at equilibrium pressure P;and W_o is the total sorption capacity; β is a constant independent of temperature and characteristic of sorbent pore structure; and is the affinity coefficient. The Dubinin plots so obtained were reasonably linear and they deviated from linearity with increasing SiO_2/Al_2O_3. This could be due to the occlusion of amorphous material in the channels of EU-1 zeolites and/or may also be due to the reduced sorption potential on account of decreased framework aluminium with increase in SiO_2/Al_2O_3. Typical Dubinin plots for n-BA sorption in EU-1 zeolites are shown in Fig 3.13. The saturation capacities and B/β^2 (β is affinity coefficient) obtained from intercept on Y axis and slopes respectively of these linear plots are tabulated in Table 3.5. Saturation capacities obtained from Dubinin plots are in general in close agreement with those obtained experimentally indicating that the data on sorption of the n-BA in EU-1 zeolites

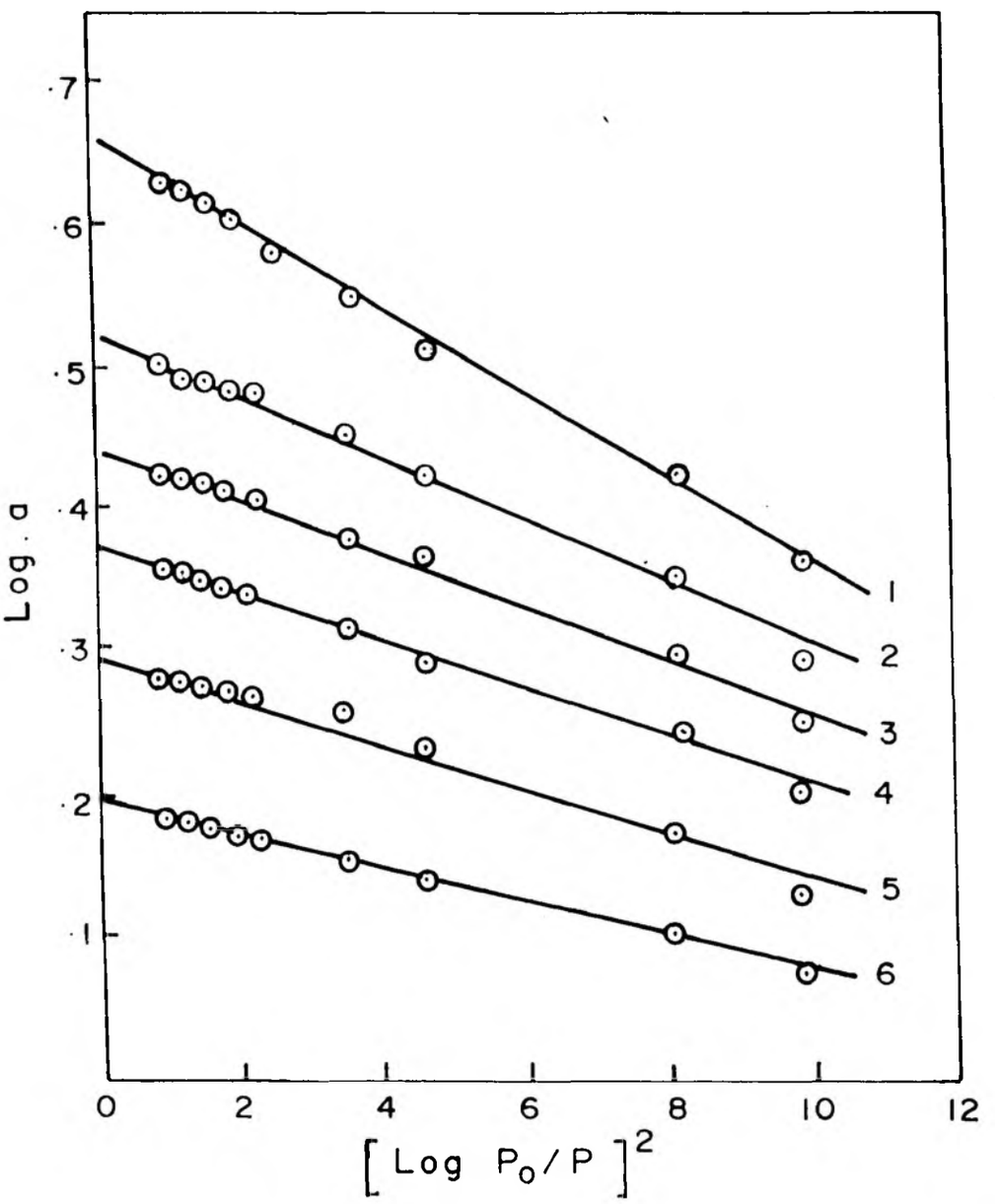

FIG.3.13: DUBININ PLOTS FOR n-BA SORPTION IN EU-1 ZEOLITE (SiO_2/Al_2O_3 = 115) AT 1) 298 K, 2) 323 K, 3) 348 K, 4) 373 K, 5) 398 K AND 6) 423 K.

Table 3.5. Saturation capacities* and B/β^2 for EU-1 zeolites from Dubinin plots.

Zeolite	298 K		323 K		348 K		373 K		398 K		423 K	
(SAR)	B/β^2	S.C.	B/β^2	S.C.	B/β^2	S.C.	B/β^2	S.C.	B/β^2	S.C.	B/β^2	S.C.
115	0.144	4.45	0.097	3.30	0.086	2.74	0.062	2.30	0.055	1.94	0.053	1.54
180	0.188	4.15	0.158	3.19	0.107	2.41	0.099	2.00	0.081	1.69	0.069	1.40
283	0.190	3.65	0.184	3.00	0.156	2.25	0.115	1.69	0.112	1.38	0.100	1.20
525	0.201	2.67	0.189	2.17	0.178	1.59	0.152	1.10	0.114	0.83	0.110	0.57

* Expressed in molecules/U.C.

S.C. = Saturation Capacity.

(SiO_2/Al_2O_3 < 283) could be satisfactorily represented by the Dubinin-Radushkevich equations. The saturation capacities decrease with increasing temperature and also with the SiO_2/Al_2O_3 ratio in the zeolite. On the other hand, the affinity coefficient, β, is found to increase with increase in the temperature / decrease in silica to alumina ratio.

3.3.6(B). BET ISOTHERM EQUATION

The application of the BET equation, the sorption of the n-BA in EU-1 zeolites yields typical linear plots and are shown in the Fig 3.14. The saturation capacities (monolayer capacitiy) obtained from the slopes of these linear plots(Table 3.6) are in good agreement with those obtained by the Dubinin equation. The linearity of the plots indicates that the n-BA sorption data of EU-1 zeolites can be described by the BET sorption model.

3.3.6(C). LANGMUIR ISOTHERM EQUATION

The n-BA sorption data were fitted to the Langmuir isotherm equation. Langmuir plots so obtained were linear for all the samples at the isotherm temperatures. Typical plots are shown in Fig 3.15. The saturation capacities (Table 3.6) obtained from the slopes of these plots are in close agreement with those obtained from the Dubinin equation and the BET equation. Both the Langmuir and BET equations could yield linear plots for the sorption of acidic molecules like CO_2 in cation exchanged Y type zeolites[194]. The sorption data of basic molecule like n-BA in

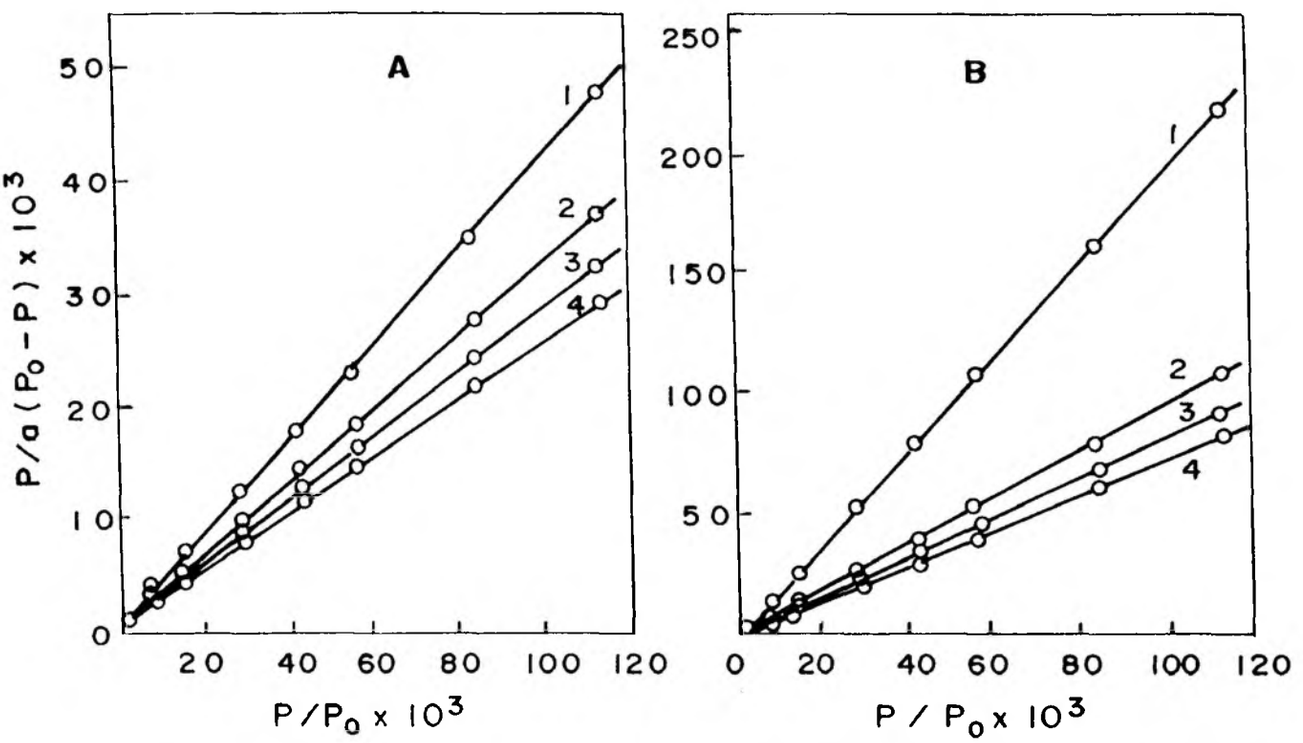

FIG. 3·14 BET PLOTS FOR n-BA SORPTION AT (A) 298 K AND (B) 423 K IN EU-1 ZEOLITES WITH SiO_2/Al_2O_3 RATIO (1) 525, (2) 283, (3) 180 AND (4) 115.

Table 3.6. Comparison of Saturation Capacities of EU-1 Zeolites

Temp. (K)	Method	Saturation capacities (molecules/u.c) for zeolites with SAR			
		115	180	283	525
298	Experimental	4.25	3.87	3.36	2.62
	BET	4.09	3.47	3.30	2.38
	Langmuir	4.25	3.88	3.37	2.63
323	Experimental	3.15	3.00	2.78	2.20
	BET	2.87	2.70	2.68	2.01
	Langmuir	3.15	3.00	2.80	2.21
348	Experimental	2.67	2.35	2.07	1.58
	BET	2.53	2.10	2.02	1.42
	Langmuir	2.69	2.36	2.08	1.60
373	Experimental	2.28	1.98	1.61	1.10
	BET	2.02	1.77	1.45	1.01
	Langmuir	2.30	1.98	1.63	1.10
398	Experimental	1.93	1.69	1.33	0.82
	BET	1.76	1.50	1.21	0.70
	Langmuir	1.94	1.61	1.34	0.82
423	Experimental	1.52	1.36	1.25	0.57
	BET	1.44	1.30	1.03	0.51
	Langmuir	1.53	1.36	1.15	0.58

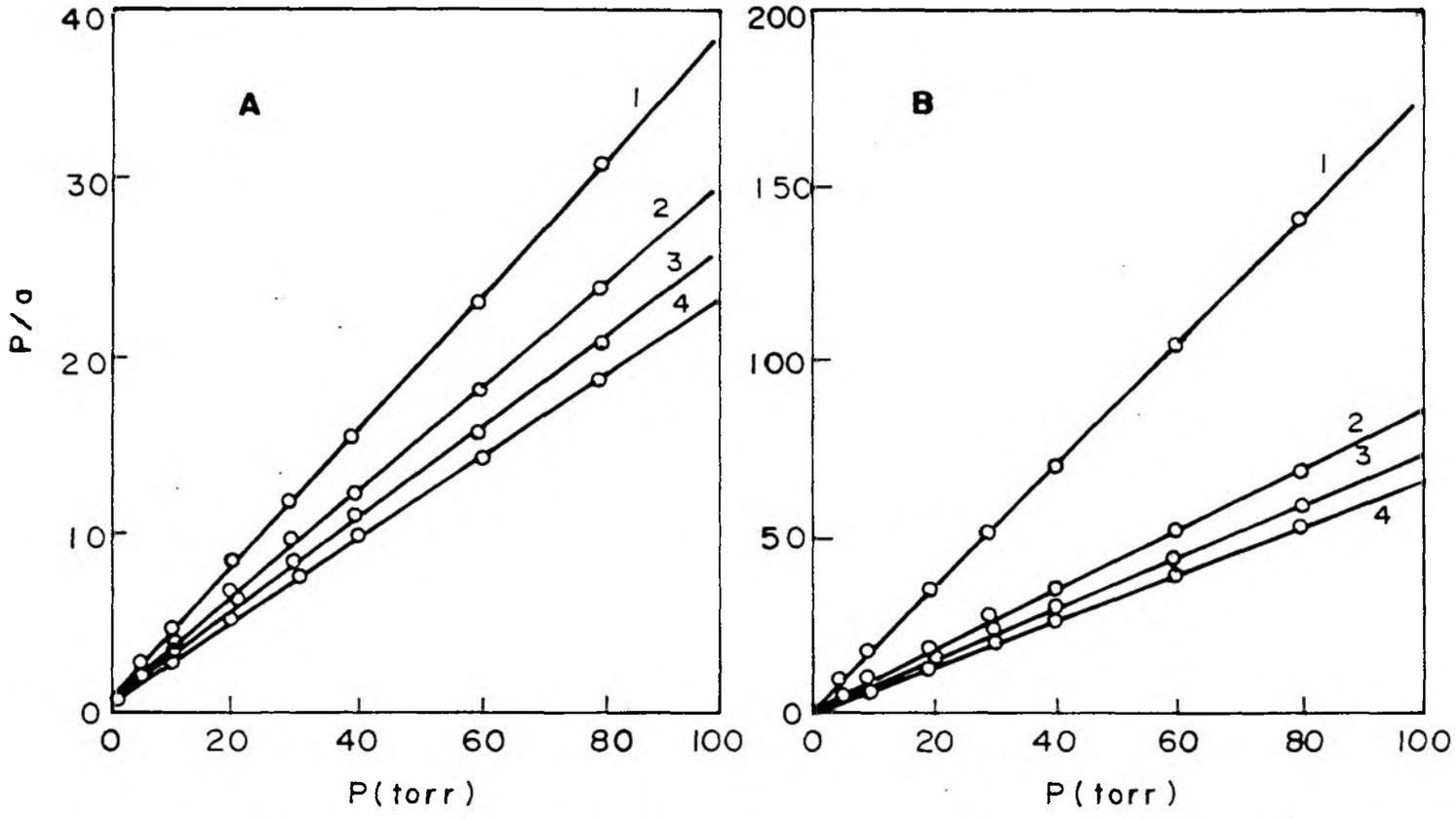

FIG. 3·15 LANGMUIR PLOTS FOR n-BA SORPTION AT (A) 298 K AND (B) 423 K IN EU-1 ZEOLITES WITH SiO_2/Al_2O_3 RATIO 1) 525, 2) 283, 3) 180 AND 4) 115.

ferric exchanged Y zeolites, gave linear Langmuir plots[195]. It was suggested [195] that the n-BA sorption is localized and a basic molecule like n-BA possesses a strong interaction with the acidic protons along with other acidic species. In the present studies, on account of localized sorption of n-BA and strong interaction with the acidic protons in EU-1 zeolites, both the Langmuir and BET isotherm equations yield linear plots and they represent the n-BA sorption data satisfactorily.

Sips equation[196] based on localized sorption with the sorbate-sorbate interaction was satisfactorily applied to CO_2[194] and NH_3[197] in cation exchanged Y zeolites. However, Sips equation was not found applicable for the n-BA sorption in the present studies. Similarly, Koble-Corrigan[198] isotherm equation based on the exact solution for dissociative sorption of sorbate molecules on two active centres could not represent the n-BA sorption data in EU-1 zeolites.

Physical models, such as those of Langmuir and Volmer, for the sorbed state describe an idealized systems and may not be applicable to the real systems, on account of deviations arising from surface heterogeneity, multilayer formations and mutual interactions between the sorbed molecules. Nevertheless, these equations have been found [194,197] to give satisfactory analysis of equilibria in energetically homogeneous systems and provide a basis for discussion of the extent of deviations in energetically heterogeneous systems. However, in the present studies on the sorption of n-BA in EU-1 zeolites, plots of K_L, K_V $\ln K_L$ & $\ln K_V$

against coverage were non-linear. The K_L Vs θ plots were curved showing increase upto a coverage of 0.8 and then passing through a maximum followed by a sharp decrease upto θ=1. $\ln K_L$ against θ plots yielded a characteristic curve with a gradual increase upto θ=0.9 and then a very sharp increase upto θ=1. No meaningful deductions were obtained from these plots.

3.3.6(D). CHEMICAL AFFINITY AND THE SELECTIVITY OF THE SORBED PHASE: A decrease in chemical affinity takes place when a gas at a standard pressure P_o is transformed reversibly and isothermally into an infinite amount of sorbent-sorbate mixture over which the equilibrium pressure is P. The chemical affinity, when the non-ideality of the sorbate is neglected, may be expressed as

$$\Delta \mu = RT \ln(P/P_o) \quad \text{----------} > \quad (9)$$

The value of $-\Delta\mu$ is often taken[199] as the quantitative measure of the chemical affinity of the sorbate for the sorbent. The plots of $-\Delta\mu$ against amount sorbed also serve as a useful criterian for the comparison of the sorption affinities of probe molecules in various cation exchanged zeolites.

Typical chemical affinity curves for the n-BA sorption in EU-1 zeolites are shown in Fig 3.16. The fig 3.16 shows that there is a constant decrease in the chemical potential with the increased coverage. The decrease becomes sharper as the temperature of the sorption increases. The decrease in the

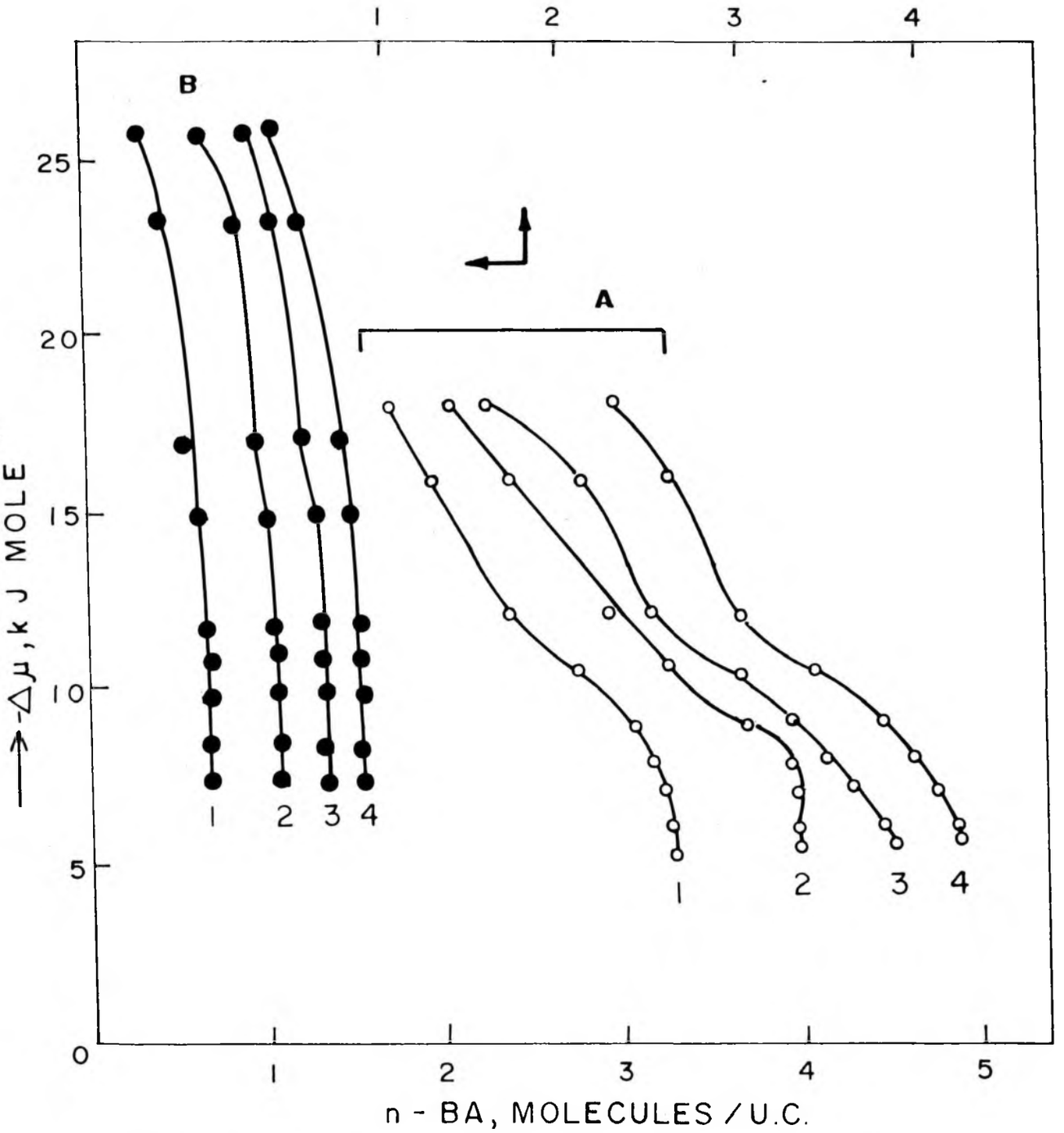

FIG. 3·16 CHEMICAL AFFINITY CURVES FOR n-BA SORPTION AT (A) 298 K AND (B) 423 K IN EU-1 ZEOLITES WITH SiO_2/Al_2O_3 RATIO (1) 525, (2) 283, (3) 180 AND 115.

chemical affinity also becomes comparatively sharper as the silica-alumina ratio in the zeolite decreases(aluminium content of the zeolite increases). Therefore, the affinity follows the sequence as EU-1 (115) > EU-1 (180) > EU-1 (283) > EU-1 (525), over the entire coverage within the temperature range of 298-423 K.

3.3.6(E). ISOSTERIC HEATS OF SORPTION (Q_{st}): The isosteric heat of sorption (Q_{st}) is derived from the sorption isosteres by applying Clausius-Clapeyron equation at a constant sorbate loading using the equation

$$-\Delta \bar{H} = Q_{st} = R \left(T_2T_1/T_2-T_1 \right) \ln(P_2/P_1) \text{ ----------> } (10)$$

If Q_{st} is temperature independent, the plots of ln(P) against 1/T should be linear. In the present studies isosteres for the n-BA sorption in EU-1 zeolites were found to be linear within experimental errors. Table3.7 lists the isosteric heats of n-BA sorption in EU-1 zeolites. Since this is an indirect method of evaluation of isosteric heat, Table 3.7 shows variation in Q_{st} values for all the zeolites over wide rangee of coverage. At the coverage of 1.11 molecules/U.C. the sequence in the isosteric heat is EU-1 (115) [130 kJ $mole^{-1}$] > EU-1 (180) [60 kJ, $mole^{-1}$] > EU-1 (283) [53 kJ, $mole^{-1}$] > EU-1 (525) [42 kJ, $mole^{-1}$]. This indicates that isosteric heats (Q_{st}) at lower coverage decreases with the decrease in aluminium content in the zeolite. Similarly Table 3.7 shows that, initially Q_{st} values decrease with the coverage i.e., n-BA molecules initially interact with

the acidic framework hydroxyls of higher strength. Once these hydroxyls get solvated n-BA molecules then interact with framework hydroxyls of lower strength. The initial decrease in the Q_{st} becomes sharp as the aluminium content increases (i.e., SiO_2/Al_2O_3 decreases). Similarly sharp fall in Q_{st} over a very narrow range of coverage indicates that there are very few acidic protons of higher strength. In the higher coverage region the sequence becomes complicated and it may be partly due to the surface heterogeneity. Such a surface heterogeneity was also observed in case of La^{+3} exchanged zeolites of type $Y^{(200)}$ during NH_3 sorption and in Fe^{+3} exchanged zeolites of type $Y^{(195)}$ during n-BA sorption. Following the intial decrease in Q_{st} in the highest coverage region, in the present studies for the n-BA sorption in EU-1 zeolites, there are maximas and minimas in Q_{st} curves.

Table 3.7. Isosteric Heats (Q_{st}) of n-BA Sorption on EU-1 zeolites

Zeolite	Q_{st} (kJ mol^{-1}) at coverages (n-BA molecules/u.c.)								
	0.50	0.75	1.00	1.25	1.50	1.75	2.00	2.50	3.25
115	--	--	--	119.0	54.0	61.5	46.0	49.0	40.0
180	--	--	--	57.0	39.0	36.5	52.0	65.0	63.5
283	--	--	49.0	51.5	52.0	42.5	49.5	34.0	36.0
525	14.5	39.	41.0	41.5	49.0	48.5	50.0	--	--

3.3.7. INFRARED SPECTROSCOPY

The IR spectra of H-Al-EU-1 zeolites shown in Fig 3.17. have been found to be practically identical with that of Na-Al-EU-1 spectra in the 300-1300 cm^{-1} region. The assignment of IR lattice vibrations in the frequency range 300-1300 cm^{-1} for EU-1 zeolite is given in Table 3.8.

Table 3.8. Framework vibration frequencies for Na-Al-EU-1 zeolite.

Wavenumber(Cm^{-1})	Assignment
450 wsh	Si-O bending
470 vs	Si-O bending
572 s	---
590 msh	ELC5
620 msh	ELC5
698 w	ELDRSS
720 w	ITSS
748 w	ELSS
795 s	ELSS
858 w	--
970 sh	ITAS
1080 vs	ITAS
1215 s	ITAS

ELC5 = external link complex 5-membered ring;
ITSS = internal tetrahedral symmetric stretch;
ELSS = external link symmetric stretch;
ITAS = internal tetrahedral asymmetric stretch;
ELDRSS = external link double-ring symmetric stretch;
s = strong;
sh = shoulder;
w = weak;
v = very
m = medium

The most intense absorption band occurs in the 950-1100 cm^{-1} region and is related to the T-O asymmetric stretching vibration (T= Si or Al). This vibration is sensitive to the Si/Al ratio, and is shifted to higher frequency with increasing content of silica[201]. The masses of Si and Al are nearly same. The

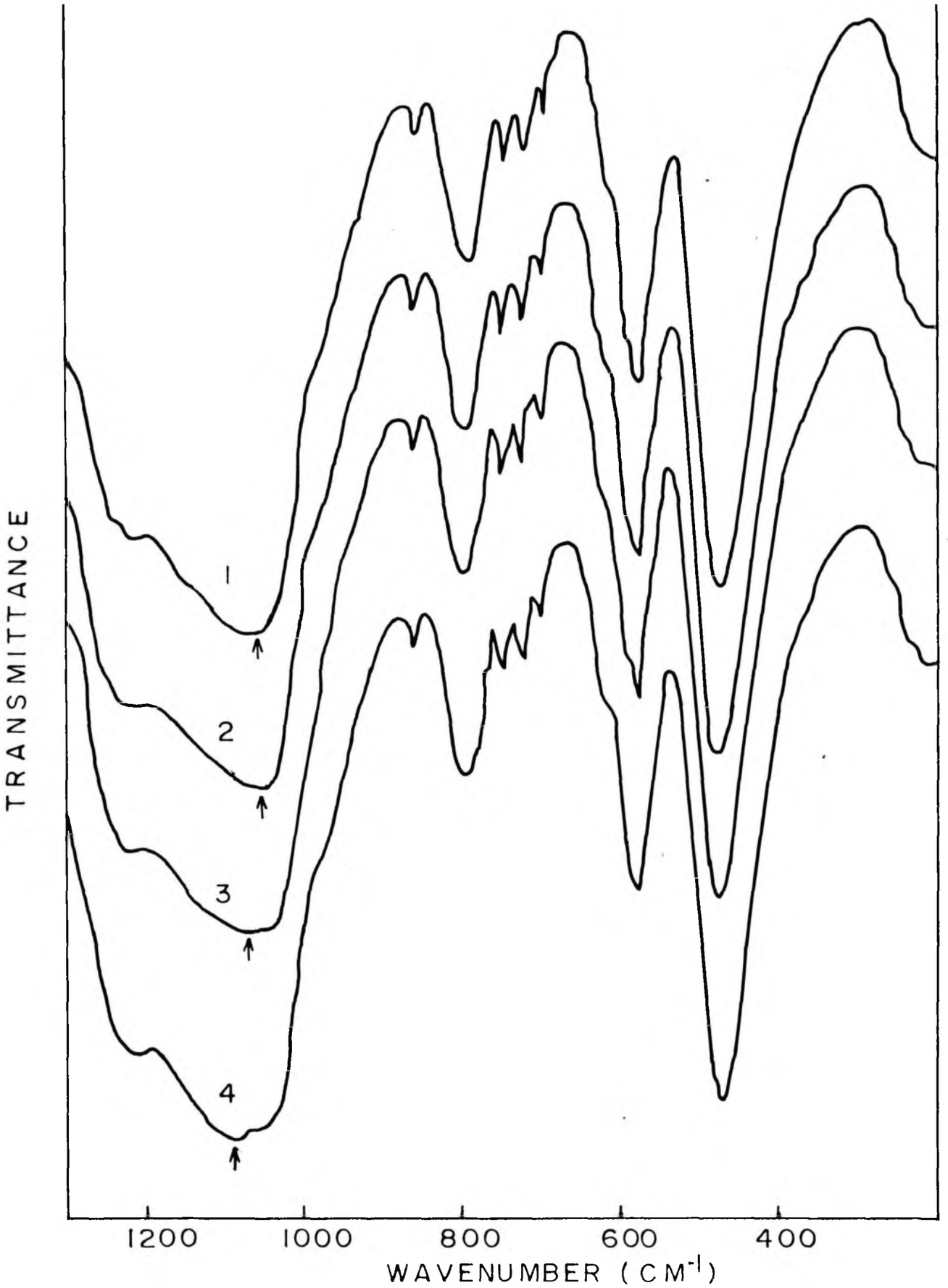

FIG.3·17. IR SPECTRA OF Al-H-EU-1 ZEOLITES 1-4 REFER SiO_2/Al_2O_3 115, 180, 283 AND 525 RESPECTIVELY.

increase in frequency with increase of Si content is related to the Al-O vibration. The lower electronegativity of Al causes a decrease in the force constant[86] of the Al-O bond and causes the frequency shift. A similar shift for varying SiO_2/Al_2O_3 ratio in zeolite had been reported by many authors[86,201,202].

3.3.8. SOLID STATE ^{29}Si AND ^{27}Al MAS-NMR

^{29}Si MASNMR spectra of as-synthesized Al-EU-1 samples with varying Al contents are shown in the Fig 3.18a. The samples exhibit two lines corresponding to Si atoms with one [at δ = -98 ppm = Si(1Al)] and zero [at δ = -110 ppm = Si(0Al)] aluminium atoms in their second coordination sphere. The NMR line intensity of Si(1Al) δ = -98 ppm is found to decrease with decrease in Al content of the samples, in accordance with the previous observations[203] for the other zeolite frameworks. In the case of higher SiO_2/Al_2O_3 ratio samples (Fig 3.18a curve 3 and 4) the line at δ =-110 ppm splits into two lines (δ = -108 ppm and = -112 ppm)indicating two crystallographically different environments of Si in high silica EU-1 zeolite[204].

It is well known that ^{27}Al nmr spectroscopy is able to distinguish between tetrahedrally and octahedrally coordinated aluminium atoms[204]. The ^{27}Al NMR spectra for samples 1,2,3 and 4 (Fig 3.18b) show a single signal at aboutδ= 52-55 ppm relative to $Al(H_2O)_6^+$ species, which is characteristic of the tetrahedrally coordinated Al atoms. Absence of a line around zero ppm with respect to $Al(H_2O)_6^{+3}$ confirms that there is no

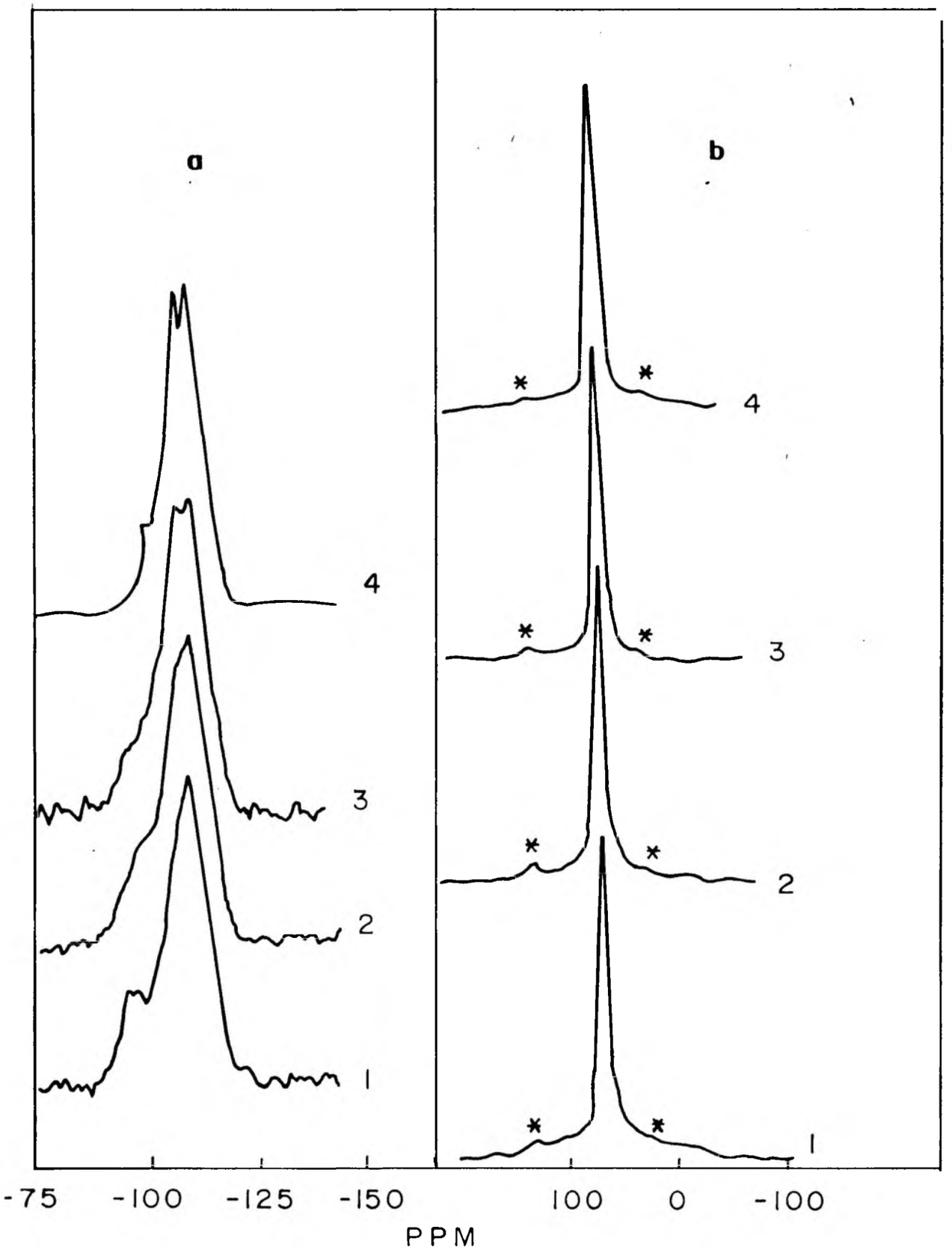

FIG. 3·18. MAS NMR SPECTRA OF AS-SYNTHESIZED Al-EU-1 SAMPLES WITH 1) 115, 2) 180, 3) 283 AND 4) 525 (a) ^{29}Si AND (b) ^{27}Al.

significant octahedrally coordinated -Al species. Most of the aluminium present is tetrahedrally coordinated in the Al-EU-1 zeolite framework.

3.3.9. TEMPERATURE PROGRAMMED DESORPTION OF AMMONIA (TPD)

Zeolite Al-EU-1 series: Acid strength distribution can be derived from the rate of desorption of chemisorbed ammonia at increasing temperatures. The zeolites release the NH_3 over a wide temperature range. The experimental technique adopted for TPD has been described previously. The ammonia TPD profiles for H-Al-EU-1 and H-Fe-EU-1 are shown in Figure 3.19. The acid strength distribution is tabulated in Table 3.9.

Three distinct stages for desorption of ammonia at about 300-373, 373-500 and 500-775 K were observed. Anderson et al.[109] have observed four TPD peaks around 400-430, 470-490, 550-600 and 780-800 K for the desorption of NH_3 from ZSM-5 zeolites. The assignment of TPD has been made[93] as follows:

1. The first peak (α -chemisorption state) is due to sites located on the external surface on some type of extraneous material, or due to interaction of ammonia molecules with surface oxide or hydroxide groups by non-specific hydrogen bonds.

2. The second peak (β -chemisorption state) is associated with the crystallites and sodium ions which are known to act as adsorption centres for NH_3 and also on weak Bronsted acid sites.
3. The third peak (γ -chemisorption state) which occurs at 500-

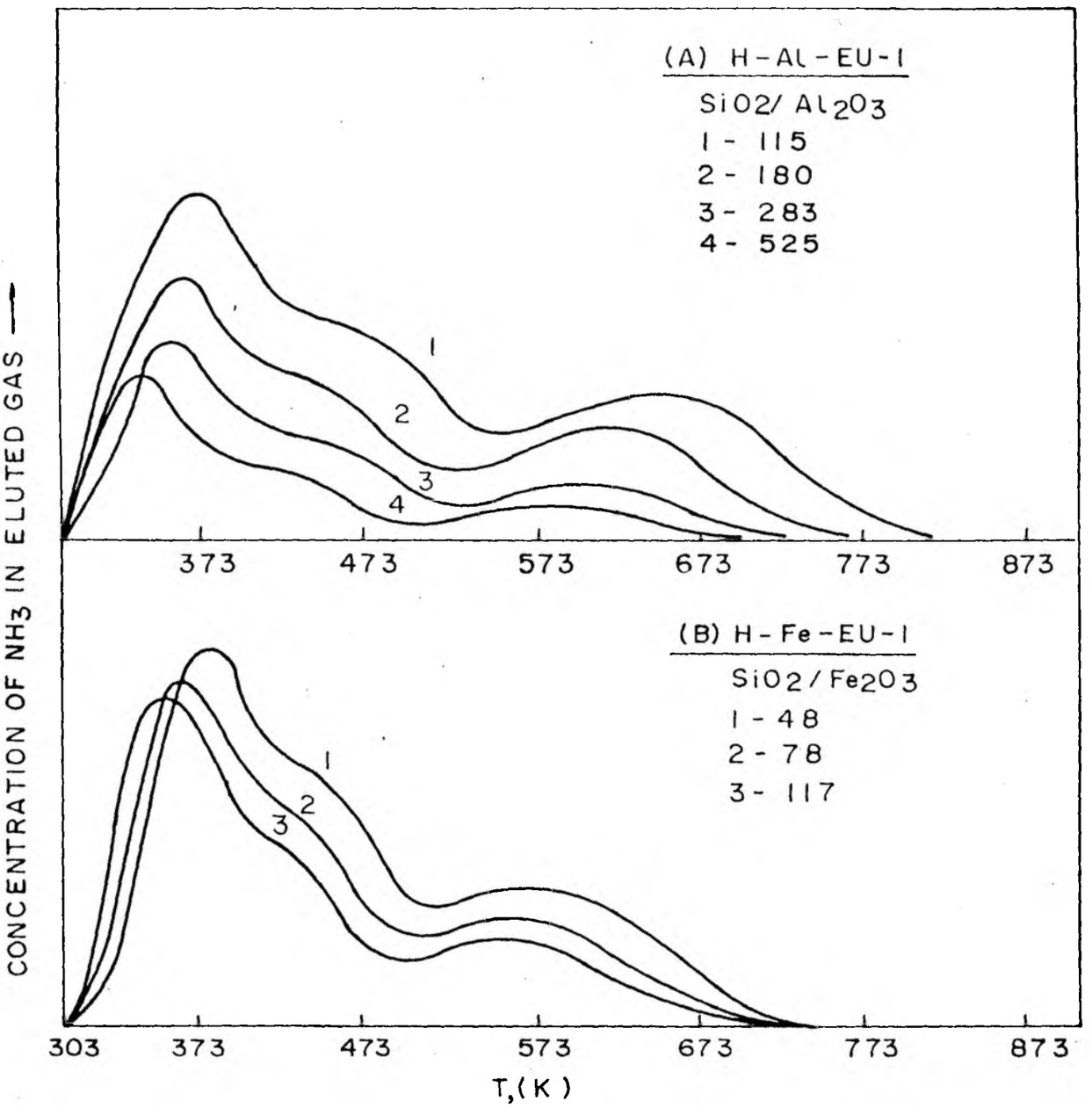

FIG. 3·19. TPD SPECTRA OF NH_3 FROM A) H-Al-EU-1, B) H-Fe-EU-1 ZEOLITES.

Table 3.9. Acid strength distribution over H-Al-EU-1 and H-Fe-EU-1 zeolites.

Sr.NO.	M*	SiO_2/M_2O_3	Chemisorption of NH_3 in α and β peaks		Chemisorption of NH_3 in γ peak	
			Peak maximum temperature T_{max} K	NH_3 molecules/U.C	Peak maximum temperature T_{max} K	NH_3 molecules/U.C
1.	H/Al	115	473	5.78	643	2.75
2.	H/Al	180	463	3.75	638	1.01
3.	H/Al	283	458	2.32	605	0.71
4.	H/Al	525	458	1.44	593	0.40
5.	H/Fe	48	448	8.09	581	3.23
6.	H/Fe	78	433	7.60	568	1.97
7.	H/Fe	117	423	5.87	563	1.30

*M = Al^{+3} or Fe^{+3}.

775 K is associated with the sorption of ammonia on strong structural Bronsted acid sites.

At higher SiO_2/Al_2O_3 ratio, it is observed that the total acidity decreases. It is expected that an increase in AlO_4 concentration in framework also increases the tendency of framework hydrolysis resulting in extra-lattice $Al(OH)_X^{3-X}$ cationic species[205]. It is also observed that T_{max} for strongest acid sites increases from about 600 to 675 K as the SiO_2/Al_2O_3 ratio decreases from 525 to 115.

Fe-EU-1 series: The nature of TPD spectra for H-Fe-EU-1 catalysts samples is also shown in Figure 3.19B. There is also a significant increase in T_{max} for the α Peak on decreasing SiO_2/Fe_2O_3 ratio. The observed T_{max} values (Table 3.9) in case of H-Fe-EU-1 were found to be lower than that of the corresponding H-Al-EU-1 analog. Based on the observed T_{max} values from TPD and expected bond strength for both the systems we may conclude that acid strength of framework hydroxyl group is in the order H-Al-EU-1 > H-Fe-EU-1.

3.4. SUMMARY

X-ray diffraction, framework IR spectroscopy and thermal analysis studies indicate that the structure of EU-1 zeolite remains stable upto 1273 K. Surface area values were found to decrease with the increase in Si/Al (M= Al^{+3} or Fe^{+3}) ratio. Values of equilibrium sorption capacities for n-hexane and cyclohexane indicates independency with Si/M ratios. However, the water sorption was inversely proportional to the Si/M ratios. The sorption data for cyclohexane confirm that the entry pore size is slightly less than 0.6nm due to the presence of 10 T-atoms windows. The BET, Langmuir and Dubinin isotherm equations were found applicable to n-BA sorption in EU-1 zeolites. The behaviour of chemisorption, chemical affinity curves has been discussed. Isosteric heat (Q_{st}) curves decrease in higher coverage region. Higher aluminium containing zeolite gave higher Q_{st} values. Evidence from ^{29}Si and ^{27}Al MASNMR measurements indicates at least two crystallographically different environments for Si atoms. Studies on the temperature programmed desorption of NH_3 indicate that the acid strength of framework hydroxyl groups in H-Al-EU-1 is greater than that in H-Fe-EU-1.

CHAPTER 4

CATALYTIC REACTIONS OVER EU-1 ZEOLITE CATALYSTS

CONTENTS

4.1. INTRODUCTION

The presence of 10-ring channels, characteristic of medium pore zeolites together with large side pockets, makes zeolite EU-1 interesting from the point of view of shape selective catalysis. In those reactions wherein the product pattern is mainly dominated by the diffusional rates of reactants/products in the zeolitic channels, EU-1 is expected to behave similar to other medium pore zeolites like ZSM-5, ZSM-48 etc,. On the other hand, in those reactions involving bulky transition states and requiring large cavities for their formation, EU-1 is expected to exhibit lower transition state shape selectivity than conventional medium pore zeolites. Kumar et al.[191] and Weitkamp and co-workers[206-208] have characterized the shape selective properties of EU-1 zeolite in reactions of paraffinic hydrocarbons. It was suggested[209,210] that shape selectivity effects in the isomerisation of m-xylene can also be used as diagnostic tools to reveal not only the size of the pores but also the presence/absence of cavities and dimensionality of the pores in zeolites of unknown structure. It is well known that the ratio of isomerisation to disproportionation in m-xylene conversion can be used as a diagnostic tool to distinguish the differences in transition state shape selectivity of the zeolite catalysts[211].

In this chapter we report the influence of the reaction temperature, WHSV and SiO_2/Al_2O_3 molar ratio on the reactions of m-xylene (isomerisation/disproportionaton) and toluene

(methylation and disproportionation) over H-EU-1 zeolite catalysts. The data are compared with those obtained using other medium pore zeolites.

4.2. EXPERIMENTAL

The catalytic reactions were carried out in a fixed bed, down flow tubular silica reactor, at atmospheric pressure. The reactor consists of a fused silica tube, 2 cm in inner diameter and 35 cm length provided with a thermowell which carries a thermocouple for sensing the reaction temperature. The reactor was inserted in a furnace. The catalyst powder was pressed, pelleted, crushed and sieved to obtain 14-20 mesh particles and 1 g of catalyst (on dry basis) was charged in the middle of the reactor in such a way that the catalyst bed was sandwitched by inert porcelain beeds. The top portion of the reactor, serving as a vapouriser-cum-preheator, was packed with inert porecelain beads. The catalytic reactor assembly shown in Fig 4.1, was attached to a product receiver system consisting of a coil condenser which is cooled by chilled water.

Prior to reaction, the catalyst was activated in a stream of air at 813 K overnight. The catalyst was then flushed with nitrogen and cooled to reaction temperature. The reactants were monitored into the reactor by a syringe pump (SAGE Instruments, Model 352) at a constant feed rate.

The reaction products were passed through the condenser cooled by chilled water. The condensed liquid products were

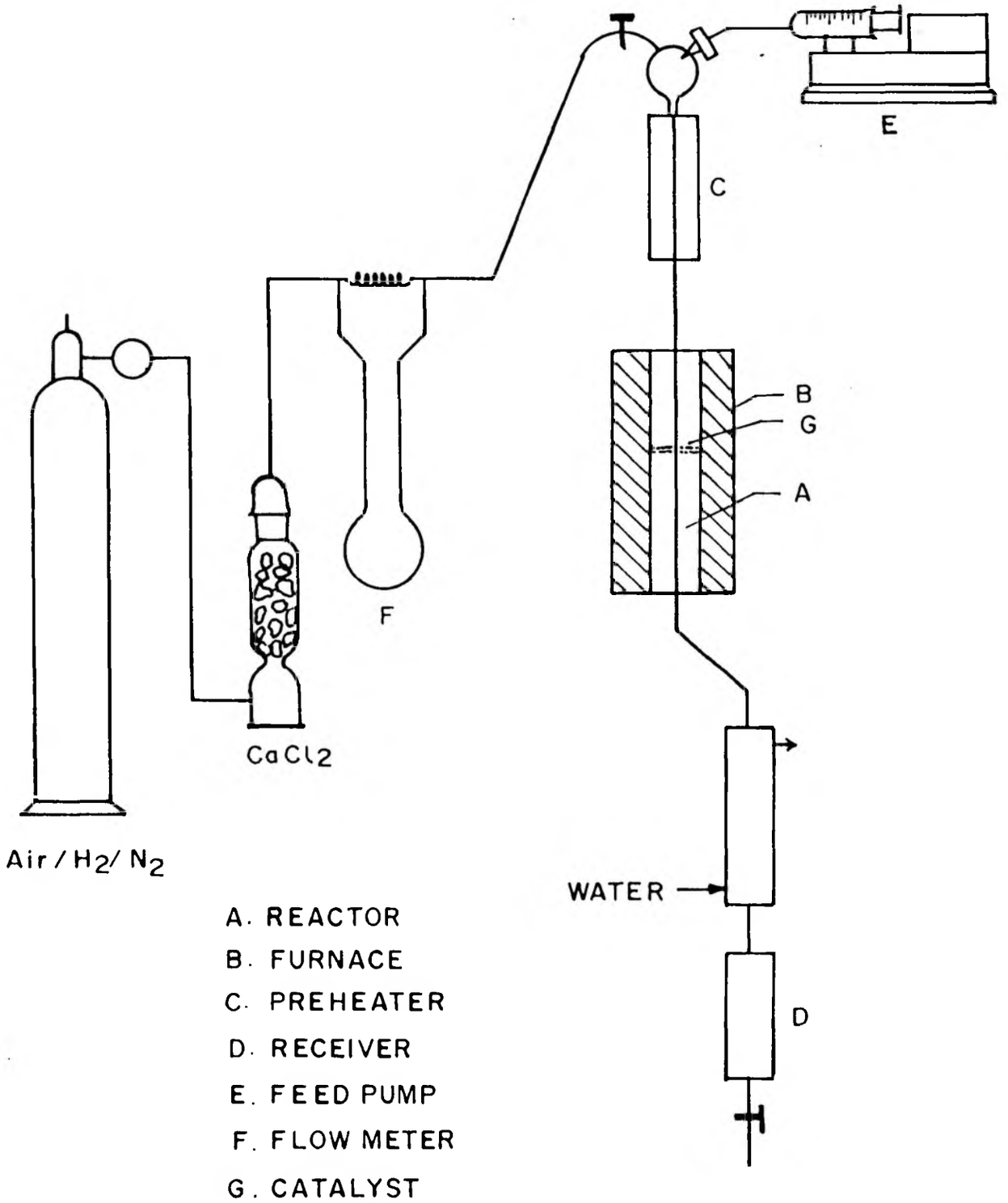

FIG. 4·1 : SILICA REACTOR USED FOR CATALYTIC REACTIONS

collected at fixed intervals and mass balances were routinely carried out in all runs and were found to be better than 97 %. The products were analysed by gas chromatography (Shimadzu) using a 5 % Bentone + 5 % Diisodecyl phthalate column.

4.3. RESULTS AND DISCUSSION

4.3.1. M-XYLENE CONVERSION

The influence of the SiO_2/Al_2O_3 ratio of H-EU-1 on the product distribution in the isomerisation of m-xylene is shown in Table 4.1. Tables 4.2 and 4.3 illustrate the influence of temperature and space velocity. As the SiO_2/Al_2O_3 ratio increases (Table 4.1) the conversion of m-xylene and the concentration of disproportionation products (toluene and trimethyl benzenes) decreases. These are direct consequences of the decreasing concentration or density of the acid sites at higher Si content[212].

In the isomerisation of m-xylene over medium pore zeolites, the relative rates of formations of para and ortho xylenes reflect their diffusionally limited transport in the pore system and may, hence, form the basis for characterising their pore structure. In addition to isomerisation, xylene molecules may also undergo transalkylation and dealkylation, the latter, especially at high temperatures. The ratio of ortho to para xylenes in the xylene fractions and the selectivity for isomerisation (equal to the content of para- and ortho xylenes in

TABLE. 4.1

Influence of SiO_2/Al_2O_3 ratio in zeolite on isomerization of m-xylene over H-EU-1.

Feed, m-xylene-hydrogen(1:4,molar);WHSV,3.5 h^{-1};temperature,633 K; H/oil ratio, 4.

Parameter	SiO_2/Al_2O_3 ratio		
	115	283	530
m-Xylene conversion (%)	38	36.5	14.1
Products (%, w/w):			
Benzene	0.1	--	--
Toluene	3.8	2.0	0.8
p-Xylene	20.2	23.3	9.0
m-Xylene	62.0	63.5	85.9
o-Xylene	9.7	9.0	3.5
1,3,5-TMB[a]	0.6	0.2	--
1,2,4-TMB	3.2	2.2	0.8
1,2,3-TMB	0.3	--	--
Xylene loss (%)[b]	8.0	4.2	1.6
Sel.Isom.[c]	0.77	0.88	0.88
Ortho/para ratio	0.48	0.39	0.39

[a]TMB = trimethylbenzene

[b]Xylene loss = (xylenes in feed-xylenes in products). 100 %.

[c]Selectivity for isomerization = (p-xylene+o-xylene)/(m-xylene converted).

TABLE. 4.2

Influence of temperature on isomerization of m-xylene over H-EU-1

Feed, m-xylene-hydrogen (1:4,molar); WHSV, 3.5 h^{-1}.

Parameter	Temperature (K)					
	543	573	603	633	663	683
Conversion(%,w/w)	3.2	12.1	18.9	38.0	44.0	47.1
Products(%,w/w):						
Benzene	--	--	0.1	0.1	0.1	0.1
Toluene	0.4	1.0	1.7	3.8	4.7	6.1
p-Xylene	1.8	6.5	10.0	20.0	20.3	20.2
m-Xylene	96.8	87.9	81.1	62.0	56.0	52.9
o-Xylene	0.9	3.3	5.1	9.7	13.7	15.3
1,3,5-TMB[a]	--	0.1	0.2	0.6	0.8	0.8
1,2,4-TMB	0.1	1.1	1.6	3.2	4.0	4.4
1,2,3-TMB	--	0.1	0.1	0.3	0.4	0.4
Xylene loss(%)[b]	0.5	2.3	3.7	8.0	10.4	11.8
Sel.Isom.[c]	0.82	0.81	0.80	0.77	0.77	0.74
Ortho/para ratio	0.50	0.50	0.51	0.48	0.67	0.76

[a-c] See Table 4.1.

TABLE. 4.3

Influence of WHSV on isomerization of m-Xylene over H-EU-1

Feed, m-xylene-hydrogen (1:4,molar); temperature, 633 K.

Parameter	WHSV (h^{-1})			
	3.5	7	13	17.5
Conversion (%,w/w)	38	29	13.9	4.2
Products (%,w/w):				
Benzene	0.1	0.1	--	--
Toluene	3.8	2.6	1.0	0.4
p-Xylene	20.2	16.2	8.1	2.4
m-Xylene	62.2	71.0	86.9	95.8
o-Xylene	9.7	7.5	3.8	1.2
1,3,5-TMB[a]	0.6	0.3	0.1	--
1,2,4-TMB	3.2	2.3	0.9	0.2
1,2,3-TMB	0.3	0.2	--	--
Xylene loss (%)[b]	8.0	5.5	2.0	0.6
Sel.Isom.[c]	0.79	0.82	0.85	0.86
Ortho/para ratio	0.48	0.46	0.47	0.50

[a-c]See Table 4.1.

the total reaction products) are used in the present study, as the indices of the shape selectivity of EU-1.

4.3.2. PX/OX RATIO

The para/ortho ratio, an index of the product shape selectivity of the zeolite [213] is around 2.2 ± 0.2for EU-1 (Table 4.3). The value decreases beyond this range (Table 4.2) at higher levels of conversion (above 40%) due to secondary reactions. The equilibrium value of this ratio is around 1.0. In Fig 4.2 the PX/OX ratio for all the medium pore zeolites, including EU-1, is plotted against conversion. The value of this ratio is higher than equilibrium composition i.e., 1.0. Even though all the three zeolites possess a normal 10-ring pore system, the observed differences in this ratios indicate that differences in other parameters, (like channel tortuosity and dimensionality of the pores) may lead to subtle differences in the shape selectivity of these zeolites. Based on our results[214], the product shape selectivity of these zeolites may be classified in the following decreasing order : ZSM-23 > ZSM-48 > EU-1 > ZSM-5.

The enhanced para selectivity in m-xylene isomerizatrion in medium pore zeolites, has been observed by various workers [209,210,213,215,216]. The formation of p-xylene can be increased further by dealumination [217,218] or by impregnation with B, P, or Mg compounds [219,220]. The increased para selectivity in meta xylene isomarisation has often been referred to as a

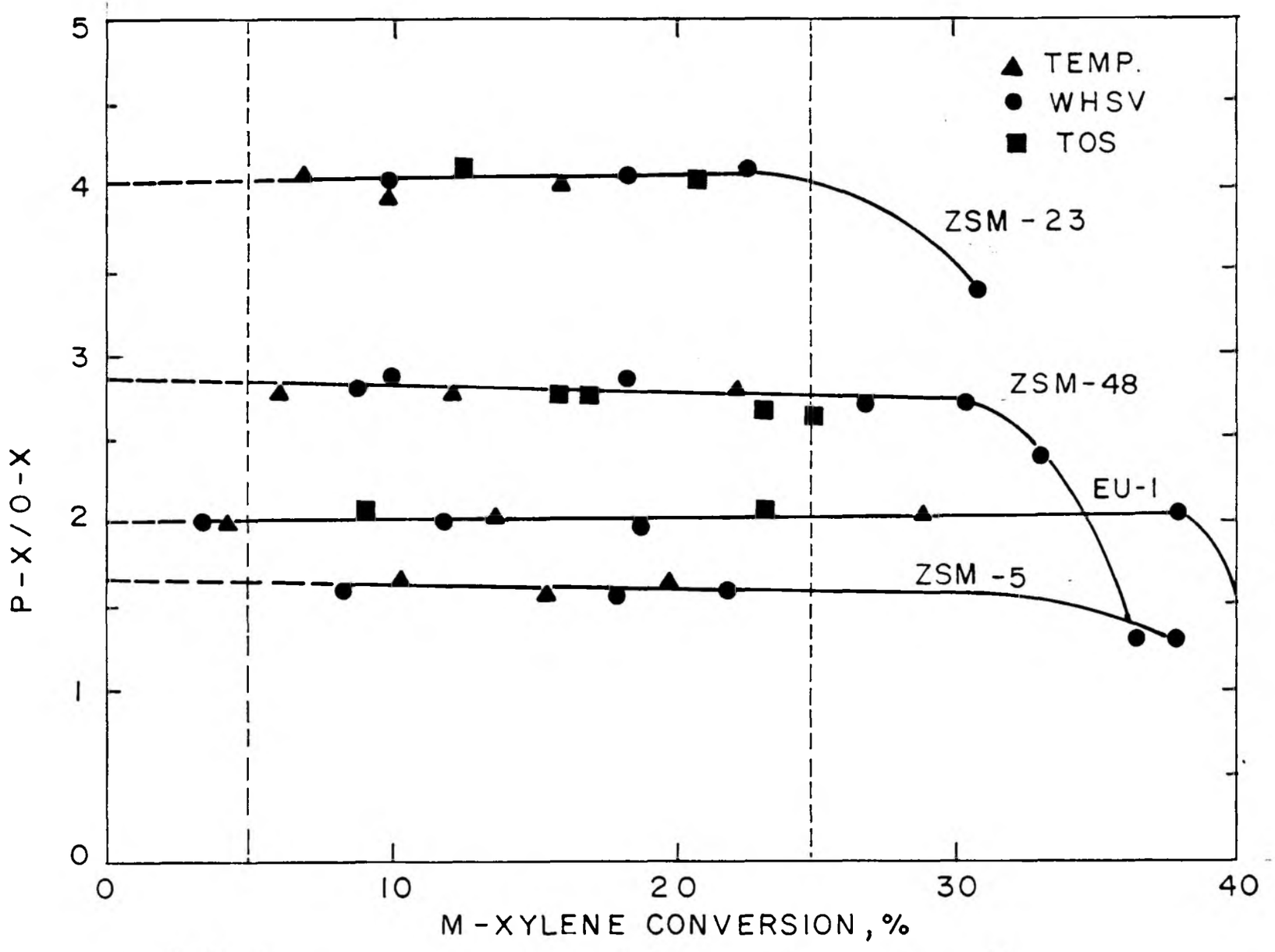

FIG. 4·2. P-XYLENE /O-XYLENE RATIO AGAINST M-XYLENE OONVERSION.

classical example of PSS, controlled by the faster diffusion of the para isomer. Isomerization of xylenes is commonly explained via classical 1,2 methyl shift mechanism (scheme-1a). In more constrained systems, such as modified ZSM-5 type zeolites, a direct interconversion of o- to p-xylene[219], the so called leakage [217] mechanism,(scheme-1b) has also been put forward to account for the increased para selectivity. Recently, in a detailed report [209] on m-xylene conversion over a large number of zeolites, it was pointed out that apart from PSS, the possibility of RTSS(due to the difference in the shape and size of protonated transition states required for the formation of p-, and o-xylenes [209,221] should also be considered to account for the para selectivity(scheme-1c). In the absence of convincing experimental evidence in favour of these hypotheses, the enrichment of p-xylene compared to o-xylene in the products of m-xylene isomerization via 1,2 methyl shift is best explained by the PSS. Fig 4.3 illustrates the routes followed in the approach to the equilibrium composition in the isomerisation of m-xylene over H-EU-1. The results are compared with those of ZSM-5 and ZSM-48 and confirm the intermediate product shape selectivity of EU-1.

4.3.3. SELECTIVITY FOR ISOMERISATION

Fig 4.4 illustrates the variation in the selectivity for the isomerisation of m-xylene at various conversion levels for EU-1. For comparative purpose, the results of ZSM-5 and ZSM-48 are also

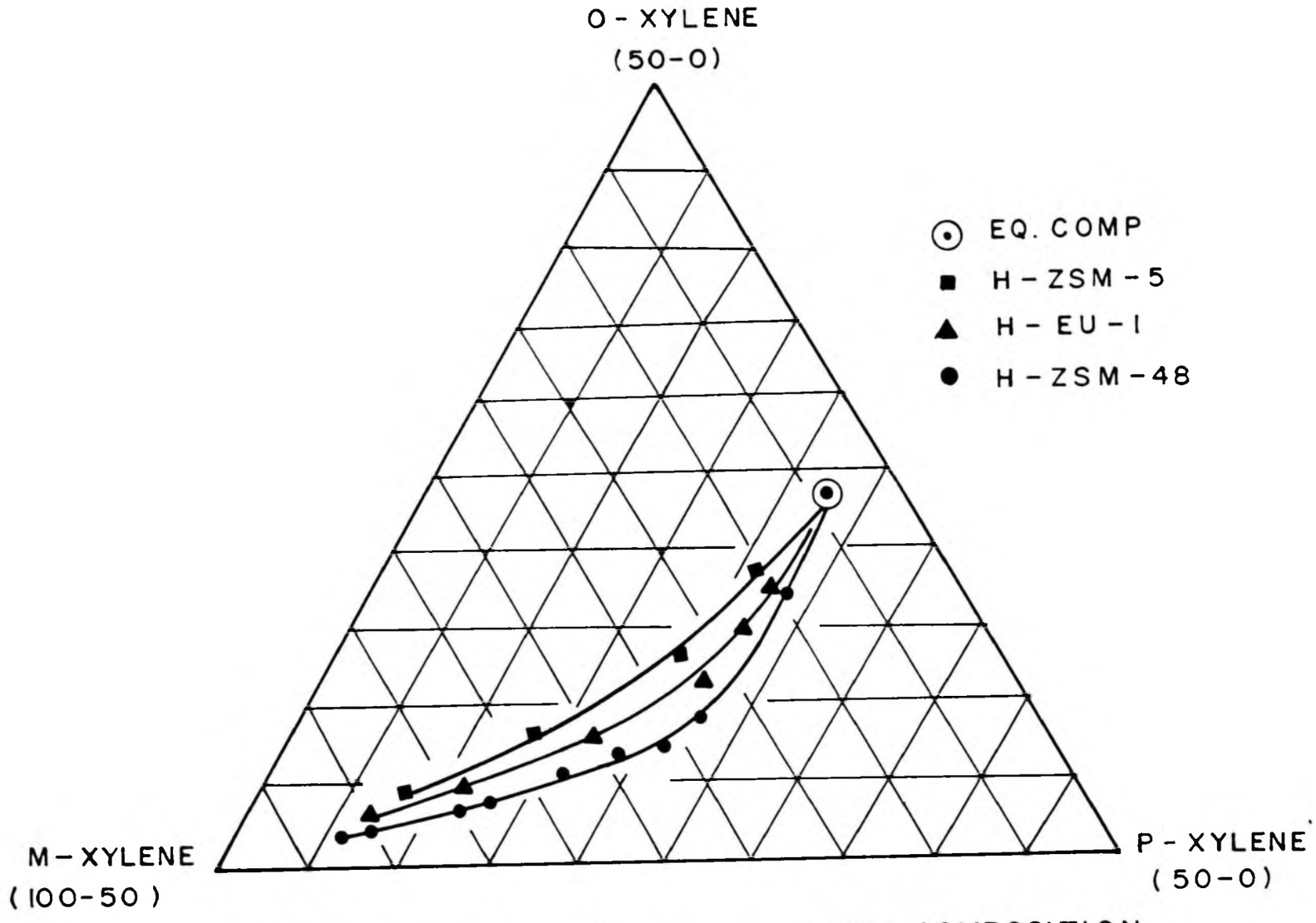

FIG. 4·3. APPROACH TO EQUILIBRIUM COMPOSITION OF XYLENE ISOMERS IN THE ISOMERIZATION OF m-XYLENE.

SCHEME – 1 a

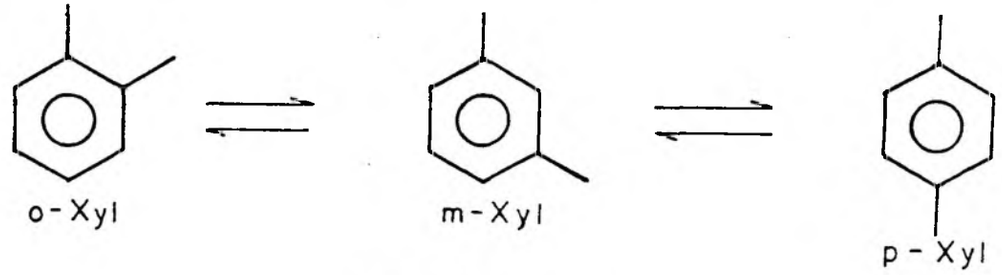

SCHEME – 1 b

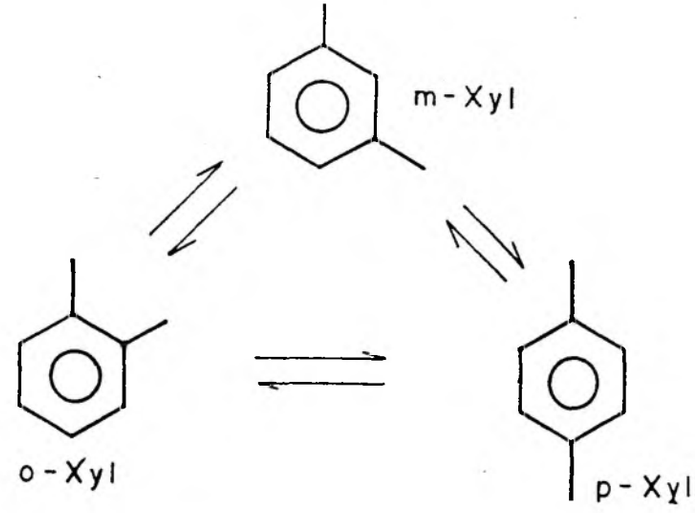

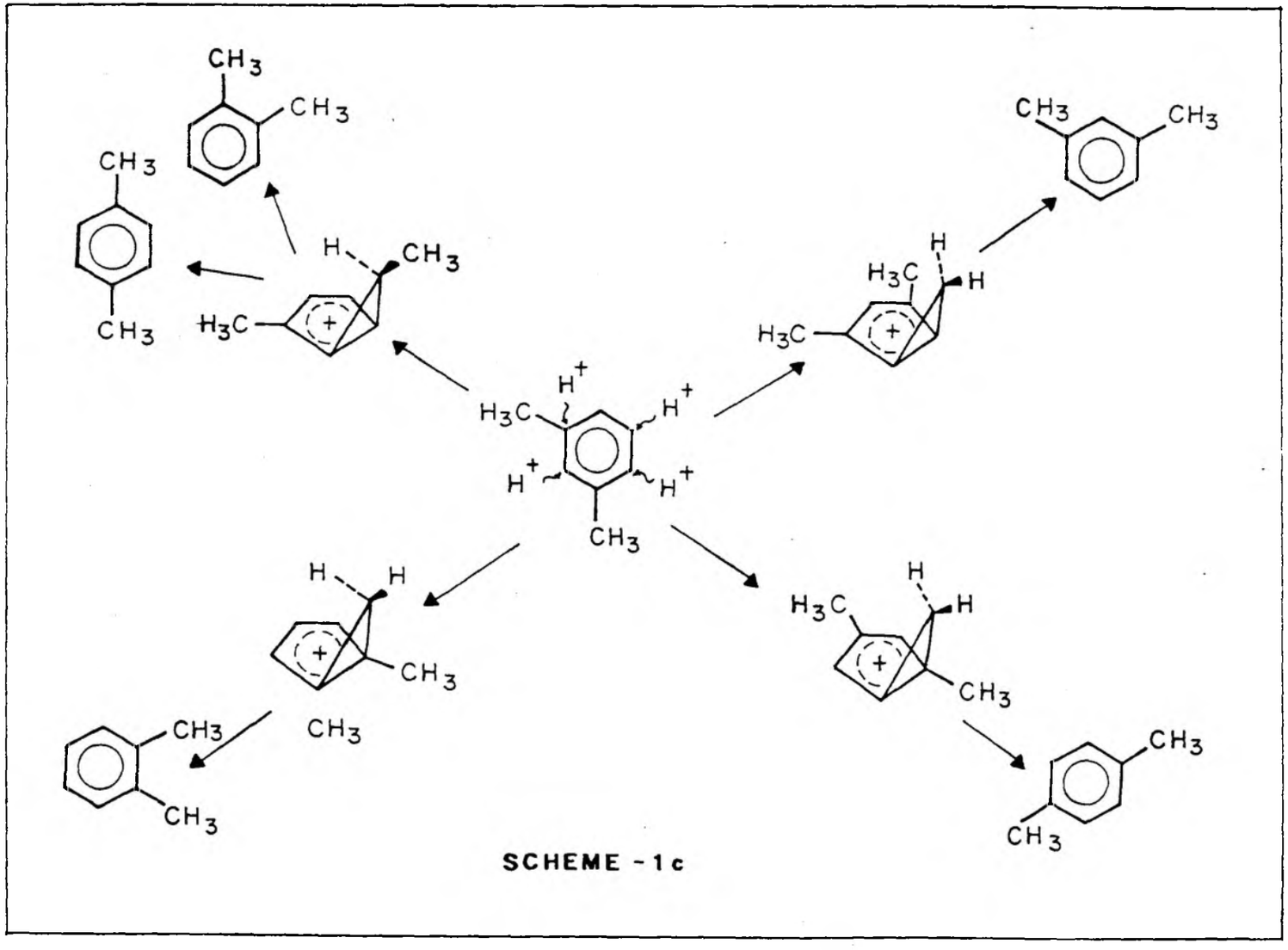

SCHEME - 1c

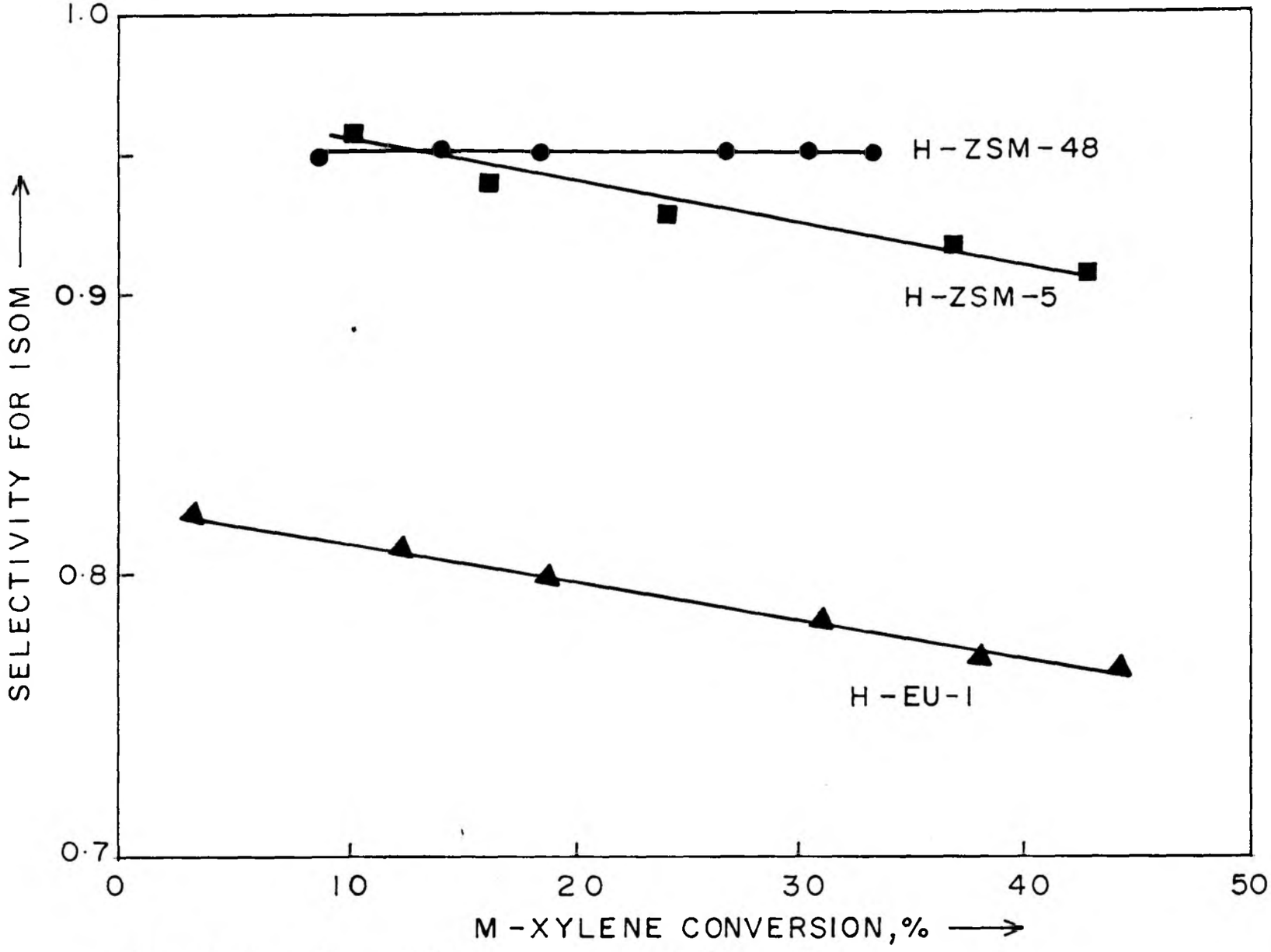

FIG.4.4. SELECTIVITY FOR ISOMERISATION AT VARIOUS LEVELS OF CONVERSION OF m-XYLENE.

included [209,210]. Two features may be noted from Fig 4.4 : (i) At all conversion levels, the three zeolites may be ranked in the decreasing order: ZSM-48 > ZSM-5 > EU-1, (ii) The decrease in the selectivity for isomerisation with increasing conversion of m-xylene is more pronounced for EU-1 and ZSM-5 than for ZSM-48. Earlier[210] it had been found that over ZSM-22 and ZSM-23, the selectivity for isomerisation of m-xylene is insensitive to the conversion level. Even though all the above five zeolites possess 10-membered channels, EU-1 and ZSM-5 differ from ZSM-48, -22 and -23 in one important aspect : The pore system of the former group includes cavities either at the intersection of the pores (ZSM-5) or as side pockets (EU-1), while those of the latter group consist of non-interpenetrating linear channels with no cavities.

The disproportionation of m-xylene into toluene, and trimethyl benzenes, TMBS, is a bimolecular reaction involving large diphenylmethane-type intermediate complexes which are bulkier than both reactants and products [222]. In such cases the intracrystalline void space of the zeolites (such as lobes and cavities either at channel intersections or as side pockets) plays a very important role in controlling the product distribution. The selectivity for TMBs in the products in m-xylene conversion may form a basis to discriminate the zeolites according to the void space contained in their pore system. These results support the suggestion of Weisz [123] and Mavrodinova et al.[223,224] that the I/D selectivity in zeolites depends

mainly on their intracrystalline void space.

Csicsery[225,226] has experimentally proved that the reduced formation of symmetrical trialkylbenzenes such as 1,3,5-trimethylbenzene from m-xylene in MOR (mordenite) is not caused by a limitation of the mobility of these bulky molecules in the pores of MOR, but is rather due to the lack of space to form the bulky transition state. Disproportionation of m-xylene is a bimolecular reaction, involving most probably 1,1-diphenylmethane intermediates, that are bulkier than the reagent and product molecules [222]. It can be anticipated that for the disproportionation of m-xylene, the space available in the cages, lobes and intersections of the zeolite channels will be more important than the dimensions of the pore openings. The reduced rates of transalkylation reactions of alkylaromatics in ZSM-5 have also been ascribed to a molecular shape-selective suppression of bimolecular reactions [211,123]. In principle three different transition states are possible for the disproportionation of m-xylene, resulting in the formation of toluene and 1,3,5- , 1.2.3- and 1.2.4- trimethylbenzene, respectively (scheme 2).

Martens et al. [209] have shown that the size of the intermediate diphenylmethane type complex required to produce the 1.2.4 TMB is smaller than that needed for 1.3.5 or 1.2.3 TMB. For all the 10 membered ring zeolites including EU-1 the 1.3.5 / 1.2.4. TMB ratio (inversely proportional to the shape selectivity of zeolites) is very low and becomes zero at zero

SCHEME-2

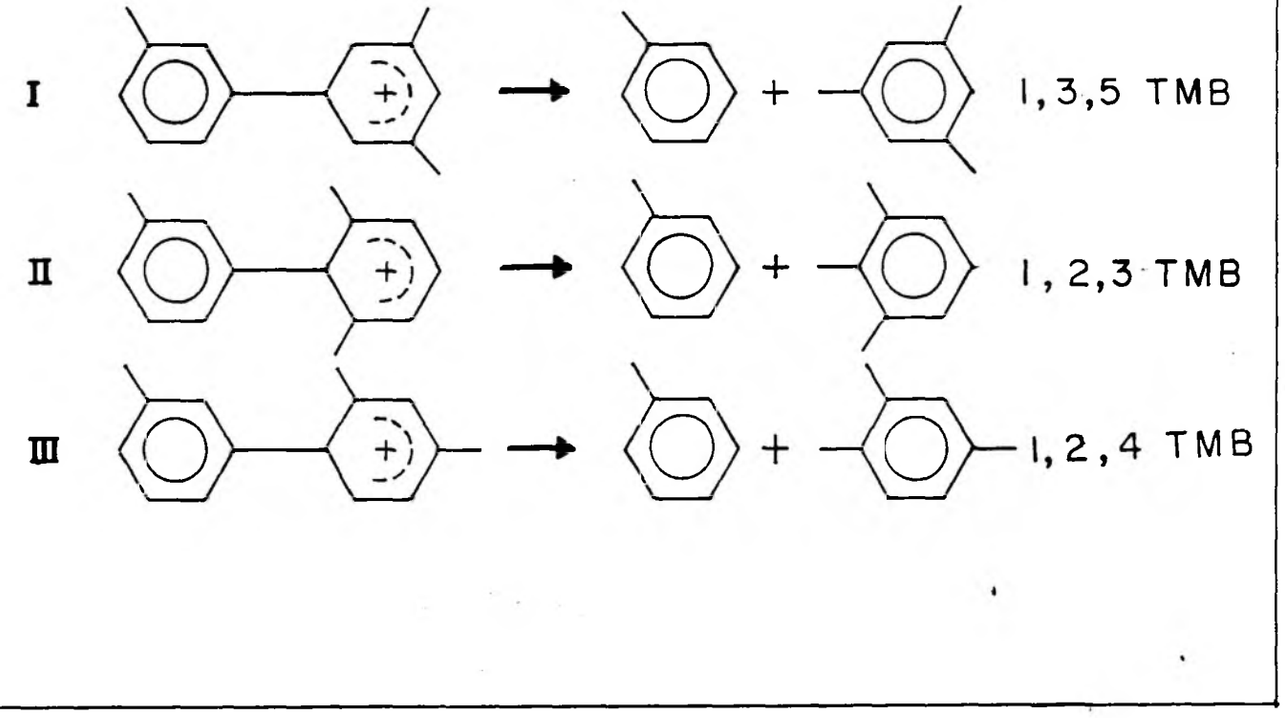

conversion (Fig 4.5). But in the case of all large pore zeolites including ZSM-12, the 1.3.5/1.2.4 TMB ratio remains positive even at zero converion of m-xylene. This suggests that in medium pore zeolites the 1.3.5 isomer is formed probably as a secondary product via isomerization of the 1.2.4 isomer, the primary product of disproportionation.

EU-1 zeolite (similar to ZSM-50) is an interesting zeolite which has large side pockets off the main unidimensional 10-ring channels[71]. Zeolite EU-1 exhibits a high product shape selectivity (Fig 4.2) in agreement with its 10-ring pore openings. However, its log I/D value (Fig 4.6) is comparble to those observed over large pore zeolites like MOR and ZSM-12. This unique feature (a high product shape selectivity combined with a low transition state shape selectivity) is due to the fact that in EU-1, while the channels are constituted by 10-membered rings, the void space in the side pockets is similar to the void volume available around the active sites in large pore zeolites. Using a combination of SI [206], CI*[207], n-decane [207] and ethylbenzene [208] reactions, it was earlier concluded [191] that EU-1 posseses the characteristics of both medium and large pore zeolites. The present results on m-xylene conversion discussed above confirm this and provide quantitative parameters to characterize the shape selectivity of EU-1 zeolite.

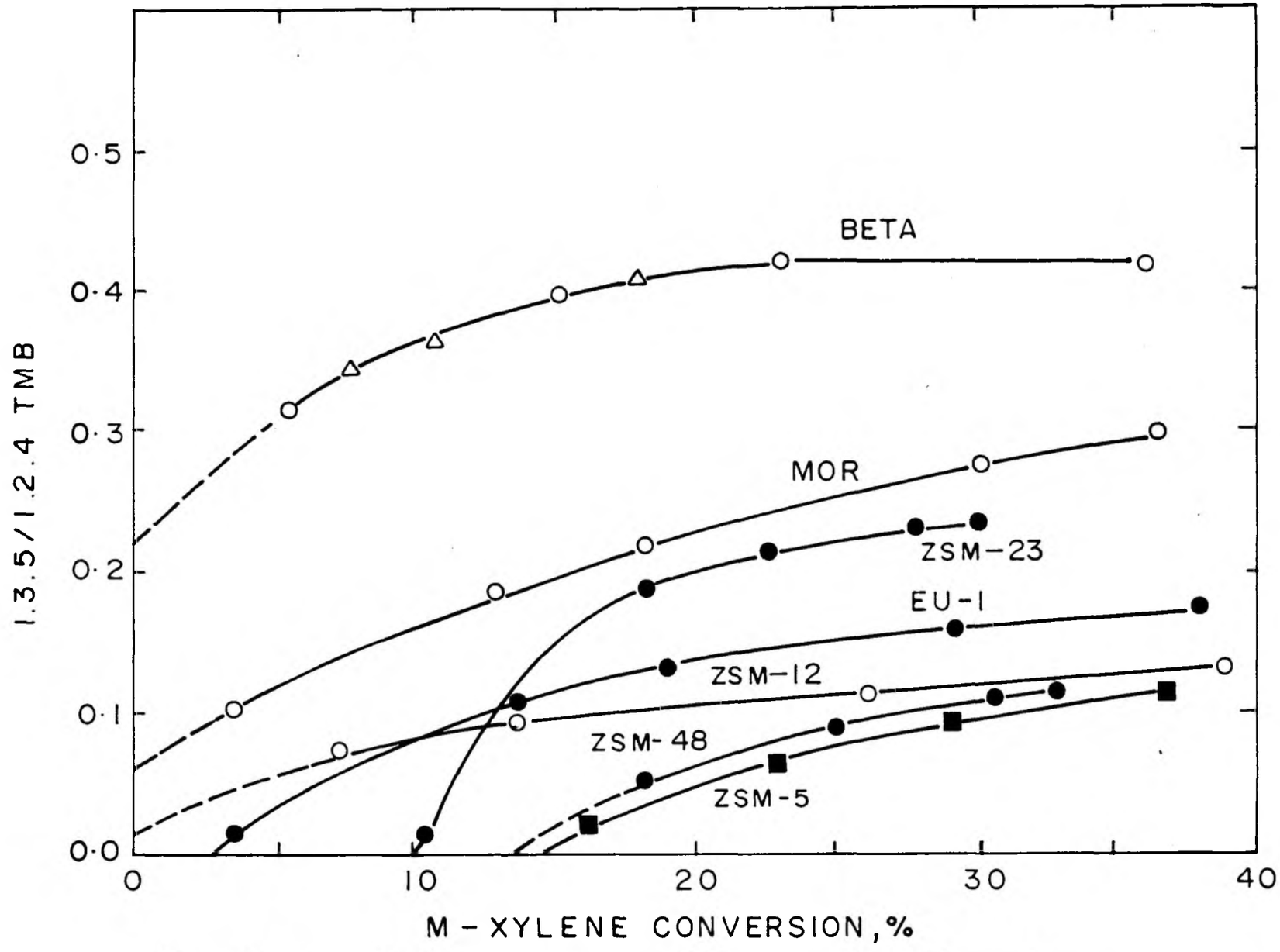

FIG. 4·5. 1.3.5 / 1.2.4 TMB RATIO AGAINST M-XYLENE CONVERSION.

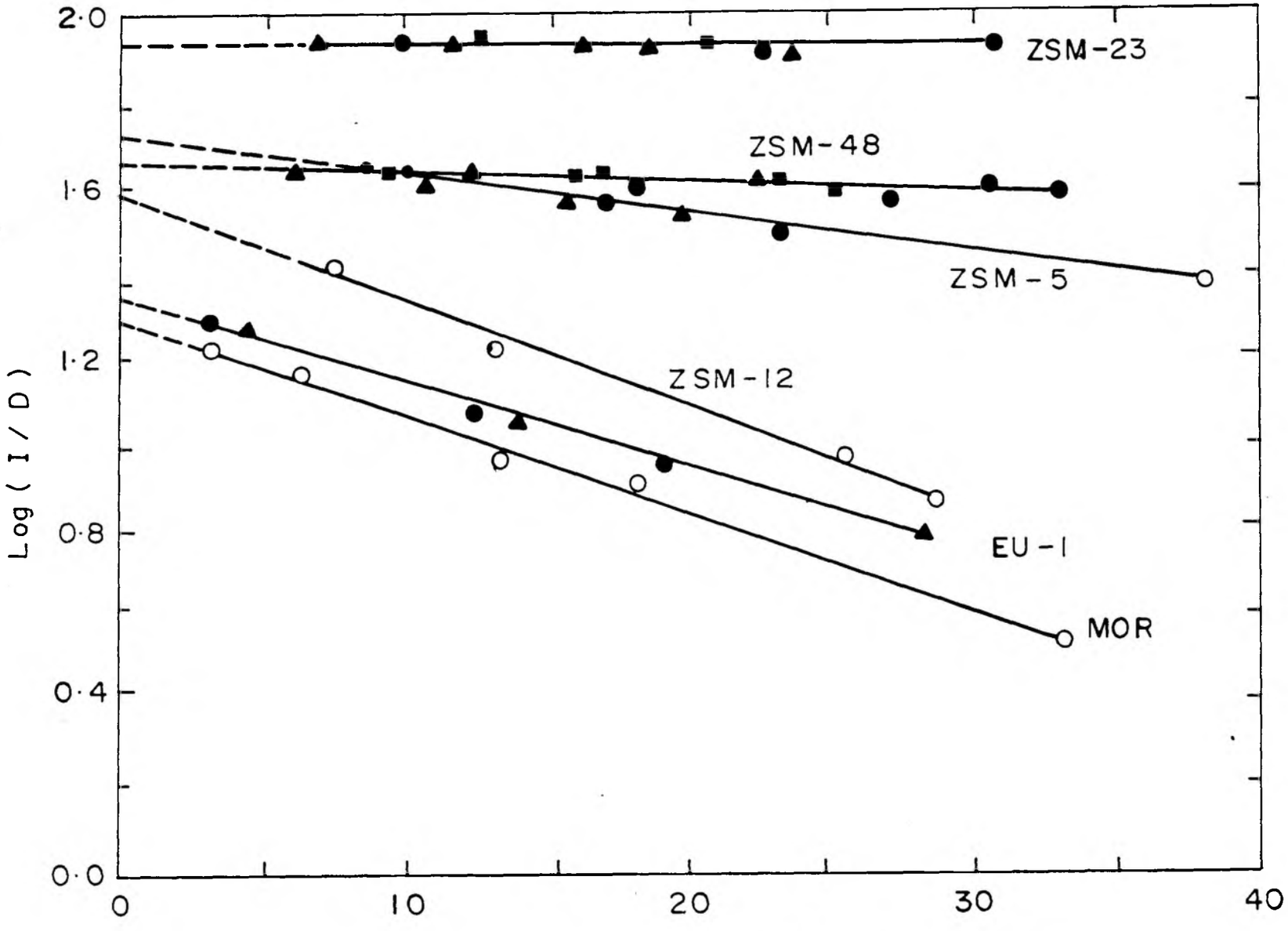

FIG. 4·6 Log (I/D) AGAINST M-XYLENE CONVERSION .

4.3.4. DISPROPORTIONATION OF TOLUENE:

The disproportionation of toluene has been used extensively to characterise the shape selectivity of medium pore zeolites, like ZSM-5 [220,227-230]. The results for H-EU-1 are shown in Tables 4.4 and 4.5 which illustrate the influence of temperature and space velocity, respectively. The benzene/xylenes (mole) ratio for all the runs reported in this study were around 1.0 indicating the absence of side reactions like (i) dealkylation of toluene to benzene and methane or (ii) disproportionation of xylenes to toluene and trimethylbenzenes. At lower temperatures, there is a slight enrichment of the para isomer in the xylenes fraction. Earlier studies [220,227,228,230], had indicated that over unmodified H-ZSM-5, the benzene/xylenes ratio increased from 1.0 to 1.8 with increasing temperature and conversion levels and was strongly dependent on the SiO_2/Al_2O_3 ratio of the zeolite. The xylene isomers were formed in equilibrium concentrations over unmodified H-ZSM-5 and enrichment in the para isomer was observed only when the ZSM-5 was rendered more shape selective by impregnation with P or Mg. For example, at a conversion level of toluene of 15 %, the benzene/xylene ratio in the product was 1.50 for H-ZSM-5 [229] to be compared to 1.0, observed for H-EU-1 (SiO_2/Al_2O_3 = 115) at the same conversion level (Tables 4.4,4.5). The higher SiO_2/Al_2O_3 value and, as a consequence, the lower acid site density of EU-1 is probably responsible for the lower benzene/xylene ratio. Under similar conditions there was no significant disproportionation of toluene

TABLE. 4.4

Influence of temperature on disproportionation of toluene over H-EU-1

Feed, toluene-hydrogen (1:2,molar); WHSV, 3.5 h^{-1}.

Parameter	Temperature (K)				
	663	683	703	733	753
Conversion (%,w/w)	8.5	9.8	11.3	15.4	21.2
Products (%,w/w):					
Benzene	3.6	4.2	4.9	6.7	9.2
Toluene	91.5	90.2	88.7	84.6	78.8
p-Xylene	1.7	1.6	1.8	2.2	3.0
m-Xylene	2.6	3.0	3.4	4.6	6.3
o-Xylene	0.6	1.0	1.2	1.8	2.5
1,3,5-TMB[a]	--	--	--	--	--
1,2,4-TMB	--	--	--	0.1	0.2
1,2,3-TMB	--	--	--	--	--
Xylenes (%):					
Para	34.7	28.6	28.1	25.6	25.4
Meta	53.1	53.5	53.5	53.5	53.4
Ortho	12.2	17.9	18.0	20.9	21.2

[a]See Table 4.1.

TABLE. 4.5

Influence of WHSV on disproportionation of toluene over H-EU-1

Feed, toluene-hydrogen (1:4,molar); Temperature,753 K.

Parameter	WHSV (h^{-1})			
	3.5	7	13	17.5
Conversion (%,w/w)	21.2	13.3	9.2	6.3
Products (%,w/w):				
Benzene	9.2	5.6	3.9	2.7
Toluene	78.8	86.7	90.8	93.7
p-Xylene	3.0	2.0	1.4	0.9
m-Xylene	6.3	4.1	2.9	2.0
o-Xylene	2.5	1.6	1.0	0.7
1,3,5-TMB[a]	--	--	--	--
1,2,4-TMB	0.2	--	--	--
1,2,3-TMB	--	--	--	--
Xylenes (%):				
Para	25.4	26.1	24.6	25.0
Meta	53.4	53.3	54.7	55.5
Ortho	21.2	20.8	20.7	19.5
R(=benzene/xylenes)	1.0	1.0	1.0	1.0

[a]See Table 4.1.

over H-ZSM-48 again emphasising the crucial role of intersections/side pockets in catalysing this reaction in medium pore zeolites. The higher para isomer selectivity observed in toluene disproportionation (vis-a-vis ZSM-5) follows the similar trend observed earlier in m-xylene isomerisation.

4.3.5. METHYLATION OF TOLUENE:

The influence of temperature and space velocity in the methylation of toluene over H-EU-1 is shown in Tables 4.6 and 4.7. This is an electrophilic reaction, the primary products being ortho and para xylenes. Meta xylene as well as C_9 aromatic products are formed by secondary reactions like isomerisation, further alkylation and transalkylation. Any enrichment of the para isomer in the reaction products is due to the shape selectivity of the catalyst and may be used as an index of the latter provided significant concentration of the secondary products is avoided. This may be seen from Tables 4.6 and 4.7 wherein at low temperatures and contact times, the ortho and para isomers predominate in the reaction product. As the reaction severity and conversion levels increase, the ortho and para xylenes isomerise to the meta isomer. At 683 K and conditions similar to those stated in Table 4.6, ZSM-48 gave a para:meta:ortho ratio of 38:40:22 [231] to be compared to 28:49:23 observed for EU-1 in this study (Table 4.6). Unmodified ZSM-5 under identical conditions yielded a distribution of the three xylene isomers similar to EU-1. Fig 4.7 compares the three

TABLE. 4.6

Influence of temperature on methylation of toluene over H-EU-1

Feed, toluene-methanol (3.4:1,molar): WHSV, 3.5 h^{-1}.

Parameter	Temperature (K)			
	633	663	683	703
Conversion (%,w/w)	2.4	6.7	17.0	28.5
Products (%,w/w):				
Aliphatics	2.8	3.0	4.2	4.1
Benzene	1.2	2.6	5.4	6.8
Toluene	93.5	89.4	79.5	68.5
Ethylbenzene	--	--	0.1	0.2
p-Xylene	0.8	1.3	2.5	4.0
m-Xylene	0.6	1.7	4.2	9.0
o-Xylene	0.5	1.0	2.0	3.0
p-Ethylbenzene	--	--	--	0.1
m-Ethylbenzene	--	--	0.2	0.2
1,3,5-TMB[a]	--	--	0.2	0.6
1,2,4-TMB	0.6	1.0	1.5	2.9
1,2,3-TMB	--	--	0.2	0.6
Xylenes(%):				
Para	42	32	28	26
Meta	32	43	49	53
Ortho	26	25	23	21
Sel.Isom. (%)[b]	52	53	54	58

[a,b]See Table 4.1.

TABLE. 4.7

Influence of WHSV on methylation of toluene over H-EU-1

Feed, toluene-methanol (3.5:1,molar); Temperature, 683 K.

Parameter	WHSV (h^{-1})			
	3.5	7	13	17.5
Conversion(%, w/w)	17.00	16.0	9.9	4.9
Products (%, w/w):				
Aliphatics	4.2	4.0	3.6	3.4
Benzene	5.4	4.3	3.0	1.9
Toluene	79.5	80.5	86.3	91.1
Ethylbenzene	0.1	--	--	--
p-Xylene	2.5	2.7	1.9	1.1
m-Xylene	4.2	4.0	2.0	1.0
o-Xylene	2.0	2.3	2.2	1.3
m-Ethylbenzene	0.2	0.1	--	--
1,3,5-TMB[a]	0.2	0.3	0.1	--
1,2,4-TMB	1.5	1.5	0.8	0.2
1,2,3-TMB	0.2	0.3	0.1	--
Xylenes (%):				
Para	28	30	31	32
Meta	49	44	33	29
Ortho	23	26	36	39
Sel.Isom. (%)[b]	54	58	60	62

[a,b]See Table 4.1.

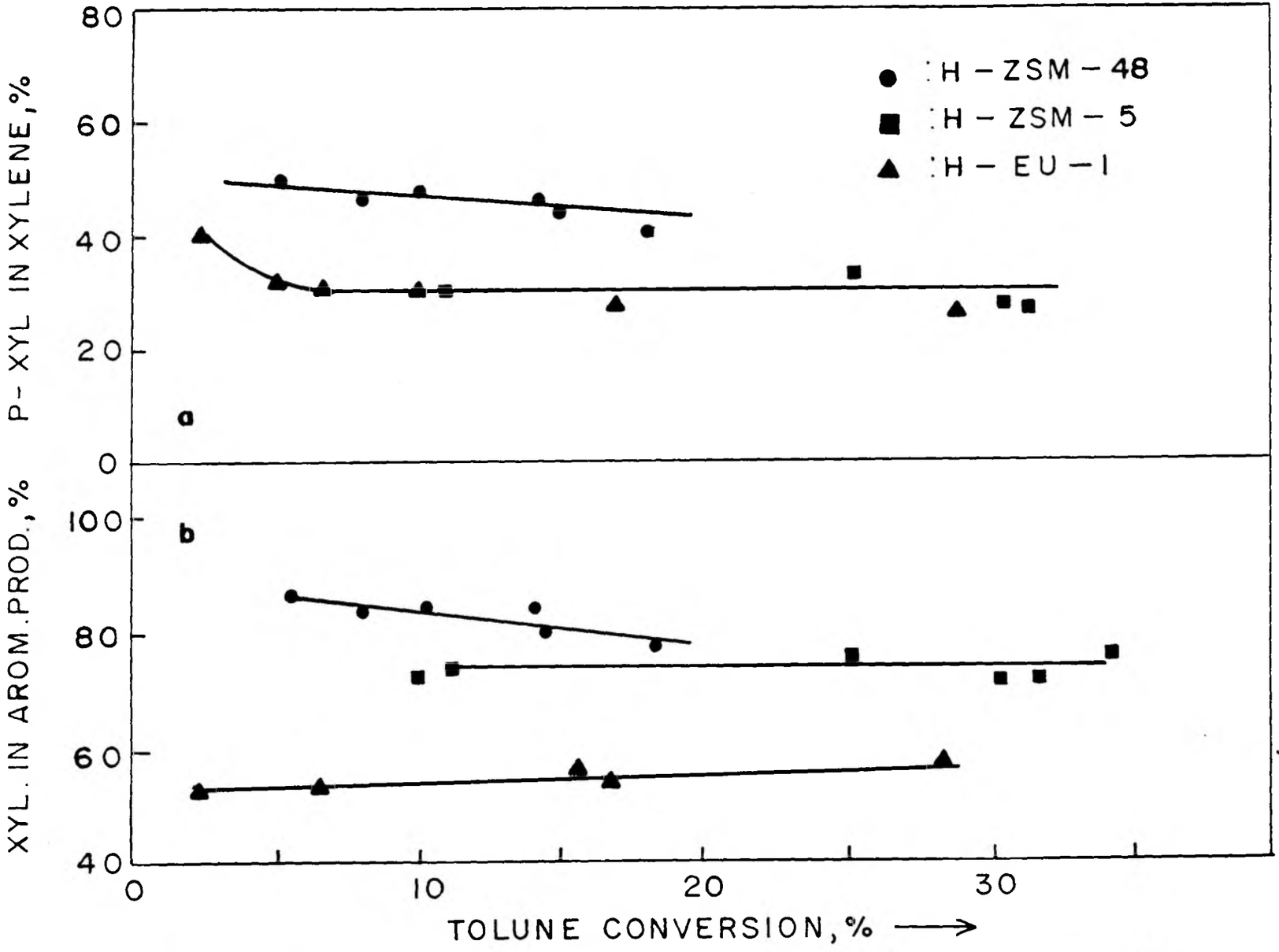

FIG. 4·7 SELECTIVITY FOR a) P-XYLENE IN XYLENE ISOMERS AND b) TOTAL XYLENES IN AROMATIC PRODUCTS.

zolites with respect to their selectivities for yielding (i) the para isomer among the xylene isomers (product shape selectivity) and (ii) xylenes amongst various reaction products (transition shape selectivity). The former decreased in the order : ZSM-22 > ZSM-23 > ZSM-48 > EU-1 ≥ ZSM-5. The restricted transition state shape selectivity of these zeolites decreases as ZSM-22 > ZSM-23 > ZSM-48 > ZSM-5 > EU-1. It may be noted that this is similar to the earlier grading of these zeolites for yielding isomerisation (rather than transalkylation) products in the reactions of m-xylene.

4.4. SUMMARY

The results on the relative shape selectivity of EU-1 in the reactions of aromatic hydrocarbons may be summarized as follows: Product shape selectivity leading to enrichment of the para isomer in the product follows the trend ZSM-22 > ZSM-23 > ZSM-48 > EU-1 > ZSM-5. On the other hand, in reactions of xylenes in which there are alternative possibilities of yielding either xylene isomers (by 1,2-alkyl shifts) or transalkyalted products, the selectivity for yielding xylene isomers (i.e., restricted transitions state selectivity) decreases in the order ZSM-22 > ZSM-23 > ZSM-48 > ZSM-5 > EU-1. The large side pockets of the channels in the EU-1 zeolites are believed to be the loci for such transalkylation reactions and lead to lower transition state shape selectivities

SUMMARY

Zeolite EU-1 belongs to the family of a high silica medium pore zeolites. The framework of EU-1 zeolite possesses an unidimensional, non-intersecting channel structure defined by 10-membered ring openings (0.58 X 0.41 nm) and deep side pockets (0.68 X 0.58 nm in cross-section and 0.81 nm in depth) off the channels. The channels lie in the [100] direction and side pockets in the [001] directions. The presence of 10-ring channels, characteristic of medium pore zeolites together with large side pockets, makes this zeolite interesting from the point of view of shape selective catalysis. Hence the detailed study was undertaken in synthesis and characterisation of novel high silica zeolite EU-1.

Factors influencing the synthesis of high silica EU-1 zeolite using mixed benzyldimethylamine (BDMA) and benzyl chloride as templating molecules have been investigated. The kinetic features of the crystallisation process, such as the influence of time, temperature, ageing of the precursor species, etc., are also studied. A synthesis procedure, using hexamethonium bromide as templating agent, for the isomorphous substitution of Fe^{+3} in place of Al^{+3} in EU-1 framework is also studied. It was found that below 453 K pure EU-1 phase crystallizes between SiO_2/Al_2O_3 ratios of 70 and 600. Above 453 K, however, the product contained either amorphous or crystalline dense phases like alpha-quartz and cristobalite. Increasing the concentration of the template enhanced the rates of both nucleation and crystallisation. It was found that under these

synthesis conditions, pure EU-1 could be obtained only in a narrow range of OH^-/SiO_2 (0.1-0.15) ratio. The apparent activation energies for both nucleation and crystallisation of EU-1 zeolite were estimated by applying Arrhenius-type equation. To describe the crystallisation process of EU-1 zeolite mathematically, the data were fitted to the Avrami-Erofeev equation. The morphology of EU-1 was examined on scanning electron microscope during nucleation and crystal growth.

The physico-chemical characterization was done by X-ray diffraction, thermal analysis, NMR, IR, TPD of ammonia, EPR, XPS, and sorption of different probe molecules such as water, nitrogen and hydrocarbons. X-ray diffraction patterns and IR spectra in framework vibration region showed typical EU-1 zeolite phase. However, the IR spectra of Fe-EU-1 zeolite shows a shift in frequency of the main asymmetric band at 1100 cm^{-1} to a lower value. Thermal analysis shows that the zeolite EU-1 phase is stable upto 1273 K. Evidence from ^{29}Si and ^{27}Al MASNMR measurements indicates at least two crystallographically different environments for Si atoms. XPS, EPR data support the presence of Fe in the framework lattice of EU-1 zeolites.

Equilibrium sorption uptake for n-hexane and cyclohexane was found to be unaffected by varying Si/M (M= Al^{+3} or Fe^{+3}) ratio. Sorption data for cyclohexane confirm that the entry pore size is slightly less than 0.6 nm due to the presence of 10 T-atoms windows. Equilibrium uptake for water was found to decrease with the increase in Si/M ratio indicating enhanced hydrophobic

character of the zeolites on increasing Si/M ratio. The BET and Langmuir surface areas were also found to decrease with increase in Si/M ratio. Sorption isotherms for n-butylamine in the temperature range 298-423 K were found to be of the Langmuir type. The number of n-BA molecules sorbed per unit cell of EU-1 zeolites decreased hyperbolically with the increase in Si/Al ratio. The n-BA sorption data satisfactorily represents the Dubinin, BET and Langmuir isotherm equations. However, Sips equation, Koble-Corrigan equation, Langmuir and Volmer coefficients (K_L & K_V) failed to represent n-BA sorption data in EU-1 zeolites. Chemical affinity curves for n-BA sorption exhibited very sharp decrease with the coverage and showed the highest chemical affinity for higher aluminium containing zeolite. Isosteric heats also showed decrease in lower coverage region with complicated behavior in the higher coverage region. Samples with higher content of aluminium showed higher Q_{st} values.

Acid strength distribution over Al-EU-1 and Fe-EU-1 zeolites have been determined by temperature programmed desorption of ammonia. Three distinct stages for desorption of ammonia at about 300-373, 373-500 and 500-775 K were observed. These three peaks are ascribed to NH_3 molecules (1) physically adsorbed, (2) chemisorbed on counter cations, and (3) bound in Bronsted acid sites, respectively. The TPD of ammonia indicated that the acid strength of framework hydroxyl groups in H-Al-EU-1 is greater than that in H-Fe-EU-1.

The shape-selective properties of H-EU-1 in the isomerization of m-xylene and the methylation and disproportionation of toluene were studied and compared with those of other medium pore zeolites. The presence of unidimensional ten-ring channel system together with deep side pockets off the channel in EU-1 leads to peculiar shape selectivity effects. The concentration of the para isomer in the isomerization products decreases in the order ZSM-22 > ZSM-23 > ZSMM-48 > EU-1 > ZSM-5. The aperture of the channels also decrease in the above order. The presence of large side pockets,in EU-1, in which bimolecular reactions such as xylene disproportionation can occur, leads to the following selectivity for isomerization (versus disproportionation): ZSM-22 > ZSM-23 > ZSM-48 > ZSM-5 > EU-1. The lower transition state shape selectivity of EU-1 is caused by the presence of large side pockets in its channel system. It is concluded that apart from the shape and size of the channel system, the presence or absence of pore intersections and cavities can also significantly affect the shape selectivity of medium-pore zeolites in catalytic reactions. It is suggested that shape selectivity effects in the isomerization of m-xylene can be used as diagnostic tools to reveal not only the size of the pores but also the presence or absence of cavities and the dimensionality of the pores in zeolites of unknown structure.

BIBLIOGRAPHY

1. Cronstedt, A., Akad. Handl. Stocholm,18, 120 (1756).

2. Damour, A., Ann. Mines, 17, 191 (1840).

3. Friedel, G., Bull. Soc. Fr. Mineral. Cristallogra., 19, 14 (1896).

4. Grandjean, F., Compt. Rendn., 149,866 (1909).

5. Weigel,O. and Steinhoff, E., Zeit. Krist., 61, 125 (1925).

6. McBain, J.W., "The Sorption of Gases and Vapours by Solids" George Routledge and Sons, London (1932).

7. Whyte, T.E.Jr. and Dalla Betta, R.A., Catal. Rev. -Sci. Eng. 24(4), 567-598 (1982).

8. Bragg, W. L., The Atomic Structure of Minerals, Cornell University Press, Ithaca, NY (1937).

9. Lok, B. M., Cannan, T. R. and Messina, C. A., Zeolites 3 282 (1983).

10. Meier, W. M. and Olson, D. H., Atlas of Zeolite structure types, structure commission of the International Zeolite Association (1978).

11. Meier, W. M., in Molecular Sieves, Society of Chem. Ind., London, p.10 (1968).

12. Barrer, R. M., Hydrothermal chemistry of Zeolites, Academic Press, London (1982).

13. Flanigen, E. M., in Proceedings of the Fifth International Conference on Zeolites,Rees, L. V. C., (ed), Heyden and Sons, London (1980).

14. Barrer, R. M., in Molecular Sieves, Society of Chem. Ind., London, p.10 (1968)

15. Sand, L. B.., Econ Geol., p.191 (1967).

16. Davis, M. E., Saldarriaga, C., Montes, C., Garces, J. and Crowder, C., Nature, 331,968-699 (1988).

17. Davis, M. E., Carlos Saldarriaga, Consuclo Montes, Juan Garoes and Cyrus Crowder, Zeolites, 8, 362 (1988).

18. Casci, J. L., Lowe, B. M. and Whitam, Thomas, V., Eur. Pat. Appl. 42226. Imperical Chemical Industries, 1981.

19. Casci, J. L. and Low, B. M., Zeolites, 3, 186 (1983).

20. Araya, A. and Lowe, B. M., Eur. Pat. 107,908 (1984).

21. Araya, A. and Lowe, B. M., Eur. Pat. 105,679 (1984).

22. Araya, A. and Lowe, B. M., Eur. Pat. 108,486 (1984).

23. Breck, D. W., Eversole, W. G. and Milton, R. M., J. Am. Chem. Soc., 1956, 78, 2338.

24. Milton, R. M., in Molecular Sieves, Soc. Chem. Ind., London, (1968), p.199.

25. Zhdanov, S. P., Adv. Chem. Ser., 101, 2 (1971).

26. Flanigen, Adv. Chem. Ser., 121, 119 (1973).

27. Breck, D. W. and Acara, N. A., U.S. Patent 2,950,952 (1960).

28. Morretti, E., Contessa, S. and Padovan, M., Chemica e Industria, 67, 21 (1985).

29. Barrer, R. M. and Denny, P. J., J. Chem. Soc., 971 (1961).

30. Kerr, G. T. and Kokotailo, G.T., J. Amer. Chem. Soc., 83,4675 (1961).

31. Barrer, R. M., Denny, P. J. and Flanigen, E. M., U.S. Patent 3,306,922 (1967).

32. Kerr, G. T., Inorg. Chem., 5, 1537; U.S.Pat. 3,247,195 (1966).

33. Wadlinger, R. L., Rosinski, E. J. and Plank, C. J., U.S. Pat. 3,375,205 (1968).

34. Kerr, G. T., Science, 140, 1412 (1963).

35. Flanigen, E. M. and Kellberg, E. R., Dutch Patent 6,710,729 (1967).

36. Barrer, R. M. and Villiger, H., J. Chem. Soc., D, 659 (1969).

37. Acara, N. A., U.S. Patent 3,414,602 (1968).

38. Rabo, J. A., Bezman, R. D. and Poutsma, M. L., Acta. Phys. Chem., 24, 39 (1978).

39. Plank, C. J., Rosinski, E. J. and Rubin, M. K., U.S. Pat. 4,086,859 (1977).

40. Rubin, M. K., Rosinski, E. J. and Plank, C. J., U.S. Pat. 4,086,186 (1978).

41. Argauer, R. J. and Landolt, G. R., U. S. Patent 3,702,886 (1972).

42. Chu, P., U.S. Patent 3,709,979 (1973).

43. Rosinski, E. J. and Rubin, M. K., U.S. Patent 3,832,449 (1974).

44. Wadlinger, R.L., Kerr, G. T. and Rosinski, E. J., U.S. Patent 3,308,069 (1967).

45. Kulkarni, S. B., Shiralkar, V. P., Kotasthane, A. N.,Borade, R. B. and Ratnasamy, P., Zeolites, 2, 313 (1982).

46. Kotasthane, A. N., Shiralkar, V. P., Hegde, S. G., and Kulkarni, S. B., Zeolites, 6, 253 (1986).

47. Casci, J. L., Proceedings of 7th International Conf. of Zeolites Tokyo 1986.

48. Casci, J. L., Lowe, B. M. and Whittam, T. V., U.K. Patent 2077709 B.

49. Casci, J. L., Lowe, B. M. and Whittam, T. V., U.S. Pat.4528171.

50. Rohrman, Jr. A. C., Lapierre,R. B., Schleuker, J. L., Wood, J. D., Valyocsik, E. W., Rubin, M. K., Higgins, J. B. and Rohrbangh, W. J., Zeolites 5 352 (1985).

51. Bibby, D. M., and Parker, L. M., Zeolites, 3, 11 (1983).

52 (a). Flanigen, E. M., Bennett, J. M., Grose, R. W., Cohen, J. P., Patton, R. L., Kirchnee, R. M. and Smith, J. V., Nature, 271, 512 (1978);
(b). Grose, R. W. and Flanigen, E. M., U.S. Pat. 4,061,724 (1977).

53. Flanigen, E. M. and Patton, R. L., U. S. Patent4,073,865 (1978).

54. Kokotoilo, G. T., Chu, P., Lowton, S. L. and Meier, W. M., Nature, 275, 119 (1978).

55. Bibby, D. M. Milestone, N. B. and Aldridge, L. P., Nature, 280, 664 (1979).

56. Grose, R. W. and Flanigen, E. M., U.S. Patent 4,104,294 (1978).

57. Stubican, V. and Ray, R., Amer. Minerol., 47, 116 (1962).

58. Hautefeuille, P., Compt. Rend., 90, 303 and 378 (1880).

59. Perry, A., Compt. Rend., 107 1150 (1888).

60. Eitel, W., Herlinger, E. and Tromel, G., Naturwiss. 18, 469 (1930).

61. Morosi, L., Stabenew, J., Schwarzmann, M., Ger. Pat.2,831,630 and 2,909,929 (1980).

62. Barrer, R. M. and Cole, J. F., J. Chem. Soc. A 2475 (1968).

63. Tielen, M., Geelen, M., Jacobs, P. A., J. Cat. 91(2), 352-355 (1985).

64. Rubin, M. K., Plank, C. J. and Rosinski, E. J., Eur.Pat. 3144, (1979). Mobil Oil Corp. USA.

65. Ratnasamy, P., Borade, R. B., Kulkarni, S. B., Kotasthane, A. N., Shiralkar, V. P. and Hedge, S. G., Indian Pat. 160212 (1983)

66. Kotasthane, A. N., Shiralkar, V. P. and Ratnasamy, P., Indian Pat. Applied (1988).

67. Ratnasamy, P., Kotasthane, A. N., Shiralkar, V. P., Thangaraj, A. and Ganapathy., ACS series 398, Chap. 28, pg.405 (1988).

68. Wilson, S. T., Lok, B. M., Massina, C. A., Cannan, T. R. and Flanigen, E. M., J. Am,. Chem. Soc., 104, 1146 (1982).

69. Lok, B. M., Messina, C. A., Patton, R. L., Gajek, R. T., Cannan, T. R. and Flanigen, E. M., U.S. Patent,4,440,871 (1984).

70. Lok, B. M., Cannan, T. R. and Messina, C. A., Zeolites 4, 289 (1984).

71. Briscoe, N. A., Johnson, D. W., Shannon, M. D., Kokotoile, G. T. and McCusker, L. B., Zeolites, 8, 74 (1988).

72. Rubin, M. K., U.S. Pat. 4,640,829 (1987).

73. Sumitami, K., Sokay, T., Yamasaki, Y. and Ohodera, T., Eur. Pat. Appl. 51318, (1982).

74. Breck, D. W., U. S. Patent, 3,130,007 (1964).

75. Culfaz, A. and Sand, L. B., Adv. Chem. Ser., 121, 140 (1973).

76. Erdem, A., M. S. Thesis, Worcester Polytechnique Institute, U.S.A. (1978).

77. Chao, K. J., Tasi, T. C., Chen, M. S. and Wang, I., J. Chem. Soc. Faraday Trans. I, 77, 547 (1981).

78. Wu, E. L., Lawton, S. L., Olson, D. H., Rohrman, Jr., A. C. and Kokotoilo, G. T., J. Phys. Chem., 83, 21, 2777 (1979).

79. Bibby, D. M., Aldridge, L. P. and Milestone, N. B., J. Cat., 72, 373 (1981).

80. Meyers, B. L., Ely, S. R., Kutz, N. A., Kaduk, J. A. and Bossche, E. V., J. Catl., 91, 352 (1985).

81. Pluth, J. J., Smith, J. V. and Bennett, J. M., Acta. Crystallog., C 42, 283 (1986).

82. Mahler, B., Z. Kristallogr., 174, 141 (1986).

83. Laves, F., Hafner, S., Norsk, Geol. Tidsski., 42, 57, (1962).

84. Wright, A. C., Rupert, J. P., Granquist, W. T., Am. Mineralogist, 53, 1293, (1968).

85. Zhdanov, S. P., Kiselev, A. V., Lygin, V. I., Titova, T. I., Russ. J. Phys. Chem., 38, 1299 (1964).

86. Flanigen, E. M. and Khatami, H., Szymanski, H.A, I. Adv. Chem. Ser., 101, 201 (1971).

87. Flanigen, E. M. and Grose, R. W., Adv. Chem. Ser., 101, 76 (1971).

88. Kutz, N., Heterogeneous Catalysis-II, B. L. Shapiro, ed., Texas A & M University Press, College Station, 121 (1984).

89. Wu, E. L., Kuhl, G. H., Whyte, T. E. Jr., Venuto, P. B., Adv. Chem. Ser., 101, 490 (1971).

90. Jacobs, P. A., Carboniogenic Activity of Zeolites, Elsevier, Amsterdam, 39 (1977).

91. Hatada, K., One, Y. and Ushik, Y., J. Phy. Chem., 37, 117 (1979).

92. Nagy, J. B., Gigot, M., Gourgue, A. and Derouane, E. G., J. Mole. Catal., 2, 265 (1977).

93. TopsOe, N.,Pendersen, K. and Derouane, E. G., J. Catal., 70, 41 (1981).

94. Jacobs, P. A. and Mortier, W. Y., Zeolites, 2, 226 (1982).

95. Chu, C. T. W. and Chang, C. D., J. Phys. Chem., 89, 1569 (1985).

96. Harris, R. K., Knight, C. T. G. and Hull, W. G., J. Amer. Chem. Soc., 103, 1577 (1981).

97. Harris, R. K., Knight, C. T. G. and Pawson, D., J. Mol. Struct., 69, 95 (1980).

98. Harris, R. K., Knight, C. T. G. and Smith, D. N., J. Chem. Soc. Chem. Comm., 726 (1980).

99. Harris, R. K. and Newman, R. H., J. Chem. Soc. Faradays Trans. II, 73, 1204 (1977).

100. Cavell, K. J., Masters, A. F. and Wilshier, K. G., Zeolite, 2, 244 (1982).

101. Nagy, J. B., Gabelica, Z. and Derouane, E. G., Chemistry Letters, 7, 1105 (1982).

102. Lippmaa, E.,Magi, M., Samoson, A., Engelhart, G. and Grimmer, A. R., J. Amer. Chem. Soc., 102, 4889 (1980).

103. Barrer, R. M. and Ibbiston, D. A., Trans. Faradays Soc., 40, 206 (1944).

104. Dibble, W. E. Jr., DeJong, B. H. W. S. and Cary, L. W., "Proc. 3rd Intern. Sympo. Water-Rock Interaction" Edmonton, Canada, 47 (1980).

105. Derouane, E. G., Nagy, J. B., Gabelica, Z. and Blom, N., Zeolite, 2, 299 (1982).

106. Engelhardt, G., Michel. D. "High-Resolution solid-state NMR of Silicates and Zeolites", John Wiley and Sons; New York, (1987).

107. Vedrine, J. C., Auroux, A., Bolis, V., Dejaifve, P., Naccache, C., Wierzchowski, P., Derouane, E. G., Nagy, J. B., Gilson, J. P., Van Hooff, J. H. C., Van Den Berg, J. P. and Wolthnizen, J. P., J. Catal., 59, 248 (1979).

108. Auroux, A., Bolis, U., Wierzchowski, P., Gravellc, P. C. and Vedrine, J. C., J. Chem. Soc. Faraday Trans. I, 75, 2544 (1979).

109. Anderson, J. R., Forger, K., Mole, T., Rajadhyaksha,R. A. and Senders, J. V., J. Catal., 58, 114 (1979).

110. Jacobs, P. A., Uytterhoeven, J. B., Steyns, M., Froment, G. and Weitkamp, J., "Proceedings, 5th Intern. Conf. on Zeolites". Naples, Italy, Y Heyden and Sons, London, 607 (1980).

111. Nakamoto, H. and Takahashi, H., Chemistry Letters, 1013 (1981).

112. Barrer, R. M. and Langley, D. A., J. Chem. Soc., 3804, 3811, 3817 (1958).

113. Breck, D. W., Zeolite Molecular Sieves, John Wiley and Sons, New York, 449 (1974).

114. Kuhl, G. H., J. Catal., 29, 270 (1973).

115. Barrer, R. M., Proc. Roy. Soc., A, 167, 392 (1938).

116. Barrer, R. M., Quart. Review, London, 3239 (1949).

117. Barrer, R. M., and Breck, D. W., Trans. Faraday Soc., 59, 2569 (1963).

118. Barrer, R. M. and Gibbson, R. M., Trans. Faraday Soc., 59, 2569 (1963).

119. Barrer, R. M., Pure and Appl. Chem., 52, 2143 (1980).

120. Derouane, E. G. and Gabelica, Z., J. Catal., 65 486 (1980).

121. Jacobs, P. A., Bayer, H. K. and Valyon, J., Zeolite, 1, 161-168 (1981).

122. Miesel, S. L., McCullough, U. J. P., Lechthalev, C. H. and Weisz, P. B., ACS meeting, Chicago, I, 11 (1977).

123. Weisz, P. B., Pure and Appl. Chem., 52, 2091 (1980).

124. Olson, D. H., Haag, W. O. and Lago, R. M., J. Catal., 61, 390 (1980).

125. Weisz, P. B., Frilette, V. J., Golden, R. L., J. Catal., 1, 301 (1962).

126. Derouane, E. G., "Catalysis by Zeolites", (ED. Imelik, B), 5 (1980).

127. Csicsery, S. M., "Zeolite Chemistry and Catalysis" (ED. Rabo, J. A.) ACS monograph 171, 680 (1976).

128. Naccache, C. and Taarit,B.Y., Pure and Appl. Chem., 52, 2175 (1980).

129.Weisz, P. B. and Frillette, V. J., J. Phy. Chem., 64, 382 (1960).

130.Weisz, P. B., Frillette, V. J., Maatman, R. W. and Mowev, E. B., J. Catal., 1, 307 (1962).

131.Wise, J. J. and Silvestri, A. J., Oil and Gas J., 74 140 (1976).

132.Chang, C.D. and Silvestri, A. J., J. Catal., 47, 249 (1978).

133.Silvestri, A. J., I and EC Proc. Desi. and Dev., 17, 255 (1978).

134.Chen, N. Y., Kaeding, W. W. and Dwyer, F. G., J. Amer. Chem. Soc., 101, 6783 (1979).

135.Dwyer, F. G., Lewis, P. J. and Schneider, F. M., Chem. Eng., 83, 90 (1976).

136.Keown, P. E., Meyers, C. C. and Wetherold, R. G., U. S. Patent, 3,751,504.

137.Chang, C. D., Lang, W. H. and Silvestri, A. J., J. Catal., 56, 268 (1979).

138.Ceasar, P. D., Brennan, J. A., Garwood, W. E. and Ciric, J., J. Catal., 56, 274 (1979).

139.Rao, U. V. S., Gormley, R. J., Hydrocarbon Proceeding, Nov. 1980.

140.Weisz, P. B., Haag, W. O. and Rodewald, P. G., Science, 206, 57 (1979).

141.Garwood, W. E. and Chen, N. Y., ACS Div. Pet. Chem., Prepr. 25, 84 (1980).

142.Chen, N. Y. and Garwood, W. E., J. Catal., 52, 453 (1978).

143.Barrer, R. M. and White, E. A. D., J. Chem. Soc., 156 (1961).

144.Regis, A. I., Sand, L. B., Calmon, C. and Gilwood, M. E., J. Phy. Chem., 64, 1567 (1980).

145.Schwochow, F. E. and Heinze, G. W., Adv. Chem. Ser., 101, 102 (1971).

146.Casci, John L., Whittam, Thomas V. and Lowe, B. M., Proc. 6th Intl. Conf. on Zeolites, Reno, p.894, (1983).

147.Dodwell, G. W., Denkewicz, R. P. and Sand, L. B., Zeolites, 153, (1985).

148.Rubin, M. K., Eur. Pat. Appl. 159845, (1985).

149.Jacobs, P. A., Derouane, E. G. and Weitkamp, P., J. Chem. Soc. Chem. Communication, 591 (1981).

150.a) Avarami, M., J. Chem. Phys., 9, 117 (1941).
b) Erofeev, B. V., C. R. Acad. Sci., USSR, 52, 511 (1946).

151.Ghamami, M. and Sand, L. B., Zeolites, 155 (1983).

152.Derouane, E. G., Detremmerie, S., Gabelica, Z. and Blom, N., Appl. Catal., 1, 201 (1981).

153.Flaniigen, E. M., Pure and Appl. Chem., 52, 2191 (1980).

154.Rollman, L. D. "Inorganic Compounds with unusual properties", Vol II (ED. R. B. King), Acs, New York, 387 (1979).

155.Gabelica, Z., Derouane, E. G. and Blom, N., Appl. Catal., 5, 109 (1983).

156.Flanigen, E. M., Adv. Chem. Ser., 173, 80 (1976).

157.Casci, John, L., U. S. Pat 4,537,754 (1985).

158.Jacobs, P. A. and Martens, J. A. in Studies in Surface Science and Catalysis, Ed. B. Delmon and J. T. Yates, Elsevier Vol. 33, p.26, (1987).

159.Chao, K. J., Proc. Natl. Sci. Counc., Roc. 3, 233 (1979).

160.Bibby, D. M., Milestone, N. B. and Aldrige, L. P., Nature, 285, 30 (1980).

161.Mory, G.W. and Ingerson, E., Econ. Geol., 607 (1937).

162.Barrer, R. M., Hydrothermal Chemistry of Zeolites, Academic Press, New York, (1982).

163.Barrer, R. M., Baynham, J. W., Bultitude, F. W., Meier, W. M., J. Chem Soc., 195 (1959).

164.Gabelica, Z., Nagy, J.B., Debras, G. and Derouane, E.G., in Proceedings of the 6th International Conference on Zeolites (Eds. D. Olson, and A. Bisio) Butterworths, Guildford. UK, p.914 (1984)

165.Flanigen, E. M., Breck, E. W., ACS 137th meeting, Cleveland, Ohio, (1960).

166.Kerr, G. T., J. Phys. Chem., 70, 1047 (1966).

167.Myrsky, Ya. V., Mirtofanov, M. G, Dorogochiniski, A. V., "New Adsorbents-Molecular Sieves", Grosnyi (1964).

168.Myrsky, YA. V., Mirtofanov, M. G., Popkov, B. M., Bolotov, L. T., Ruohko, L. F., "Zeolites, Their Synthesis, Properties and Utilization", Nauka, Moscow Leningrad, 192 (1965).

169.Zhadnov, S. P., "Molecular Sieves", Soc. of the Chemical Industry, London, 62 (1968).

170.Zhdanov, S. P., Egorova, E. N., "Chemistry of Zeolites", Nauka, Leningrad, (1968).

171.Senderov, E. E., Khitarov, N. E., "Zeolites, Their Synthesis and conditions of Formation in Nature", Nauka Publishing House, Moscow, (1970).

172.Zhdanov, S. P., Advances, Chem. Ser., 101, 20 (1973).

173.Breck, D. W., Flanigen, E. M. "Molecular Sieves", Society of the Chemical Industrys, London, 47 (1968).

174.Kerr, G. T., J. Phys. Chem., 72, 1385 (1968).

175.Ovsepyan, M. E., Zhdanov, S. P., Izv, Akad. Nauk SSSR, Ser, Khim., 11 (1965).

176.Barrer, R. M., Cole, J. F., J. Chem. Soc., A, 1516 (1970).

177.Culfaz, A., Sand, L. B., Adv. Chem. Ser., 121 152 (1973).

178.Kerr, I. S., Gard, J. A., Barrer, R. M., Galabova, I. M., Amer. Mineral, 55, 441 (1970).

179.Derouane, E. G., Mestdagh, M.,and Vielyove, L., J. Catal, 33, 169 (1974).

180. McNicol, B. D. and Pott, G. T., J. Catal., 25, 223 (1972).

181.Wichterlova, B., Zeolite, 1, 181 (1981).

182.Wichterlova, B. and Jiru, P., React. Kinet. Catal. Lett., 13 197 (1980).

183.Castner, T. Jr., Newell, G. S., Hotton, W. C., and Slichter, C. P., J. Chem. Phys., 32, 668 (1980).

184.Stencel, J. M., Diehl, J. R., Dougles, L. J., Spitler, C. A., Crowford, J. E., and Nelson, G. A., Colloids Surf. 4, 331 (1982).

185.Tsitsishvili, G. V. and Andronikashvili, T. G., Adv. Chem. Ser., 102, 217 (1971).

186.Ballivet, D., Pichat, P. and Barthomeuf, D., Adv. Chem. Ser., 121, 469 (1973).

187.Johnson, M. F. L., J. Catal., 52, 425 (1978).

188.Tsitsishvili, G. V., Adv. Chem. Ser., 121, 291 (1973).

189.Smith, J. V., Adv. Chem. Ser., 101, 171 (1971).

190.McDaniel, C. V. and Maher, P. K., "Molecular Sieves", Soc. Chem. Ind., London, 186 (1968).

191.Kumar, R., Ernst, S., Kokotailo, G. T., and Weitkamp, J., Stud. Surf. Catal., 37, 451 (1988).

192.Breck, D. W., "Zeolite Molecular Sieves," John Wiley and Sons, New York, 529 (1974).

193.Dubinin, M. M. and Radushkevich, L. V., Proc. Acad. Sci., USSR, 1974, 55, 327.

194.Shiralkar, V. P. and Kulkarni, S.B., Zeolites, 4, 329 (1984).

195.Kulkarni, S. J. and Kulkarni, S. B., Ind. J. Chem., 1989, 28A, 6.

196.Sips, R., J. Chem. Phys., 1948, 16, 491.

197.Shiralkar, V. P. and Kulkarni, S. B., J. Colloid and Interface Sci., 1985, 108, 1.

198.Koble, R. A. and Corrigan, T. E., Ind. Engg. Chem., 1952, 44, 383.

199.Shiralkar, V. P. and Kulkarni, S. B., Zeolites, 1985, 5, 37.

200.Shiralkar, V. P. and Kulkarni, S. B., J. Colloid and Interface Sci., 1986, 109, 115.

201.Lahoduy-sarac, O. and White, J. L., J. Phys. Chem., 53, 2408 (1971).

202.Pichat, P. Beaumont, R. and Barthomeuf, D., J. Chem. Soc. Faraday Trans. I, 70 1402 (1974).

203.Klinowski, J., Thomas, J. M., Fyfe, C. A., and Gobbi, G. C., Nature 296, 533 (1982).

204.Fyfe, C. A., Gobbi, G. C., Klinowski, J., Thomas, J. M. and Ramadas, S., Nature (London), 296, 530 (1982).

205.Jacobs, P. A., J. Phys. Chem, 86, 3050 (1982).

206.Weitkamp, J., Ernst, S., and Kumar, R., Appl. Catal. 27, 207 (1986).

207.Martens, J.A., Ticklen, M., Jacobs, P.A., and Weitkamp, J., Zeolites, 4, 98 (1984).

208.Weitkamp, J., Ernst, S., Jacobs, P.A., and Karge, H.G., Erdol. Kohle - Erdgas - Petrochem., 39, 15 (1986).

209.Martens, J.A., J. Parez - Parient, Sastre., E., Corma, A., Jacobs, P.A., Appl. Catal. 45, 85 (1988).

210.Kumar, R., Rao, G.N., and Ratnasamy, P., in Jacobs, P.A., and Varsamlin, R.A.(editors), Stud. Surf. Sci. and Catal. 49 B, 1141 (1989).

211.Csicsery, S.M., Zeolites, 4, 202 (1984).

212.Prakash Babu, G., Kulkarni, S. B. and Ratnasamy. P., J. Cat. 79, 215 (1983).

213.Dewing, J., J. Molecular Catal. 27, 25 (1984).

214.Rao, G.N., Kumar, R., and Ratnasamy, P., Appl. Catal. 49, 307 (1989).

215.Gnep, N.S., Tejada, J., and Guisnet, M., Bull.Soc. Chim. Fr., 1, 5 (1982).

216.Ribeiro, F.R., Lemos, F., Parot, G., and Guisnet, M., in Setton R. (editor), Chemical Reactions in Organic and Inorganic Constrained Systems, Nato ASI Ser. C . No. 165, D.Reidel, Dordrect , p 145, (1986).

217.Joensen, F., Blom, N., Tapp, N.J., Derouane, E.G., and Fernandez, C., in P.A. Jacobs and R.A. van Santen (editors), Stud. Surf. Sci. and Catal. 49 B, 1989, Elsevier, Amsterdam, p 1131.

218.Richter, M., Fiebig, W., Jerschkewitz, H.-G., Lischke, G., and Ohlmann, G., Zeolites, 9, 238 (1989).

219.Kaeding, W.W., Chu, C., Young, L.B., Weinstein, B., and Butter, S.A., J.Catal. 67, 159 (1981).

220.Young, L.B., Butter, S.A., and Kaeding, W.W., J. Catal. 76, 418 (1982).

221.Corma, A., Cortes, A., Nebot, I., and Tomas, F., J. Catal. 57, 444 (1979).

222.Olson, D.H., Haag, W.O., in Catalytic Materials: Relationship Between Structure and Reactivity, ACS Symp. Ser. No. 248, 275 (1984).

223.Mavrodinova, V., Penchev, V., Lohse, U., and Stach, H., Zeolites, 9, 197 (1989).

224.Mavrodinova, V., Penchev, V., Lohse, U., and Gross, T., Zeolites, 9, 203 (1989).

225.Csicsery, S.M., J. Catal. 108, 433 (1987).

226.Csiscery, S.M., J. Catal. 110, 348 (1988).

227.Kaeding, W.W., Chu, C., Young, L.B., and Butter, S.A., J. Catal. 69, 392 (1981).

228.Meshram, N.R., Hegde, S.G., Kulkarni, S.B., and Ratnasamy, P. Appl. Catal. 8, 359 (1983).

229.Meshram, N.R., Hegde, S.G., and Kulkarni, S.B., Zeolites, 6, 434 (1986).

230.Meshram, N.R., J. Chem. Technol. Biotechnol. 37, 111 (1987).

231.Kumar, R., and Ratnasamy, P., J.Catal. 118, 68 (1989).